Circadian regulation of the AhR signaling pathway

Dissertation

to obtain the academic degree
Doctor rerum naturalium (Dr. rer. nat.)
submitted to the Department of Biology, Chemistry, Pharmacy
of Freie Universität Berlin

by

Melina Mihelakis

Berlin, 2024

The doctoral thesis was carried out at the Federal Institute for Risk Assessment (BfR) between 03/2020-02/2024 under the supervision of Dr. Norman Ertych.

1st reviewer: Prof Dr. Gilbert Schönfelder
2nd reviewer: Prof Dr. Florian Heyd

Date of defense: 23.07.2024

Acknowledgement

First, I would like to thank Prof. Dr. Gilbert Schönfelder for giving me the opportunity to carry out research at the German Federal Institute of Risk Assessment (BfR). Also, I would like to express my gratitude to Prof. Dr. Florian Heyd for agreeing to review this thesis and giving me some good advice on my research.

Next, I would like to thank Dr. Michael Oelgeschläger, who not only entrusted me with the topic of this thesis but also offered constructive criticism and valuable scientific input, as well as supported me from the beginning of my work at the BfR. Furthermore, I can´t thank enough Dr. Norman Ertych for being an excellent mentor, sharing his solid expertise with me, our chaotic but helpful scientific (or not) conversations, as well as guiding me through the challenges of failed experiments and redirecting me again towards the right path.

I would like to acknowledge the help I received from everyone in unit 93, with sincere thanks to Tanina Flore and Dorothee Storm for their technical assistance on the circadian project. I would also like to thank Dr. Johanna Ndikung for her contribution to the circadian project during her doctoral studies, that laid the foundation for my thesis, and her support to have a seamless start at the BfR. A heartfelt thank you to Tra-my, Sven, Miriam, Mirjam, Julia, Ann-Sophie, Marlene, Lars, and Sarah for making my daily work-life more enjoyable. Next, I would like to express my gratitude to Elena von Coburg, who from office-buddy evolved to a good friend, for her positive energy that always cheered me up during the day and for supporting our coffee addiction by supplying our office with her amazing coffee machine. The time during my thesis would not be the same without her and I hope at some point we are office-buddies again but this time with a daily croissant delivery service and a lab dog. At this point, I would also like to thank Dr. Peter Douglas, in whose lab I conducted my master thesis, for always inspiring me with his knowledge, his continuous support and pivotal role in my scientific career by convincing me to pursue a doctoral degree.

One of my most special thanks goes to my parents and my friends who are like family, Haris, Despoina and Eleanna, for always caring about me, supporting me in everything I pursue, even if they probably still wonder what exactly I do at work, and knowing exactly what to say to cheer me up in difficult times. Also, thanks to all the friends I made during the time of this thesis in Berlin: Alex, Christina, Delphine, Emiliano, Kathrin, Luca, Marco, Matthieu, Miguel, Nader, Sven, and Valeria. You all together with Haris and Despoina made my life outside of work so delightful, especially with all the dances, vacations, and conversations we had together and help me maintain the cultural aspect in my life. Because of all of you, I can now happily say: “Disturbing my own day-night rhythm while studying circadian rhythms for my doctoral thesis will always be an ironic story worth telling”.

Declaration of Independence

Herewith I certify that I have prepared my thesis with the title “Circadian regulation of the AhR signaling pathway” independently and that I have not used any sources and aids other than those indicated by me. The thesis was carried out at the German Federal Institute of Risk Assessment in Berlin under the guidance of Prof. Dr. Gilbert Schönfelder from March 2020 to February 2024.

X

Berlin, 27.02.2024

Outline

Summary

Common *in vitro* cell culture systems are widely used to understand physiological processes and disease development. However, these have a number of limitations such as the lack of the physiological 3D tissue architecture but also regulatory mechanisms, such as the circadian rhythm. For that reason, *in vitro* methods need to be improved to mimic as closely as possible the *in vivo* situation found in humans, and the regulatory framework of toxicological relevant pathways should be studied to better understand physiological processes. Even if the circadian rhythm has been linked to various important physiological processes, the molecular mechanism of these circadian regulations remains unravelled. The circadian rhythm is characterized by internal oscillations of physiological processes with a recurring periodicity of approximately 24 h and its synchronization depends mainly on the light-dark periods of the day. On the molecular level, the circadian rhythm is driven by the recurring expression of CLOCK genes, which regulate up to 48% of all human genes and ensures the proper daytime-depended activity. The uniform circadian rhythm of all cells in a tissue is often lost in common 2D *in vitro* cell culture systems but can be easily restored through artificial synchronization of these cells. Subsequently, such synchronized cell culture systems lead to enhanced quantitative and qualitative cellular response with a higher human relevance.

A highly toxicological relevant pathway, which might be under circadian control is the AhR (Aryl hydrocarbon Receptor) signaling pathway. In particular, in synchronized human breast cells the cellular response upon AhR-ligand binding shows a circadian pattern indicating a circadian regulation of the AhR pathway. This study describes for the first time important aspects of the mechanism behind the circadian regulation of the AhR signaling pathway. The circadian expression of AhR target genes, e.g. *CYP1A1*, is caused by a circadian activation of the *CYP1A1* promoter but not a circadian expression of AhR itself. Upon ligand exposure, e.g. TCDD (2,3,7,8-Tetrachlordibenzodioxin), AhR translocates into the nucleus and binds not only with ARNT but also with the circadian rhythm regulator BMAL1. These interactions seem to be circadian phase-dependent, indicating a possible competition in AhR binding. Additionally, the AhR co-factor, p23, negatively modulated the circadian regulation of the AhR signaling and SP1 was identified as a novel AhR co-factor exhibiting a circadian protein expression, which possibly sustains the proper circadian regulation of the AhR pathway. Besides that, preliminary data suggest that GSK3β could be involved in the circadian regulation of the AhR pathway.

Summarizing, all the findings of this thesis propose a possible mechanism for the circadian regulation of the AhR pathway and this work contributes to a better understanding of the circadian regulation of an important toxicological pathway, that might lead to the development of improved cell culture-based *in vitro* systems for toxicological and risk assessment strategies as well as for drug development with a higher human relevance.

Zusammenfassung

Um physiologische Prozesse und die Entstehung von Krankheiten zu verstehen, werden häufig konventionelle *in vitro* Zellkultursysteme verwenden. Diese haben jedoch entscheidende Nachteile, denn sie weisen keine physiologische 3D-Gewebestruktur auf und zum anderen sind in diese Systeme keine Regulationsmechanismen wie der circadiane Rhythmus hinreichend abgebildet. Es ist von entscheidender Bedeutung, solche *in vitro* Methoden zu verbessern und neu zu entwickeln, um ein möglichst realistisches Abbild der physiologischen Eigenschaften des Menschen widerzuspiegeln. Darüber hinaus würde in der toxikologisch-biomedizinischen Forschung ein vertieftes molekulares Verständnis von relevanten Signalwege und Regulatoren zur Optimierung von vorhandene *in vitro* Systemen beitragen und die Aufklärung physiologischer Prozesse vorantreiben. Einer von diesen zentralen Regulatoren ist der circadiane Rhythmus. Obwohl dieser mit verschiedenen wichtigen physiologischen Prozessen verknüpft ist, wie z.B. mit dem Fremdstoffmetabolismus, bleiben molekulare Mechanismen der circadianen Regulation des Fremdstoffmetabolismus weiterhin ungeklärt. Der circadiane Rhythmus wird als biologische Oszillation mit einer wiederkehrenden Periodizität von 24 Stunden definiert, welche durch den Tag-Nacht Rhythmus vorgegeben wird. Auf zelluläre Ebene wird der circadiane Rhythmus durch eine oszillierende Expression von CLOCK-Genen angetrieben. Diese können bis zu 48% aller menschlichen Gene regulieren und determinieren so die tageszeitliche Aktivität von Geweben und Organen. In konventionellen 2D *in vitro* Zellkultursystemen folgt jede Zelle ihrem eigenen circadian Rhythmus, wodurch die tagesabhängige Synchronität eines Gewebes in einem Organismus nicht abgebildet wird. Diese Synchronität kann aber wiederhergestellt werden, indem die rhythmische Expression der CLOCK-Gene artifiziell stimuliert wird. In der Folge führen solche synchronisierten Zellkultursysteme zu einer verbesserten quantitativen und qualitativen zellulären Reaktion mit einer höheren humanen Relevanz.

Der toxikologisch relevante AhR-Signalweg (*Aryl hydrocarbon Receptor*) scheint einer von den Prozessen im Fremdstoffmetabolismus zu sein, der eine circadiane Regulation aufweist. So zeigt die Zellantwort von synchronisierten humane Brustzellen nach Exposition mit AhR Liganden einen circadianen Rhythmus. Mit dieser Arbeit konnten nun erstmals wertvolle Erkenntnisse hinsichtlich des Mechanismus der circadianen Regulation des AhR-Signalwegs gewonnen werden. So konnte gezeigt werden, dass die circadiane Expression von AhR-Zielgenen, wie z.B. *CYP1A1,* nicht auf einer circadianen Expression des Rezeptors zurückzuführen ist, sondern auf eine circadiane Aktivierung des XRE Promotors. Dabei wird der AhR nach Exposition mit dem Ligand TCDD in den Zellkern transportiert. Dort bindet er nicht nur mit ARNT, um die Expression seiner Zielgenen zu initiieren, sondern auch mit dem circadianen Regulator, BMAL1. Möglicherweise führt das zu einer

kompetitiven Bindung zwischen AhR, ARNT und BMAL1, und somit zu einer circadianen regulierten Interaktion. Zusätzlich wurde gezeigt, dass der AhR Co-faktor, p23, die circadiane Regulation vom AhR-Signalweg negativ beeinflusst und SP1 wurde als ein AhR Co-faktor identifizieret, der die circadiane Promotoraktivität positiv reguliert. Interessanterweise konnte für SP1 auch eine circadian Proteinexpression nachgewiesen werden, die möglicherweise die physiologische, circadiane AhR-Regulation aufrecht hält. Präliminäre Daten deuten auf eine GSK3β-Abhängigkeit der circadianen Regulation des AhR-Signalwegs hinaus. Zusammenfassend ermöglichen die Ergebnisse dieser Studie die Ableitung eines potenziellen Mechanismus für die circadiane Regulation des AhR-Signalwegs und tragen somit zu einem besseren Verständnis der circadianen Regulation eines bedeutenden toxikologischen Signalwegs bei. Dadurch können zukünftig verbesserter zellkulturbasierte *in vitro* Systeme entwickelt werden, die für toxikologische und biomedizinischen Forschung aber auch für Risikobewertungsstrategien von hoher Wichtigkeit sind.

List of tables

List of figures

List of abbreviations

%	percentage
°C	celsius
µ	micro-
ADME	absorption, distribution, metabolism and excretion
AhR	aryl hydrocarbon receptor
AHRR	AhR repressor
ALAS1	aminolevulinic acid synthase
ALDH	aldehyde dehydrogenase
AMPK	adenosine monophosphate -activated protein kinase
APS	ammonium persulphate
ARA9	aryl hydrocarbon receptor-associated 9
ARNT	aryl hydrocarbon receptor nuclear translocator
ATP	adenosine triphosphate
bHLH-PAS	basic helix-loop-helix – period/ARNT/single minded
BMAL1	brain muscle arnt-like protein-1
bp	base pair
BSA	bovine serum albumin
c-	centi
Ca+	calcium
cAMP	cyclic adenosine monophosphate
CAR	constitutive androstane receptor
CCGs	clock-controlled genes
Ccl2	CC-chemokin-ligand-2
cDNA	complementary stranded DNA
CK	casein kinase
CK-MB	creatine kinase MB
CLOCK	circadian locomotor receptor cycles output kaput
cPLA2	phospholipase A2
CRY	cryptochrome
CTL	cytotoxic T lymphocytes
Da	Dalton
DBP	albumin site D-Binding Protein
dd	double destillated
DER	dioxin response elements
DMSO	dimethyl sulfoxide
DNA	deoxyribonucleic acid
DPBS	Dulbecco's phosphate-buffered saline
DTT	dithiothreitol
E-box	enhancer-box
EDC	endocrine disrupting chemicals
EDTA	ethylenediaminetetraacetic acid
EGFR	epidermal growth factor receptor
EPH	epoxide hydrolases
Era	estrogen receptor α
F	fahrrad
FAK	focal adhesion kinase
FGF21	fibroblast growth factor 21
FICZ,	6-formylindolo[3,2-b]carbazole
g	gram
GFP	green fluorescent protein
GLUT	glucose transporter

GSH	glutathione-S-transferases
GSK3β	glycogen synthase kinase 3 beta
h	hour
H_2O	water
hERT	human telomerase reverse transcriptase
HLF	hepatocyte leukemia factor
HME1	human mammary epithelial cell line
HPA	hypothalamus–pituitary–adrenal
HSP90	heat shock protein 90
HSPCs	hematopoietic stem progenitor cells
Hz	herz
I3C	indole-3-carbinol
IDO1	indoleamine 2,3-dioxygenase-1
IL	interleukin
IP	immunoprecipitation
ipRGC	photosensitive retinal ganglion cells
k-	kilo-
KLF6	Krüppel-like factor 6
L	liter
LPS	lipopolysaccharide
LUC	luciferin
M	molar
m	meter
m-	milli
M13SV1	human breast epithelial cells (SV40 immortalized)
mGS	muscle-specific glycogen synthase
min	minutes
mRNA	messeger RNA
MRP	multidrug resistance-associated proteins
n-	nano
NaCl	sodiumchloride
NAS	nicotinamide adenine dinucleotides
NAT	N-acetyltransferases
NC-XRE	non-consensus XRE
NF1L	nuclear factor interleukin
NF-kB	nuclear factor kappa B
NIR	near-infrared
NQO	nicotinamide adenine dinucleotide phosphate (NAD(P)H) quinine oxidoreductases
NR1D1	nuclear receptor subfamily 1, group D, member 1
O_2	oxygen
PARbZip	proline and acidic amino acid rich basic-leucine zipper
PBS	phosphate-buffered saline
PCB	polychloride biphenyls
PCR	polymerase chain reaction
PDK	pyruvate dehydrogenase kinase-4
PER	period
P-gp	p-glycoprotein
PIAS1	protein inhibitor of activated STAT 1
PKC	protein kinase C
POR	P450 oxidoreductase
pp	phosphatase
PPAR	peroxisome proliferator–activated receptors
PXR	pregnane X receptor

REV-ERBa	reverse erythroblastic leukemia viral oncogene homolog alpha
RHT	retinohypothalamic tract
RISC	RNA-induced silencing complex
RNA	ribonucleic acid
ROR	retinoic acid orphan receptor
RORE	retinoic acid orphan receptor element
rpm	revolutions per minute
RT	room temperature
RT-qPCR	real-time quantitative polymerase chain reaction
SCN	suprachiasmatic nucleus
SCR	scrambled
SDS-PAGE	sodium dodecyl sulfate-polyacrylamide gel electrophoresis
sec	second
SENP1	sentrin-specific protease 1
siRNA	small interfering RNA
SIRT	sirtuin
SP1	specificity protein 1
SULT	sulfotransferase
SV40	Simian virus 40
TBS	tris-buffered saline
TBST	tris-buffered saline with tween20
TCDD	2,3,7,8-tetrachlordibenzodioxin
TEF	thyrotroph embryonic factor
TEMED	tetramethylethylenediamine
TGF-b	transforming growth factor-β
TNF	tumor necrosis factor
TNS	trypsin neutralizing solution
TTFL	transcription-translation feedback loops
UGT	uridine 5'-diphospho-glucuronosyltransferase
UGT1A6	uridine 5'-diphospho-glucuronosyltransferase family polypeptide A6
V	volt
VEGF	vascular endothelial growth factors
WHO	World Health Organisation
Wnt	wingless-type MMTV integration site family
XCOX2	cyclooxygenase 2
XRE	xenobiotic response elements
YFP	yellow fluorescent protein
Ω	ohm

1 Introduction

1.1 The circadian rhythm

Earth´s rotation on its axis causes daily environmental changes, e.g. in temperature and light, at any geographical location. Living organisms have evolved a circadian clock that follows a rhythm of approx. 24 h (*circa diem* = approximately one day) and enables the adaptation of physiological and behavioral processes to external daily changes [1, 2].

The French astronomer Jean Jacques d'Ortous de Mairan first scientifically described the circadian rhythm in a plant called *mimosa pudica* in 1729 by placing the plant in darkness and still observing canonical daily leaf movement [3]. Later, Kleitman and Richardson showed that humans also have an endogen circadian rhythm by spending 32 days in a cave with a strict sleeping/ working schedule and the absence of light and noise as well as a constant temperature [4]. Another pioneer of the circadian rhythm, Erwin Bünning, described the genetic basis of the circadian rhythm by studying beans. He proposed that the circadian rhythm in plants is inherited, as plants with intermediate circadian periods were generated by crossing of strains with different periods [5]. These first observations, together with several other studies, first led to approval of the existence of the circadian rhythm and second stimulated research that focused on a better understanding of the mechanism mediating the circadian system [6, 7]. In 2017, three chronobiologists Jeffrey Hall, Michael Rosbash, and Michael Young were awarded with the Nobel Prize for describing the molecular machinery of the circadian rhythm by conducting studies in *Drosophila melanogaster* [8, 9]. Until now, the circadian rhythm has been described in several organisms from cyanobacteria, plants, and flies to mice and humans [10].

The circadian rhythm is characterized by three significant hallmarks that are universal for all species [11]. First, they are self-sustained and not influenced by external environmental cycles, i.e. they maintain their rhythm despite the absence of external stimuli, such as the (natural) dark-light cycle. Therefore, they are also called free-running rhythms [12, 13]. The second characteristic property is the persistence of a period of approx. but not exactly 24 h, which helps the period length to adjust to non-rhythmic changes in the natural environment of the organism, e.g. temperature variation [11, 14]. Last, circadian rhythms can be synchronized by external stimuli, called *zeitgeber*. External stimuli, such as the light-dark cycle, are used as reference points from the circadian rhythm to align with their cues. This property is of crucial importance, as it allows an organism to adapt to the prevailing environmental conditions and is essential for maintaining the health of the organism.

1.2 The circadian system in mammals

1.2.1 The organization of the circadian system: central and peripheral oscillators

The circadian rhythm is generated by cell-autonomous circadian oscillators, i.e. each individual cell has its own molecular circadian rhythm but is part of an interconnected system that ensures a synchronized (uniform) rhythm throughout the organism. Multicellular species, e.g. mammals, form a hierarchical circadian system containing multiple self-sustained oscillators with a pacemaker at the top of the hierarchy setting the rhythm of the peripheral oscillators and enabling clockwork alignment to environmental changes [11, 13].

In mammals, for instance, the SCN (suprachiasmatic nucleus), located at the anterior hypothalamus, serves as the central clock, coordinating the rhythm of downstream tissue such as the liver, lungs, kidney, muscles, abdomen, or heart, the so-called peripheral clocks (Figure 1) [15]. The SCN is not only required to coordinate the phases of the peripheral clocks to not drift apart but also to transmit environmental entrainment signals to light-insensitive tissues. Changes in light intensity are perceived by photosensitive ipRGC (retinal ganglion cells) located within the retina of the eye and forward through the retinohypothalamic tract to the SCN [16, 17]. A series of electrical and biochemical reactions result in the induction of intracellular calcium (Ca^{+}) and cAMP (cyclic adenosine monophosphate) levels, which cause the regulation of genes and a subsequent time-of-day-dependent phase response of the SCN clock. Next, neuronal and endocrine signals transmit the light-dark cycle information from the SCN brain region to non-SCN brain clocks leading to synchronization of the peripheral clock rhythms and adaptation to external environmental stimuli [16, 18, 19]. All in all, the circadian rhythm system consists of a complex SCN/ peripheral tissue network, and gene expression in the peripheral organs is under the control of various indirect factors, like temperature, exercise, feeding/ rest, or endocrine signaling.

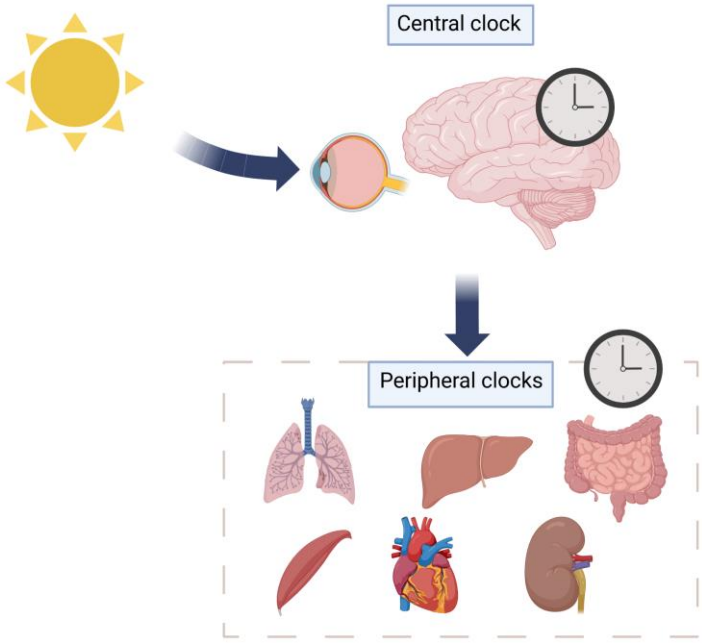

Figure 1: The organization of the mammalian circadian system
The mammalian circadian clocks are organized in a hierarchical manner. The SCN (suprachiasmatic nucleus) serves as the central clock and the pacemaker for the oscillation of the other peripheral clocks, e.g. in the liver, lungs, kidney, muscles, abdomen, and heart. The light signal, as a *zeitgeber*, is sensed by the photosensitive retinal ganglion cells in the eye and transmitted to the SCN through the RHT (retinohypothalamic tract). Then, biochemical signals are released from the SCN to the peripheral clocks, resulting in the alignment of the rhythms between the different organs and with the environmental stimuli, i.e. light-dark cycle, regulating endocrine, and behavioral rhythmicity. The peripheral organs can have differences in the rhythmicity pattern and can also be entrained by rest-activity, feeding-fasting, and (body) temperature cycles. (The illustration was created with BioRender.com).

1.2.2 The molecular mechanism of the mammalian clock

SCN and peripheral clocks have the same core molecular mechanisms that generate and maintain their circadian rhythmicity. This consists of several transcription factors organized in auto-regulatory TTFLs (transcription-translation feedback loops), which drive a self-sustained and intrinsic rhythm of approx. 24 h [20, 21]. Almost up to 43% of all human genes in various tissues are regulated by this mechanism and indirectly control biological and physiological processes in a circadian manner [22–24].

In the positive (activating) site of the TTFLs system, the BMAL1 (brain muscle arnt-like protein-1, also known as ARNTL) and CLOCK (circadian locomotor receptor cycles output kaput) proteins heterodimerize in the cytoplasm and translocate to the nucleus, where the BMAL1:CLOCK complex binds to non-canonical or canonical enhancer (E-box) elements (5′-CACGTG-3′) of CCGs (clock-controlled genes) (Figure 2) [21]. Among others, the heterodimer induces the expression of the clock genes *PER1, PER2* (*period 1 and 2*), and *CRY1, CRY2* (*cryptochrome 1 and 2)*, which form the negative loop (inactivating) of the

TTFLs. PERs and CRYs also form a heterodimer in the cytoplasm and translocate to the nucleus to inhibit the transcriptional activity of the BMAL1:CLOCK complex (Figure 2) [25, 26]. In order to restart the 24 h cycle, PER and CRY undergo post-translational modification, which leads to ubiquitin-dependent degradation and a subsequent reactivation of the BMAL1:CLOCK formation [21, 27]. More specifically, PER can be degraded either by the E3 ubiquitin ligase β-TrCP (also known as F-box/WD repeat-containing protein 1A), after its phosphorylation by the Casein Kinase, CK1δ, CK1ε, and CK2, or through its de-acetylation by SIRT1 (sirtuin 1). These, together with the phosphatases PP1 and PP2, play an important role in the degradation rate or the nuclear translocation of the PER:CRY complex as well as the period length of the clock system (Figure 2) [21, 28–30]. Besides that, the BMAL1:CLOCK complex induces the expression of the nuclear receptor REVERBα (*NR1D1*, nuclear receptor subfamily 1 group D member 1), as well as the RORα (retinoic acid orphan receptor), which together form another feedback loop [26, 31]. In particular, REVERB inhibits and ROR induces the transcription of *BMAL1* by binding to the RORE (retinoic acid receptor-related orphan receptor element) of the *BMAL1* gene promoter (Figure 2) [32].

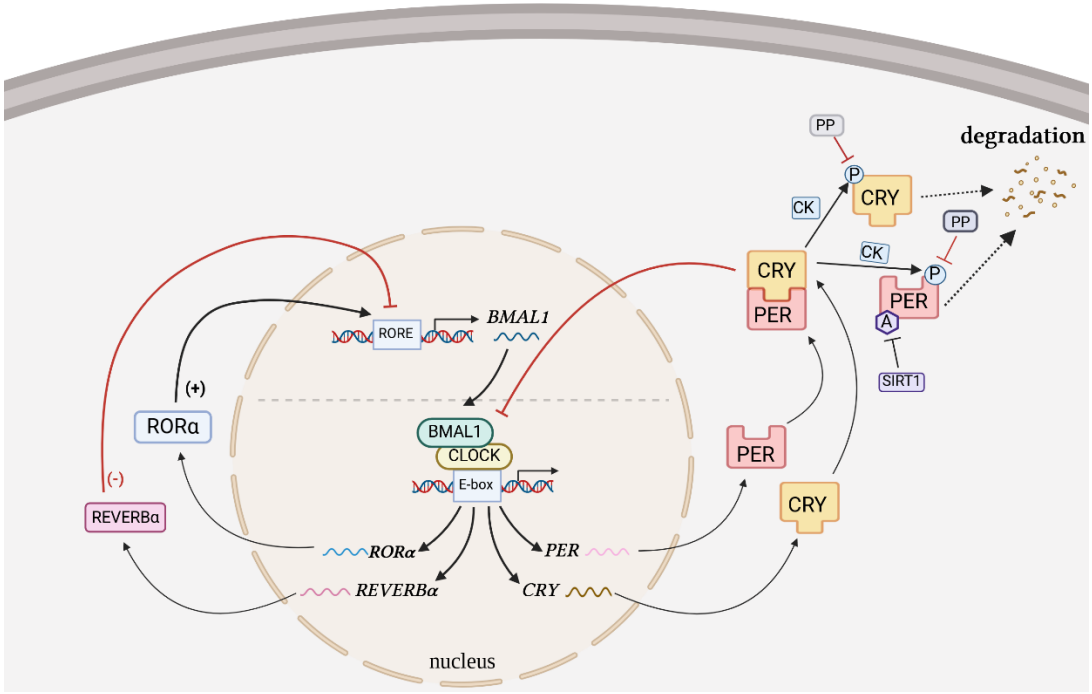

Figure 2: The molecular mechanism of the circadian system
The circadian system is organized at the molecular level in autoregulatory feedback loops. In the first/core loop, BMAL1 and CLOCK form a heterodimer, which activates the expression of CCGs, including C*ry* and P*er*. These two form a heterodimer that inhibits the transcriptional activation of the BMAL1:CLOCK complex. After completing their cycle, CRY and PER are phosphorylated by CKs (casein kinases) to undergo proteasomal degradation. De-acetylation of PER by SIRT1 also promotes its degradation, where PPs (phosphatases) stabilize the CRY:PER complex through dephosphorylation. In the interlocking/ second loop, the BMAL1:CLOCK drives the expression of *RORα* and R*EVERBα.* REVERBα inhibits, whereas RORα induces the expression of *Bmal1* by binding the RORE response element. (The illustration was created with BioRender.com).

While transcriptional regulation is critical for the proper functioning of the TTFL, post-transcriptional and post-translational modifications also play an important role in the regulation of the clock proteins and the maintenance of the circadian rhythm. The stability and activity of circadian rhythms are highly affected by phosphorylation, ubiquitination, acetylation, and sumoylation of clock proteins [33]. Phosphorylation of PER and CRY by CKIε and CKIδ, respectively, as well as ubiquitination by the E3 ubiquitin ligase complex, SCFβ-TrCP, leads to their degradation and maintenance of the circadian rhythm [27, 30, 34]. Besides that, phosphorylation of BMAL1 by the protein kinase GSK3β results in its degradation and maintenance of the canonical circadian rhythmicity. Also, GSK3β phosphorylates REVERBα and represses its transcriptional activity, which induces the expression of *BMAL1* [35, 36]. Further, BMAL1 is acetylated by HAT p300/CBP (CREB-binding protein) promoting its transcriptional activity and supporting the positive feedback loop, as well as deacetylated by the histone deacetylase SIRT1 contributing to the negative feedback loop [37, 38]. Last, BMAL1 is sumoylated by SUMO ligase PIAS1 (protein inhibitor of activated STAT 1), and Per2 is desumoylated by SUMO protease SENP1 (sentrin-specific protease 1) to help together with all other components maintain the circadian rhythmicity of the cell [39–41].

1.3 Circadian regulation of physiological processes

The day-night rhythm influences a plethora of physiological processes, highlighting the importance of maintaining circadian rhythmicity for optimal health and well-being. Besides the sleep-wake cycle, the circadian rhythm orchestrates various processes in the cardiovascular, immune, and endocrine systems, as well as the (xenobiotic) metabolism (schematic overview in Figure 3) [42]. Circadian disruption, i.e. altered light-dark cycles, occurring during shift work, jet lag, or sleeping disorders, compromises the above-mentioned systems and leads to the development of various diseases. In particular, epidemiological studies focusing on shift workers and recent laboratory studies in mice have shown that circadian misalignment increases the risk of developing cardiovascular diseases, obesity, diabetes, and some types of cancer [43, 44]. Next, a more detailed overview of the current knowledge regarding the connection between circadian rhythm and these (patho-) physiological systems will be provided, which is also implemented in the development of potential therapeutic strategies for managing circadian-related disorders.

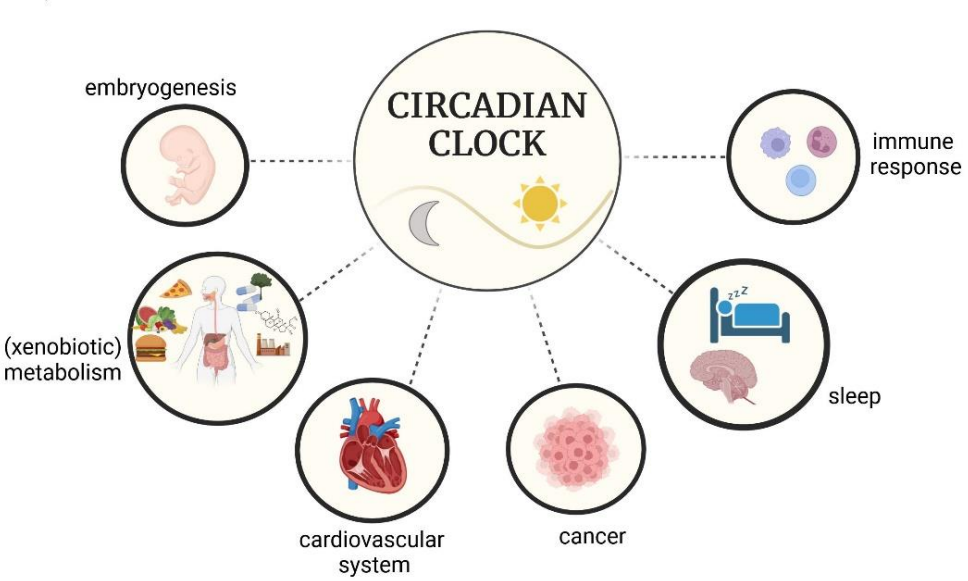

Figure 3: Overview of circadian regulated physiological processes
The circadian clock plays an important role in the proper function of several physiological processes inside the organism and in health maintenance. Besides its association with sleep, it is also involved in embryonic development and immune response via inflammation. The circadian rhythm is linked to tumorigenesis as well as cancer progression and is established as a target for cancer treatment with chemotherapy. Last, the metabolic and cardiovascular systems are also highly affected by the circadian clock, and several diseases in these systems have a higher risk of showing up at a specific time of the day. (The illustration was created with BioRender.com).

The cardiovascular system ensures proper oxygen and nutrient flow to all other organs, and the activity of the heart and the blood flow, i.e. pressure, change depending on different circadian phases. All of the core clock genes are expressed in the heart, and approx. 13% of all genes expressed in it oscillate in a circadian manner [45]. In humans, heart rate, blood pressure, and the platelet or endothelial function show a diurnal rhythm and help the cardiovascular system anticipate changes from the inactive state with low heart rate, sympathetic tone, and high vagal tone to an active state with high heart rate, sympathetic tone, and low vagal tone. This change occurring in the morning indicates that humans are more prone to cardiovascular incidents, such as ischemic strokes, myocardial infarction, arrhythmias, and sudden cardiac death, in the early morning hours. However, it is unclear, whether this pattern is due to behavioral and environmental factors or the endogenous circadian rhythm [46–49]. Clock gene knockout studies in mice have shown that the molecular circadian clock directly regulates diurnal changes in heart rate and blood pressure [46, 50]. Further, it also regulates key enzymes involved in catecholamine synthesis and metabolism that explain the circadian pattern of epinephrine and norepinephrine in human plasma [50, 51]. Human and rodent studies support that circadian disruption by either shift work, sleeping disorders, or environmental changes is highly

associated with heart diseases, e.g. ischemic stroke and myocardial infarction [52–54]. This highlights the need to consider the circadian clock in treating and preventing heart diseases and understand more about its role in physiology and pathophysiology for the benefit of patients with cardiovascular diseases.

Several parameters of the immune system exhibit a circadian rhythm, such as the number of hematopoietic cells, the blood levels of hormones, or the cytokines. Among others, the levels of adrenalin, noradrenaline, glucocorticoids, the pro-inflammatory cytokine TNF (tumor necrosis factor), and IL-1β (interleukin-1β) peak at the beginning of the active phase [55, 56]. In contrast, the amounts of HSPCs (hematopoietic stem progenitor cells) and several mature leukocytes peak at the resting phase, at which they are released from the bone marrow into the bloodstream [56–58]. In this context, the circadian clock can fine-tune the amplitude and duration of immune responses, ensuring optimal function of the defense mechanisms and maintenance of immunosurveillance. Disruption of the circadian rhythm affects the immune system by disturbing the balance between anti- and pro-inflammatory mechanisms, which can lead to a pro inflammatory microenvironment and inflammatory chronic diseases. Indeed, humans working in shifts or often subjected to jet lag can be more sensitive to infection from pathogens, including the cold, flu, and COVID-19 viruses, as well as potentially cope less effectively with tissue injury [59–61]. In summary, disruption of the light-dark cycle affects the proper function of the immune cells by dysregulating their transport and production, as well as compromises the immune surveillance of the organism by shifting it to a pro-inflammatory state, which can lead to chronic inflammation and promote tumorigenesis.

The circadian clock is affected by food consumption and is directly or indirectly connected with various metabolic processes, including carbohydrate, lipid, protein, and NAD^+ metabolism. Food is considered an external *zeitgeber* for peripheral clocks, and a misalignment between food uptake and the resting/ active phase could lead to several negative health outcomes and metabolic disorders [62, 63]. Indeed, high-fat diet studies in mice have shown that animals with impaired clock genes, such as PER2 or CLOCK, gain more easily weight and are more prone to developing metabolic diseases [64–66]. Further, rodent and human studies have proven that unregular eating habits shift the phase of certain circadian rhythms, indicating that a non-canonical feeding schedule is a possible circadian disruptor, leading to an increased risk for obesity, type 2 diabetes, high blood pressure, and hyperlipidemia [63, 67–69]. On the other hand, glucose metabolism follows a circadian pattern, which is influenced by factors like increased physical activity and food consumption during the day. Circadian regulation affects glycogen levels by modulating the balance between glycogenesis and glycose consumption through rhythmic enzyme

expression [70]. Insulin, crucial for blood glucose homeostasis, exhibits a daily oscillation overlaid by a distinct increase after food consumption. It has been reported that its canonical secretion can be impaired by circadian disruption, causing hypoinsulinemia [71, 72]. Interestingly, patients with type 2 diabetes maintain their insulin sensitivity, but the circadian oscillation of insulin secretion is impaired [73]. Last, metabolic processes or components such as the equilibrium of the NAD(P)H/ $NAD(P)^+$ (nicotinamide adenine dinucleotides) redox reaction, the AMPK (AMP-activated protein kinase), which senses low energy and nutrients, and SIRT1, regulating transcriptional silencing, genome stability, longevity, and stress resistance during caloric restriction, are tightly connected with clock control genes [74–76]. All in all, time-restricted eating as well as better understanding of the mechanistic link between circadian misalignment and metabolic dysregulation may help in the development of novel medical regimes to prevent or intervene in the metabolic consequences of a circadian disruption and vice versa [72, 77, 78].

1.3.1 Crosstalk between circadian rhythms and endocrine system

The endocrine system plays an important role in the distribution of circadian rhythmicity within the organisms. It enables communication between the central and peripheral clocks and thus facilitates adaptation to environmental changes. Circadian rhythms have been described in all endocrine organs of mammals, e.g. pituitary, adrenal, and pineal glands, pancreas, liver, and adipose tissue [79, 80]. Various hormones, such as prolactin, melatonin, and nutrient-sensitive hormones, such as insulin and adipokines, as well as glucocorticoids and thyroid, growth, or sex hormones, show a diurnal oscillation. In addition, they respond to *zeitgebers*, e.g. food and light, and transmit circadian cues between the different clock tissues [79, 81]. More specifically, melatonin production is directly regulated by the light signal reaching the SCN and subsequently acts as an internal *zeitgeber* [82]. Indeed, studies in rodents have shown that melatonin can induce circadian oscillation of the clock components PER1, BMAL1, CLOCK, and CRY, as well as studies in blind subjects have shown that ectopic administration of melatonin can entrain or phase shift the circadian clock [83–85]. Further melatonin is produced less in the daylight and increases during the night to induce sleep. The connection of melatonin with sleep promotion is debatable, as in nocturnal animals, it is still peaking at night when the animals are active, and it is decreasing in the morning when the animals normally fall asleep [86]. However, administration of a melatonin agonist to patients with insomnia reduces sleeping latency and promotes sleep. Besides that, melatonin also affects blood pressure, and alterations in proper melatonin production are linked with an increased risk of breast and colorectal cancer, sleeping disorders, and metabolic diseases [87, 88]. On the other hand, cortisol, as a glucocorticoid,

is characterized by a circadian rhythm that peaks at the end of the sleeping phase, preparing the body to be energetic for the active phase. This peaking is related to the time of awaking and is not light-dependent, meaning that nocturnal animals, e.g. mice and rats, have the peak in the evening and humans in the morning [89, 90]. Cortisol is produced after the release of a series of hormones belonging to the adrenal gland of the HPA (hypothalamus pituitary adrenal) axis. It is essential for many biological processes, such as stress release, fat and protein metabolism, cardiovascular function, and inflammatory response, as well as for the regulation of the circadian expression of clock genes. Besides that, cortisol also acts as a *zeitgeber* of the circadian system [90–92]. Last, not only insulin displays circadian rhythmicity but also its sensitizer adiponectin, which exhibits a circadian oscillation with peeking in the middle of the active phase to promote increased insulin levels later in the day.

EAS (endocrine active substances), which interact or interfere with normal hormonal function, or EDS (endocrine disrupting substances) that are EAS leading to an adverse effect are linked to circadian rhythms. As already described before, the endocrine system is tightly connected with the circadian rhythms, indicating that circadian disruption could lead to several endocrine pathologies. Also, EDCs could potentially induce circadian disruption and cause related reproductive, neuroendocrine, cardiovascular, and metabolic health issues, or increase the risk for cancer [80] [93]. The connection between EDCs and circadian disruption is already described, but the mechanistic background is still undiscovered [94]. For example, Zhang *et al.* described the effect of cadmium on circadian clock genes and thyroid cancer [95], and Bahougne *et al.* showed that in rats, impaired luteinizing hormone, which is important for follicle development and also functions as a *zeitgeber* in gonads, increases abnormal pregnancies and reduces fertility upon shift work conditions [96]. Further, several studies across different organisms, especially aquatic ones, showed that EDCs interfere with the proper clock gene expression and function in the HPG (L) axis [80, 97]. In addition, EDCs bind to nuclear receptors that are circadian regulated, such as ROR α/β/γ and PPARs [80, 98], and several estrogen and androgen receptors seem to underlie circadian regulation. Indeed, the PR (progesterone receptor) is tightly connected with PER1 in initiating and maintaining endometrial decidualization [99], and ERα (estrogen receptor α) signaling is linked to PER2 disruption in breast cancer [100, 101]. Moreover, the connection between estrogen signaling and circadian rhythm described in shift-work-mediated hormone-related tumorigenesis or progression remains debatable, as the systematic review by Salamanca Fernandez *et al.* showed only a correlation of 62.5% between breast or prostate cancer and circadian disruption [102]. The rhythmic expression of these nuclear receptors in correlation with the EDC action, as well as its mechanism,

need to be further studied, as it could have a major impact on disease treatment and risk assessment. This would also help to identify potential pollutants or pharmaceuticals that have both EDCs and circadian disruption properties, preventing circadian and endocrine related diseases. All in all, it is very important to understand the crosstalk between circadian rhythms and the endocrine system, as both have a major impact on keeping the human body in a healthy balance.

1.3.2 Circadian regulation of xenobiotic metabolism

Besides the utilization of natural substances, metabolism and detoxification from xenobiotics (i.e. external synthetic chemical substances) are similarly important. Humans are in contact with a variety of xenobiotic substances, e.g. drugs, pesticides, chemicals in food, preservatives, or environmental contaminants. The organism, especially the liver, is able to metabolize and excrete some of those substances in order to preserve healthy conditions [103]. Importantly, several enzymes involved in xenobiotic metabolism display a circadian pattern, indicating that the daily detoxification in the organism, especially in the liver and the intestine, is under the circadian influence [104, 105]. It is reasonable that the xenobiotic metabolism is circadian regulated, as during the daytime the contact with contaminants (e.g. through food consumption) is more prominent [106]. Besides that, the xenobiotic metabolism pathways should be taken into consideration at drug administration during disease treatment in order to achieve the highest efficacy and avoid side effects [107]. Indeed, chronopharmacology and chronopharmacokinetics, which specialize in the time-dependent physiological response to drugs, are widely accepted in clinical medicine, and the time-dependent drug administration is highly considered in the principle of ADME (absorption, distribution, metabolism, and excretion) [108]. However, in the field of toxicology, time-dependency in risk assessment is rather neglected, and toxicity test systems lack the implementation of the circadian clock, even though it apparently influences many toxicological relevant pathways and overall xenobiotic metabolism [109].

The xenobiotic metabolism is divided into three phases: In phase I, xenobiotics are introduced to reactive groups; in phase II, they are conjugated into polar compounds; and in phase III, they are further processed to be recognized by transporters operating the excretion of compounds from the cells. Each of the phases involves proteins with characteristic detoxification functions and several of them are circadian regulated [103, 110]. More in detail, the phase I group is characterized by microsomal P450 cytochrome super-family enzymes with oxidase, reductase, or hydroxylase activities. Several cytochrome P450 enzymes are regulated by clock genes and display a circadian rhythm. For example, in the mouse liver, *CYP2C19* and *CYP3A4* are regulated by DBP and BMAL1,

respectively [111], and *CYP2A4* and *CYP2A5* exhibit a circadian expression pattern [112]. Further, in human liver cells, CYP1A1, CYP2B6, and CYP3A4 are linked to the circadian clock [113]. Phase II involves conjugating enzymes, i.e. they alter lipophilic compounds into more hydrophilic ones. Among those are SULTs (sulfotransferases), UGTs (UDP-glucuronotransferases), NQOs (NAD(P)H quinine oxidoreductases), EPHs (epoxide hydrolases), GSHs (glutathione-S-transferases), and NATs (N-acetyltransferases). Indeed, in mice liver, each of these families incorporates circadian expressed proteins, such as Sult1a1 (regulated by BMAL1), GST-α1, or Ugt2b (regulated by REVERBα) [114–116]. Last, the role of the phase III group is to transport the hydrophilic compounds generated by the phase II enzymes for excretion via bile, feces or urine. This group involves proteins such as the MRP (multidrug resistance-associated protein) and the P-gp (p-glycoprotein). The last is well described to have a diurnal expression in the intestine and is under the control of BMAL1, which suppresses *E4bp4* (negative regulator of P-gp) and activates *Hlg* (positive regulator of P-gp) [117, 118]. Last, not included in any of the groups mentioned before but highly involved in the circadian regulation of Phase I enzymes (e.g. P450 enzymes), are the ALAS1 (aminolevulinic acid synthase) and the POR (P450 oxidoreductase) [119–123].

The transcription and activation of the proteins involved in xenobiotic metabolism are regulated by so-called xenobiotic receptors. The most important receptors are CAR (constitutive androstane receptor), PXR (pregnane X receptor), and the dioxin receptor AhR (aryl hydrocarbon receptor). Upon xenobiotic response, these receptors translocate into the nucleus, where they activate the transcription of phase I, II, and III genes [124]. CAR is an important regulator of CYP2b10, which seems to be robustly circadian expressed. Indeed, the CAR expression is modulated by PARbZip (proline and acidic amino acid-rich basic-leucine zipper) transcription factors, such as DBP (albumin site D-Binding Protein), TEF (thyrotroph embryonic factor), and HLF (hepatocyte leukemia factor). These are directly circadian regulated by the circadian core clock genes and bind as homo- or heterodimers, DNA elements of the consensus sequence 5′-VTTAYGTAAY-3′ (where V is C, G or A, and Y is C or T) [123, 125, 126]. Besides that, PARbZib proteins bind in a circadian manner at the promoter of ALAS1 and POR, mediating circadian expression of cytochrome P450 enzymes [127, 128]. Interestingly, the PARbZip proteins display no feedback-regulating-effect on the clock core genes. AhR and his dimerization partner ARNT (aryl hydrocarbon receptor nuclear translocator), which will be discussed in detail in the next chapter, are circadian expressed in several organs, including the liver [129, 130]. Interestingly, the CYP1A1 expression, an indirect measurement of AhR activation, also displays a circadian rhythmicity in several tissues in support of a circadian activation of the receptor [131, 132]. All in all, the xenobiotic metabolism seems highly circadian regulated, highlighting the

importance of acknowledging daytime-dependence in drug development and toxicity testing.

1.4 The Aryl hydrocarbon Receptor (AhR)

Living organisms are exposed every day to many chemicals via air, water, or food that can pose a potential health risk if not quickly eliminated from the body. Various enzymes and transporters metabolize and eliminate these potentially dangerous compounds. The detection and detoxification of such chemicals are mediated by xenobiotic receptors, which serve as transcription factors. One of the highly toxicological relevant receptors is the AhR (aryl hydrocarbon receptor), which not only has a function in xenobiotic metabolism, but is also recognized for its role in cell proliferation, adhesion, cell migration, and biological processes, e.g. cardiovascular function, immune system, embryonic development, metabolism, and cancer development [133–135].

Figure 4 shows a schematic overview of the two-dimensional structure of AhR and ARNT. AhR belongs to the bHLH-PAS family (basic helix-loop-helix – period/ ARNT/ single minded) and contains three important domains: the bHLH domain; the PAS domain, which is divided into two structural repeats, A and B; and a C-terminal domain, which contains three subdomains [136]. The bHLH domain enables the dimerization with ARNT, the binding of DNA, the interaction with chaperones such as HSP90 (heat shock protein 90), and the nuclear import and export of AhR. PAS domain A enables AhR to dimerize with ARNT and domain B to bind with ligands. The three subdomains of the C-terminal are enriched with acidic residues (glutamate or aspartate), glutamine (Q-rich), and serine, threonine, proline, respectively. These allow the interaction of AhR with co-activators and co-repressors [137–140]. ARNT has a similar structure to AhR, but it lacks two subdomains in the C-terminal, and despite containing a PAS B domain, it is not able to bind ligands [137, 140, 141].

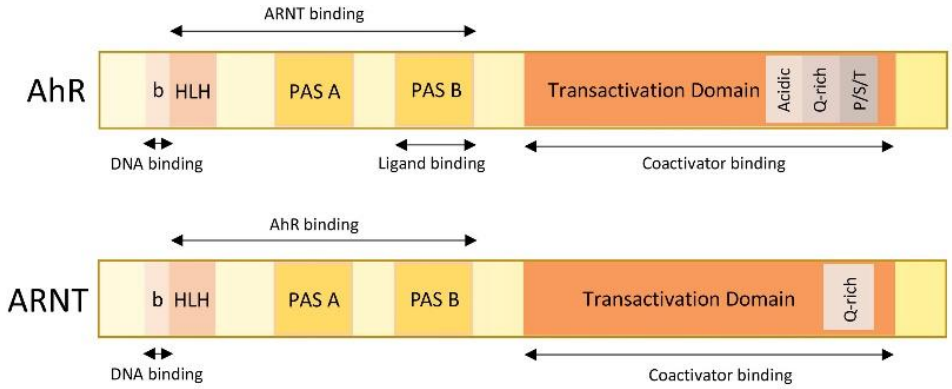

Figure 4: Functional domains of AhR and ARNT
Two-dimensional structure of AhR and ARNT. The bHLH, PAS A, and PAS B domains enable the interaction between AhR and ARNT, and specifically, the bHLH enables their binding to DNA. AhR, in comparison to ARNT, can bind to different ligands via the PAS B domain. The transactivation domain allows binding to other cofactors and corepressors. (Figure adapted from Larigot *et al.* [137]).

1.4.1 Canonical AhR signaling pathway

In the past years, numerous endogenous and exogenous AhR ligands from different sources have been identified. Among others are the endogenous metabolites of tryptophan, I3C (indole-3-carbinol) in broccoli or coffee, and dioxins or PCB (polychloride biphenyls) as environmental pollutants that pose a high risk to human health [142–146]. Indeed, high doses of dioxins in industrial accidents can cause chloracne, and long-term exposure can cause neurodamage, thyroid malfunction, or impaired steroid hormone function [147, 148]. Dioxins and PCB have been classified as group 1 and group 2A carcinogens, respectively, by the IARC (International Agency for Research on Cancer) [149]. This example, among many others, suggests that various AhR ligands are involved in disease development, such as cancer, neurodevelopmental abnormalities, cardiovascular malfunction, and embryonic development, making the AhR signaling pathway an interesting tool to understand xenobiotic-dependent diseases and to be used in favor of developing new testing strategies, such as a more sensitive *in vitro* test system, specifically laid out on the AhR pathway and its ligands [150].

Based on ligand binding, different pathways can be activated by AhR, with the genomic pathway described in Figure 5 being the most well-known and well characterized. In the absence of a bound agonist, AhR is located in the cytoplasm, forming a complex with HSP90, p23 (also known as PTGS3), and AIP (aryl hydrocarbon receptor-interacting protein, also known as ARA9 and XAP2) [151–153]. HSP90 prevents AhR from translocating into the nucleus and enables binding with different ligands, whereas p23 stabilizes the AhR-HSP90 interaction [151, 154]. Indeed, p23 mediates the transport of AhR into the nucleus by enhancing the ability of the receptor to recognize import protein β [155].

Moreover, Chan *et al.* showed that p23 protects AhR from ubiquitin-mediated protein degradation and proposed that AhR is phosphorylated by GSK3β in a p23-dependent manner. This p23/ GSK3β-mediated phosphorylation is required for proper AhR target gene transcription and drives AhR rather to lysosomal than autophagosomal degradation [156, 157]. In contrast, AIP facilitates proper AhR folding in the cytoplasm and consequently enhances AhR signaling. Once hydrophobic ligands, such as the dioxin TCDD, diffuse through the cell membrane, they bind to cytosolic AhR, change its conformation, and cause AhR translocation into the nucleus [158]. Hence, AhR forms a complex with its heterodimeric partner, ARNT, binds to dioxin response elements (DREs) or xenobiotic response elements (XREs) within the genome with the common DNA consensus motif 5'-TNGCGTG-3', and initiates the expression of target genes [137, 159]. Among these genes are xenobiotic metabolizing enzymes, such as the cytochromes P450 CYP1A1, CYP1A2, CYP1B1, the UGT1A6 (UDP glucuronosyltransferase 1 family polypeptide A6), or aldehyde dehydrogenase family members, e.g. ALDH3A1 [159, 160]. Moreover, the AHRR (Aryl Hydrocarbon Receptor Repressor) is also an AhR target gene that represses AhR activity by binding to the ARNT:XRE complex as an antagonist to the AhR:ARNT:XRE complex [161]. This negative regulatory loop, together with the degradation of AhR by the ubiquitin-proteasome pathway prevents overstimulation of the pathway by agonists [137, 153].

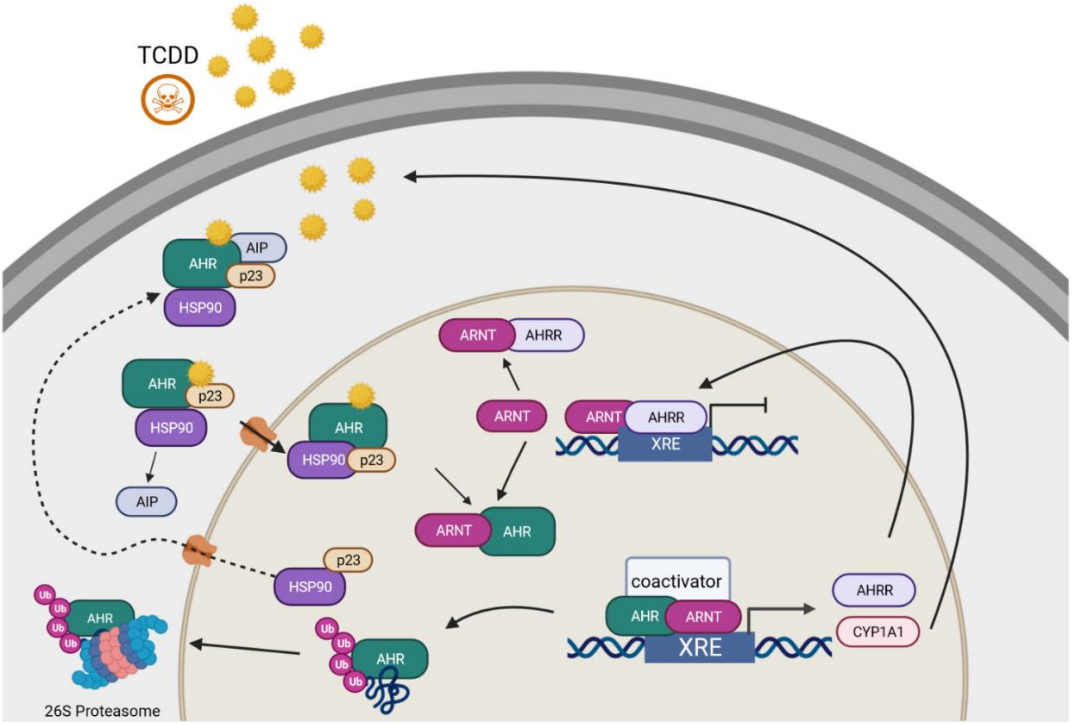

Figure 5: The genomic AhR signaling
In the cytosol, AhR stays inactive in a complex with HSP90 (heat shock protein 90), p23, and AIP (aryl hydrocarbon receptor-interacting protein). Once an AhR ligand, such as TCDD, passes the extracellular membrane, AhR is translocated to the nucleus. There, it dimerizes with ARNT (aryl hydrocarbon nuclear translocator), binds to XRE (xenobiotic response elements) within the genome and transactivates with the help of other coactivators the expression of target genes, such as *CYP1A1* and *ALDH3A1*, which are important for metabolizing the AhR ligands and detoxification. AHRR (AhR repressor) is also an AhR target gene and once translated, it binds with ARNT on the XREs antagonizing the AhR/ ARNT binding to inhibit AhR target gene expression. AhR undergoes ubiquitination and proteasomal degradation in the cytoplasm after activating the expression of target genes. (The illustration was created with BioRender.com).

1.4.2 Non-canonical/ -genomic AhR signaling pathways

Besides the AhR canonical genomic pathway, several non-canonical AhR signaling pathways have been described in the past years. For example, TCDD-mediated AhR activation triggers the activation of EGFR (Epidermal Growth Factor Receptor), which is a receptor tyrosine kinase and is involved in cellular processes such as proliferation, differentiation, and apoptosis. More in detail, after AhR activation, a part of the SRC complex activates, via EGFR, the FAK (focal adhesion kinase), which disrupts focal adhesion points, as well as activates MAP kinases leading to transcription of COX2 (cyclooxygenase 2) and induced cell proliferation. In addition, TCDD increases intracellular calcium that activates PKCa (protein kinase C a) and the synthesis of arachidonic acid, via phosphorylation of cPLA2 (phospholipase A2) [162–164]. Finally, arachidonic acid is used by COX2 to produce prostaglandin and cause inflammation [165, 166]. On the other hand, AhR can also bind with other factors besides ARNT, such as ERα (estrogen receptor α), KLF6 (Krüppel-like factor 6), or transcription factors of the NF-κB (nuclear factor kappa B) family (e.g. RelB)

[167, 168]. The AhR/ KLF6 heterodimer recognizes novel NC-XRE (non-consensus XRE) and regulates genes that are involved in the cell cycle [168]. Interestingly, AhR can form a heterodimer with a subunit of NF-kB (ReIB) regulating chemokines and cytokines expression that leads to a decreased binding with ARNT and expression of *CYP1A1* [166, 167, 169]. Lately, the crosstalk between the AhR and Wnt pathways has been intensively discussed. Dioxin-mediated AhR activation has been described to interact with the Wnt/ β-catenin pathway in the liver [170, 171]. Studies have shown that AhR and β-catenin are cooperating in the induction of AhR transcription target genes such as *CYP1A1*, and AhR activation leads to downregulation of several Wnt/ β-catenin target genes, causing alteration in cell adhesion, E-cadherin-mediated cell-cell junctions, and G1-S transition of liver progenitor cell lines [167, 171]. Last, AhR can act as an E3 ubiquitin ligase, inducing the proteasomal degradation of target proteins such as p53, MYC, FOS, OCT4, and HIF1α, This competes again with ARNT availability, its binding to AhR, and the activation of AhR-mediated transcription [172].

1.5 AhR regulation of biological processes

The first studies on AhR signaling focused on its toxicological relevance because it is mainly involved in xenobiotic metabolism, especially in the metabolization of environmental pollutants. Since then, it has been highlighted that AhR is involved in many other biological processes and has become an interesting target for new therapeutic approaches, such as applying specific AhR inhibitors to restore immune response and suppress tumor progression, as well as using AhR ligands (e.g. tryptophan) for topical treatment to enhance wound healing [173, 174]. Indeed, AhR has been linked to a plethora of ligands and to numerous physiological functions of the cardiovascular, immune, gastrointestinal, epidermal, and circadian system [130, 133, 175–178].

AhR could potentially be a perfect therapeutic target for obesity as it is tightly associated with energy metabolism by regulating several genes involved in lipid metabolism, adipogenesis, and glucose homeostasis [175]. In addition, it could also be a target for cardiovascular diseases as it is linked to cardiovascular physiology and cardiovascular diseases (e.g. thrombosis and atherosclerosis). AhR regulates fatty acid and cholesterol synthesis, playing an important role in glucose homeostasis, insulin resistance, and diabetes development [179–181]. Moreover, Tischkau *et al.* and Girer *et al.* reported that AhR affects energy balance through FGF21 (fibroblast growth factor 21), which plays a crucial role in sweet taste preference, regulation of energy metabolism via the nervous system, and weight loss. Besides that, AhR is activated by ligands produced by the gut microbiota and vice versa [182, 183]. Thus, AhR could be target to restore gut immunity

and prevent the progression of diseases, such as colitis, as well as modulate host metabolic processes (e.g. fatty acid and glucose metabolism) [184]. On the other hand, studies using *AhR* knockout mice have shown the important role of AhR in cardiac morphogenesis, angiogenesis, and vascular remodeling [185, 186]. Last, AhR activation modulates vascular function by impacting endothelial cells and is implicated in lipid metabolism and inflammation by accumulating lipids and immune cells in the arteria walls [175].

Looking into the immune system, AhR has been implicated in the regulation of T cell, B cell, and natural killer cell development and differentiation [187]. Further, AhR activation initiates expression of the pro-inflammatory IL-6 (interleukin-6) or STAT3, which also play a key role in the expression of IDO-1 (indoleamine 2,3-dioxygenase-1). At the same time, IDO-1 converts tryptophan into kynurenine, which is an AhR ligand, creating a IDO1-AhR-IL-6-STAT3 signaling loop [188, 189]. Further, AhR regulates pathogen defense, immunosuppression, immune tolerance, and autoimmunity via modulation of pro-inflammatory cytokines and chemokines. From a cancer point of view, AhR activation has been shown to enhance anti-tumor immune responses by promoting the activation and function of immune cells, such as natural killer cells and cytotoxic T lymphocytes (CTLs) [185, 187, 190]. Taken together, AhR is involved in several important processes and is considered a promising target to treat various diseases. However, most of the studies are conducted in mice, highlighting the importance of performing additional studies in a more human related system to fully understand the mechanism and role of AhR in human physiology.

1.6 Circadian rhythm meets AhR signaling in physiological processes

The circadian rhythm and AhR signaling affect numerous similar processes in an organism, indicating a physiological crosstalk between them to ensure health maintenance. The circadian rhythm organizes cellular processes from sleep-wake cycles until metabolic functions to align with the 24-h rotation of the Earth. Also, it is affected by external environmental changes (e.g. light and temperature) or other *zeitgebers* such as food intake and hormones. In parallel, AhR emerges as a key regulator in cellular responses to endogenous and exogenous signals, which are also under circadian influence. Thus, AhR signaling and circadian rhythms probably cooperate to fine-tune the proper function of these and allow time-sensitive molecular processes to interconnect with environmental cues [121, 191]. The interaction of AhR signaling and circadian rhythm is reciprocal, which means that activation of AhR can change the expression of circadian clock genes and inhibit molecular

rhythms, and vice versa, alteration of the circadian clock can affect AhR signaling and the sensitivity to AhR agonist and AhR target genes [130, 191, 192]. This may indicate that disturbance in this interplay, either by circadian disruption or impairment of the AhR signaling pathway could possibly lead to a higher risk of disease, such as obesity, cardiovascular diseases, or malfunction of the immune system, as well as a higher risk of environmental hazards [129, 193].

Several studies indicate a direct interaction between AhR and the clock machinery, but the actual mechanism behind this interplay is poorly understood [131, 132]. Interestingly, the master regulators of the circadian rhythm, BMAL1, PER, and CLOCK, belong to the same bHLH/ PAS domain protein family as AhR and ARNT. This similarity indicates an interaction between the circadian clock proteins and the AhR or its regulators [191, 194]. For example, BMAL1 shows a 44.3% homology to ARNT, implying physical interaction between AhR and BMAL1 [195]. However, a direct interaction between AhR and BMAL1 remains controversial, and more studies have to be conducted in different tissues to get a clear answer. Two hybrid system studies show no interaction between these two candidates. In contrast, data derived from mouse cells (Hep1c1c7) indicate the formation of a complex between AhR and BMAL1, which competes with the BMAL1/ CLOCK complex for binding to the E-Box of the *Per1* promoter [193, 196]. Moreover, studying the effect of AhR ligands on the circadian clock system revealed in mice that ligands derivate from food consumption such as tryptophan, indole metabolites, and flavonoids activate the AhR pathway and subsequently might suppress BMAL1/ CLOCK-mediated transcription, as the circadian oscillation of metabolites, e.g. insulin and glucose, was altered [197]. Further, FICZ, a high affinity AhR ligand and photoproduct of tryptophan, alters the expression of clock genes and inhibits the glutamate-induced phase shifting in the SCN of mice, affecting also peripheral clocks, e.g. the liver [198]. Besides that, studies argue about the effect of TCDD-mediated AhR activation on circadian synchrony. Several studies show that TCDD alters the clock machinery in the SCN, ovary, liver, and bone marrow of mice, which is important in locomotor activity, feeding, and serum hormone homeostasis [192, 199, 200]. However, Pendergast and Yamazaki *et al*. showed that TCDD does not affect the circadian rhythmicity of the SCN and peripheral tissue by using a PER2::luciferase mice system, as well as Ndikung *et al.* showed that TCDD has no influence on the circadian expression of clock genes, e.g. *BMAL1* and *PER2*, in the breast [201–203]. Last, AhR has only an effect on the circadian clock machinery when it is activated by an exogenous agonist [203].

On the other hand, the circadian expression (mRNA or protein) of AhR varies between tissues. In rodent liver, lungs, and thymus, AhR and ARNT proteins are expressed in a diurnal pattern compared to the spleen, where the protein levels remain stable for 24 h.

Similarly, the expression of *AhR* mRNA exhibits a circadian oscillation in rodent hepatocytes and the SCN, but for example, not in human breast epithelial cells [131, 204, 205]. Moreover, AhR transcripts and their sensitivity to agonists, such as TCDD, are rhythmic in several tissues. More specific, data from mouse liver and mammary glands showed that activation of AhR (e.g. by TCDD exposure) enhances the amplitude of *CYP1A1* during the night compared to the daytime because of PER1 and PER2 regulation [206]. Also, studies in *CLOCK* mutant mice showed that the expression of *AhR* mRNA was lower and non-circadian regulated compared to the wild-type, as well as benzo[α]pyrene-induced *CYP1A1* expression was modulated by CLOCK via AhR [132]. Looking into *in vitro* data, studies using synchronized cells to oscillate in the same phase revealed a circadian oscillation with a 24 h periodicity of AhR target genes, such as *CYP3A4* and *CYP1A1* in hepatic and breast epithelial cells, respectively. More specifically, heat shock-synchronized HepG2 cells revealed a DBP-mediated circadian transcription of *CYP3A4* in the daytime and a NF1L (nuclear factor interleukin 3 or E4BP4)-dependent circadian suppression of CYP3A4 during the rest of the day [207]. Similar, Ndikung *et al.* showed in breast epithelial hTERT-HME1 cells, an AhR-mediated circadian oscillation of *CYP1A1*, with the *AhR* expression itself staying constant over time [201]. In general, AhR target genes like *CYPs* are induced by ligand-mediated AhR activation regardless of the time of day, but the responsiveness depends on the phase of the circadian synchrony. Collectively, all studies indicate that depending on the tissue and the species, AhR signaling and the circadian clock work together to maintain the proper function of biological processes and regulate the homeostatic function of peripheral and central clocks. Thus, the elucidation of the unknown molecular mechanisms underlying the functional interactions between these two should be highest priority.

1.7 Relevance of AhR and circadian rhythms in disease treatment, drug development, and toxicology

The circadian clock controlled drug metabolism plays an important role in the pharmacokinetics of drugs and their efficiency [208]. In addition, AhR signaling, as an important detoxification pathway and displaying a time-dependent response to binding ligands, is of highest interest for the pharmacological and toxicological fields. Indeed, AhR signaling is one of the most toxicological relevant pathways and is often integrated in drug development or disease treatment, as well as in the generation of new test systems and risk assessment [209, 210]. Because of its circadian regulation, it is important to integrate the circadian aspect to not only drug development and treatment, which is already quite

established, but also in toxicology and the development of new test systems for risk and hazard assessment.

Several pharmaceuticals, especially anticancer drugs, such as 5-FU, etoposide, doxorubicine, vinca alkaloids, and cisplatin, exhibit a circadian effect in pharmacokinetics and a day-time-dependent mode of action [211–214]. Chronotherapy, i.e. time-of-day-dependent treatment, makes obvious sense in diseases that exhibit day-time-dependent variation in the symptoms, such as in heart failure diseases or bronchial asthma, but it is also applied in the treatment of diseases such as cancer [215]. In cancer treatment with chemotherapy, the chemotherapeutics must be dosed high enough to kill the cancer cells, but the concentration should also be low enough to prevent damage in healthy cells and tissues. This indicates that pharmacokinetics and dynamics can only operate in a small window to achieve successful treatment [214, 216]. Considering that drug metabolism is highly circadian regulated, drug efficacy can change during the course of the day, which makes chronotherapeutic strategies particularly important [217–219]. AhR signaling is described as having both pro- and anti-tumorigenic activities. Thus, together with being activated by several different ligands, it is often targeted in cancer treatment [220]. With AhR also being circadian regulated, it is even more important to consider day-time-dependent treatment, as its activity and response are altered not only according to the ligand but also to the time of the day or the chronotype of the patient. With chronotype is meant the “phase of entrainment” of each individual, as the behavioral and physiological rhythms can range from an early (morning larks) to a late (night owls) type or somewhere in between. A simple estimation of the internal circadian time of an individual, for example through blood or saliva samples, would allow a more customized and probably more successful therapy [221, 222]. Combining AhR target therapy with chronotherapy as well as fully understanding its regulatory mechanism and the circadian influence, could achieve an even more accurate and successful treatment for diseases, such as cancer, or other AhR-linked diseases [105, 208]. All in all, AhR targeting in cancer treatment is a good example, of why parameters such as mechanism of action, metabolism, and toxicity in cooperation with circadian rhythmicity should be taken into consideration while planning treatment strategies or drug development.

Looking into the field of toxicology, the implementation of the circadian clock in identifying potential hazards and risk assessment is rather neglected, even though there is evidence supporting that the time of the day at which an organism comes in contact with a xenobiotic leads to differences in the reaction sensitivity [223–225]. This is supported by studies, particularly in rodents, which show a circadian oscillation of xenobiotic metabolizing enzymes, like the CYPs [112, 226]. Another study in humans showed that cleaning products

could be more efficiently metabolized by CYPs during the daytime than at night [227, 228]. Additionally, xenobiotics can alter the circadian rhythmicity of an organism, implying circadian disruption as part of compound toxicity and a toxicological endpoint that needs more consideration in risk assessment. The identification of circadian disruptors, including endocrine active substances, and their effect on disease development and progression would improve the toxicological assessment of environmental and industrial chemicals and pharmaceutical drugs [109].

There is an ongoing challenge to level up toxicological relevant *in vitro* test systems to mimic the *in vivo* situation as well as remain uncomplicated, cheap, and quick in analysis to prevent toxicity and health harm caused by specific compounds. An easy way to improve these systems is by implicating the circadian rhythm, for example, by synchronizing the cells to oscillate in a uniform circadian phase. This would not only improve the significance of toxicological test systems but could also be used in drug development to find the optimal treatment window [109]. Three studies focusing on AhR signaling show that restoration of circadian synchrony enhances the cell response to specific xenobiotic compounds [201, 229, 230]. More in detail, studies in rodents show that benzo[a]pyrene modulates temporally CYP1A1 induction in mammary glands as well as liver toxicity, which is modulated by the circadian AHR-mediated CYP1A1 expression [229, 230]. In addition, Schmitt *et al*. showed that benzo[a]pyrene also temporally modulates CYP1A1 induction in breast cancer cell lines [229]. Finally, Ndikung *et al.* highlighted that circadian synchronization of a cell culture system enhances cellular response to xenobiotics that activate the AhR pathway [201]. Thus, easy cell synchronization can improve the assay sensitivity, and more physiologically relevant results can be achieved about potential toxicants for human health. Besides that, it is of highest priority to make *in vitro* systems used in toxicology or pharmacology more accurate and sensitive to minimize animal testing and improve animal welfare in studies according to the 3R principle (replace, reduce, and refine). Optimized *in vitro* test systems would provide more human relevant data, as until now most studies were conducted in rodents. Studying circadian rhythms in rodents often results in irrelevant data for human health and risk assessment, as rodents are nocturnal animals compared to humans, which are active in the daytime, i.e their circadian patterns are completely opposite [231]. Summarizing, it is of highest priority to refine the *in vitro* studies, e.g. through synchronization of the cells, not only to improve the outcome in favor of humans but also to minimize animal testing until more complex test systems such as 3D organoids or microfluidic systems are well established, simplified and commonly available, which again could profit from synchronization.

1.8 Aim of the study

The importance of developing and improving cell culture-based *in vitro* methods to mimic as closely as possible the *in vivo* situation for toxicological assessment strategies has already been highlighted in the previous chapters. Therefore, toxicological relevant pathways, such as AhR signaling, and their regulatory framework should be further studied for a better understanding of physiologically relevant pathways. On the other hand, circadian rhythmicity is often neglected in common toxicological *in vitro* systems, even though it seems to highly interact with the xenobiotic metabolism, which is addressed in these systems to determine and characterize the cellular response to xenobiotics. More in detail, in the common *in vitro* test systems, every cell follows its own circadian rhythm, which does not reflect the *in vivo* situation, and provides only limited information about the physiological cellular response to xenobiotics.

Ndikung *et al.* showed that circadian synchronization of cells in *in vitro* test systems, both quantitative and qualitative, enhance the cellular response [201]. In particular, the activation of AhR and the expression of its target genes, e.g. *CYP1A1* and *ALDH3A1,* upon various chemicals are enhanced in synchronized human mammary epithelial cells. This might be caused by an elevated transcriptional activation of the AhR receptor and not by a higher expression of AhR itself. Besides that, the data highlight that there is a circadian regulation of the AhR pathway, as the cellular response is more pronounced or rather moderate in different circadian phases, but the exact mechanism is still unclear. The aim of this project is to unravel this mechanism at a cellular and molecular level in order to better understand the impact of circadian rhythmicity on the physiological response to xenobiotic exposure and improve the development of toxicological *in vitro* test systems. In particular, the following question will be addressed:

1. Is the transcription, translation, or post-transnational modification of any AhR-signaling cofactors, e.g. p23, ARNT, AIP, AHRR, and HSP90 circadian regulated?
2. Is the (trans-) localization of AhR signaling cofactors circadian regulated after exposure to various chemicals?
3. Is AhR interacting with cofactors after exposure to various chemicals regulated in a circadian manner?
4. Is AhR or its cofactors directly interacting with the clock machinery?
5. Are clock components involved in the regulation of the AhR-mediated *CYP1A1* promoter activity?

2 Materials and methods

All chemicals, equipment, software, kits and working reagents used in this thesis are listed in tables 32-37 in chapter 2.9.

2.1 Cell culture

The cell lines used in this thesis are listed in Table 1 and their respective growth medium in Table 2. Cell lines were chosen according to their synchronization ability, their response to TCDD by activating the AhR signaling, their human origin and their relevance in the field of toxicology and disease studying. Cell lines were frozen in 1 mL complete medium supplemented with 10% DMSO and stored in a liquid nitrogen tank.

Cell lines were subcultured twice a week at a ratio of approx. 1:4 and grown at 37 °C, 5% CO_2, and 95% humidity. Growth medium was aspirated, cells were washed twice with sterile DPBS, and supplemented with Trypsin/ EDTA solution (1.5 mL for a 10 cm plate, 2.5 mL for a 15 cm plate). HME1_PLB cells were trypsinized with Trypsin/EDTA 0.025% solution (Lonza) and M13SV1 with 0.25% Trypsin/ 0.02% EDTA (PAN) for 5-7 min at 37 °C in 5% CO_2. The reaction was neutralized in HME1 cells by using a double volume of Trypsin Neutralizing Solution (TNS) and in M13SV1 a double volume of growth medium. Subsequently, the cell suspension was transferred into 50 mL Falcon tubes and centrifuged for 5 min at 200 x g in order to remove the Trypsin/ EDTA. The cell pellet was resuspended in fresh growth medium and dispensed into new culture plates.

Table 1: Cell line types

Cell line	Description	Supplier
HME1_PLB	Human breast epithelial cells (hTERT immortalized) expressing a firefly luciferase reporter of *PER2* promoter (*PER2*::*LUC*)	Pr. Dr. Kramer (Charite Universitätsmedizin Berlin) [232]
HME1_BLH	Human breast epithelial cells (hTERT immortalized) expressing a firefly luciferase reporter of *PER2* promoter (*BMAL1*::*LUC*)	Pr. Dr. Kramer (Charite Universitätsmedizin Berlin) [232]
M13SV1	Human breast epithelial cells (SV40 immortalized)	[233]

Table 2: Growth Media

Description	Main medium	Supplements
HME1 growth medium	MEBM™ Mammary Epithelial Cell Growth Basal Medium, Phenol Red Free (Lonza)	MEGM™ Mammary Epithelial Cell Growth Medium SingleQuots™ Kit (without Hydrocortisone) (Lonza) 25 mM Hepes 1% Penicillin/ Streptomycin 0.1 µg/ mL Hydrocortisone (ATCC)
M13SV1 growth Medium	MSU-1 basal media (Biochrom)	1% Penicillin/ Streptomycin 10% FBS

2.2 Synchronization and treatment of cells

For studying the circadian regulation of the AhR signaling pathway, the cells were treated with 1 µM dexamethasone to bring them in the same phase of oscillation. The day before synchronization, the cells were seeded according to Table 3, in order to be 100% confluent the next day. Simultaneously, for the non-synchronous condition, cells were seeded to have a 30% confluency on the day of synchronization, i.e. on the next day. The cells, which were 100% confluent were treated for 1 h with 1 µM dexamethasone. Then, they were washed twice with DPBS and either cultured in growth medium or treated with TCDD.

Table 3: Cell seeding numbers

***Plat*e format**	**96-well**		**6-well**		**24 cm**	
Confluency on next day after seeding	**30%**	**100%**	**30%**	**100%**	**30%**	**100%**
M13SV1 (million cells/ well)	0.02	0.1	0.3	1	0.04	0.2
HME1 (million cells/ well)	0.02	0.1	0.3	1	0.04	0.2

2.3 Transfection of cells

Transfection of cells with siRNA (2.3.1) or plasmid (2.3.2) is widely used to generate gene modification in mammalian cells and study mainly the function of genes by downregulating or enhancing specific gene expression and their recombinant proteins. In this thesis, specific cofactors of the AhR pathway were repressed or overexpressed by using these techniques to understand their role in the circadian regulation of this pathway.

2.3.1 Small interfering RNA (siRNA)

Small interfering RNA (siRNA) is a class of double stranded RNA that can degrade post-transcriptional mRNA with complementary nucleotide sequences, prevent its translation and inhibit protein synthesis. This process is based on the natural mechanism in which long dsRNA, e.g. from hairpin, is cleaved by the endoribonuclease, DICER, generating many short double stranded interfering RNAs (siRNAs). When entering the cell, these form with other proteins the RISC (RNA-induced silencing complex) and single strand siRNAs are produced, which recognize and bind to complementary mRNA inducing its cleavage and silence gene expression.

M13SV1 cells were seeded into a 6-well plate or a 10 cm plate to have a 70% confluence on the day of transfection. The siRNAs concentration and sequence used in this thesis are listed in Table 4. All steps were performed using RNAse free filter tips and tubes.

Table 4: Mix of siRNA transfections

	siRNA	**Stock**	**C_{final} (6-Well)**	**C_{final} (10 cm plate)**	**Sequence (5´->3´)**
Transfection solution (100 µL)	*SCR*	10 µM	120 µM (12 µL of stock)	120 µM (72 µL of stock)	CAUAAGCUGAGAUACUUCA
	p23				GGAUGUAGAUUUACCAGAA
	SP1				GCCAAUAGCUACUCAACUA
	AhR				AAGCGGCAUAGAGACCGACUU
	HSP90				GCAGAUAUCUCUAUGAUUG
	AIP				CCAGUUCCUCUGUGACAUCAA
	AHRR				GCAACGAUCGUGGACUAUC
	BMAL1				UCGGCACGCGAUAGAUGGAAA
	ARNT				UGGGCUCAAGGAGAUCGUUUA
	Medium without supplements		88 µL	528 µL	
	HiPerFect		12 µL	72 µL	

On the day of transfection, in a 1.5 mL tube, siRNA was mixed well with medium without supplements to an end volume of 100 µL according to Table 4. HiPerFect™ was added and immediately mixed by using a vortex for 10 sec. In the meantime of the transfection solution incubating for 10 min at RT, the cells were washed twice with DPBS and each well was supplemented with 1 mL of medium without any supplements. Then, the transfection mix was added dropwise to the cells and incubated at 37 °C and 5% CO_2. After 5- 6 h of incubation, the cells were washed twice with DPBS and normal growth medium with

supplements was added. In the next days, the cells were reseeded on different plate formats, synchronized and treated with substances, e.g. DMSO or TCDD, and subsequently, 48 h after transfection, analyzed by Western blot or RT-qPCR.

2.3.2 Plasmid transfection via electroporation

Transfection via electroporation is used to temporarily permeabilize the membrane of the cell, enabling macromolecules, as plasmids DNA, to enter the cell and modify its genome. In this thesis, plasmid transfection via electroporation was used to overexpress genes (e.g. p23 and SP1), YFP- tag proteins (AhR) for microscopy experiments or create stable lines expressing luciferase induced promoters. The plasmids used in transfection via electroporation are listed in Table 5. On the day of the electroporation, 4 mm electroporation cuvettes were prepared with directly pipetting 10-15 µg plasmid on the bottom of the cuvette. M13SV1 cells were harvest and 1.6 million cells were resuspended in 400 µL. In the meantime, a 6-well plate was prepared by adding 1 mL medium in each well. Then, the cell suspension was added to the cuvette, mixed well and electroporated at 950 µF, 220 V, ∞ Ω. The transformed cells were transferred in one well of the previous prepared 6-well plate. After 5-6 h, the wells were washed twice with DPBS and fresh medium was added. After 48 h, the cells were further analyzed by Western blot, RT-qPCR, microscopy, or luciferase assays.

Table 5: List of plasmids

Name	Description	Vector backbone	Origin
PL318, pGFP-N2-p23	p23 WT	pGFP-N2	[234]
PL319, pGFP-N2-p23-D108A	p23 overexpression	PGF2-N2	[234]
PL320, pGFP-N2-p23-D112A	p23 overexpression	pGFP-N2	[234]
PL321, pGFP-N2p23- D1-110	p23 overexpression	PGF2-N2	[234]
PL270, pLKO.1- p23 shRNA 1475 (#3)	p23 shRNA	pLKO.1	[234]
RSV-SP1	SP1 overexpression	RSV	Addgene (#12098)
CMV-SP1	SP1 overexpression	CMV	Addgene (#12097)
pN3-Sp1FL	SP1 overexpression	pN3	Addgene (#24543)
pcDNA3	Empty Vector	pcDNA3	Invitrogen (V79020)

2.4 Circadian reporter bioluminescence assay

2.4.1 Generation and activity measurement of circadian reporter cell lines

Circadian reporter bioluminescence assays were performed to visualize circadian rhythms, ensure successful synchronization of the cells, and analyze the effects of substances on the circadian rhythm. In this thesis, the assay is based on the reaction of the luciferase, derivate from the firefly, *Photinus pyralis*, catalyzing luciferin, O_2 and ATP to emit a photon, which can be measured at a 560 nm well length. Clock gene, such as BMAL1 or PER2, promoters can be tagged with *luciferase*-based reporter systems and be expressed stable or transiently in the cell. Thus, the activity of the promoter can be monitored live on the abundance of luciferin by using a photometer. In this way, an indirect visualization of the circadian rhythm could be achieved, and the promoter activity could be measured for up to 72 h.

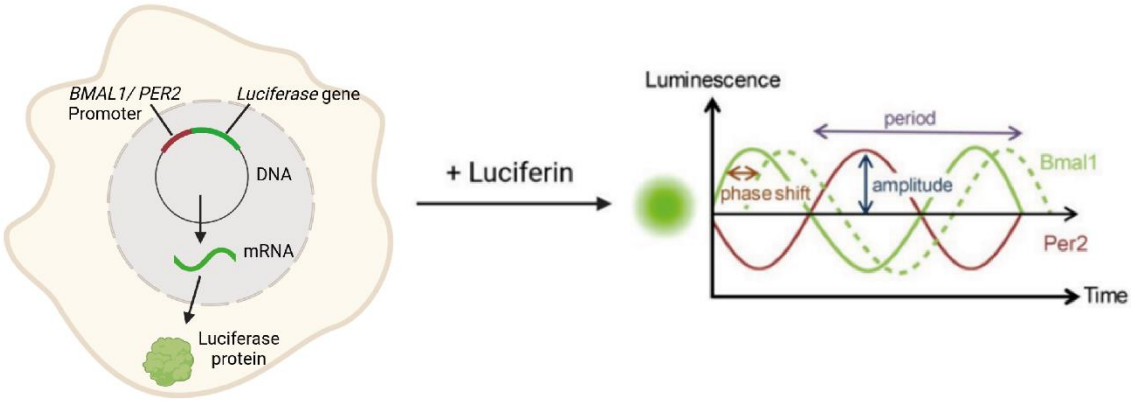

Figure 6: Schematic overview of the circadian bioluminescence reporter system and assay
In the construct used for the circadian bioluminescence reporter system, the luciferase gene is regulated through the *BMAL1* or *PER2* promoter. When the promoter is activated, a luciferase signal is released upon luciferin, and the promoter activity can be indirectly determined by measuring this signal. Upon synchronization of the cells, the circadian regulation of the clock gene promoter can be visualized by monitoring the oscillating luciferase signal through a plate reader at a well length of 560 nm. Parameters like phase shift, amplitude, and period can be determined to characterize the curve of the circadian rhythm. (The illustration was created with BioRender.com).

A stable HME1 cell line expressing a PER2 promoter-controlled luciferase system was kindly provided by Prof. Dr. Achim Kramer and used to monitor the circadian rhythm upon treatment with different potential circadian rhythm disrupting substances. Also, M13SV1 cells were transient-transfected (2.3.2) with a PER2 or BMAL1 promoter-controlled luciferase system construct (Table 6) and further analyzed after 48 h of transfection. Control cells were transfected with a GFP expression vector to check the transfection efficiency.

Overall, cells were seeded on a 96-well plate from Greiner (Cat.no. 655098) in order to be 100% confluent on the day of synchronization, and non-synchronized control cells were seeded at a density of 30%. Then, the cells were synchronized for 1 h with 1 µM dexamethasone and the medium was exchanged with 0.25 mM D-luciferin growth medium containing (or not) testing substances. The bottom of the plate was covered with a white sticker, and the plate was placed in the plate reader, Synergy Neo2, already heated up to 37°C and submitted with 5% CO_2. The reporter activity was determined by measuring the bioluminescence with a photon count of 6.5 sec per well and a gain of 125, every 30 min for 72 h.

Table 6: Circadian reporter bioluminescence constructs

Name	Description	Vector backbone	Origin
PLB::LUC	Firefly luciferase reporter of PER2 promoter (PLB::LUC)	pAB	[235]
BLH::LUC	Firefly luciferase reporter of BMAL1 promoter (BLH::LUC)	pAB	[236]
H2B-GFP	GFP expression vector	pEGFP-N1	Clontech®

2.4.2 Analysis of circadian bioluminescent data with ChronAlyzer

Luciferase signals can easily be measured by the photometer, but the further analysis of the obtained rhythmic time-series data can be challenging, as the rhythmic signals have a biological origin with systemic variabilities that impair the direct derivation of parameters, such as phase shift, amplitude and period, which are important in defining oscillations, i.e. circadian rhythms. Therefore, the software tool ChronAlyzer was developed to process rhythmic *in vitro* data series and identify characteristic rhythmic parameters by the Department 9 of the German Federal Institute of Risk Assessment (BfR). First, the ChronAlyzer tool automatically normalizes the raw data in order to be able to use curve fitting algorithms based on the comparison of measurements and a curve, which includes the following parameters: period length, phase-shift, amplitude, and damping. Second, a MATLAB® (MathWorks) optimization function (fminsearch) is built-in, which changes those parameter values according to their specific algorithm, until an exit condition to the iteration sequence is met and no further changes can improve the fitting. Subsequently, to determine the rhythmic parameters, the software uses the following model function:

$$y_{\mathrm{model}}(t) = \cos(2\pi \cdot ((t - p_{\mathrm{shift}})) \,/\, P) \cdot A_0 \cdot e^{(-d \cdot t)}$$

The p_{shift} stands for phase-shift, the period length is abbreviated by *P,* and the starting amplitude is denoted with A_0. The damping*, i.e* the extent of the oscillating amplitude

reduction over time, is shortened by *d*. After further adjustments to model function above, the obtained residual signal is oscillating around the x axis and an optimal representative fit for the measured time-series is determined.

2.4.3 Dual luciferase reporter assay for measuring promoter activity

The *CYP1A1* promoter activity upon 48 h of synchronization and treatment with TCDD was analyzed by using a *CYP1A1* promoter construct, i.e a firefly luciferase reporter plasmid containing a 1200 bp fragment of the human CYP1A1 promoter, and mutants of this construct, in which the *CYP1A1* promoter is constantly induced at its maximal activity. The plasmids used for this assay are in detail described in Schulthess *et al.* [237] and listed in Table 7. M13SV1 cells were co-transfected via electroporation with the wild-type promoter or the mutant types of the promoter and a *Renilla* luciferase construct, as a control reference for the number of the transfected cells. For the transfection, 10 mg and 5 mg were used for the wildtype/ mutant constructs and the *Renilla* luciferase construct, respectively. 24 h after electroporation (2.3.2), the cells were trypsinized and reseeded on four 96-well plates, one for each time point of 12 h, 24 h, 36 h, and 48 h, after synchronization and TCDD treatment. For non-synchronized and synchronized conditions, cells were seeded in an amount of 60,000 million cells per well and 150,000 million cells per well, respectively. Triplicates were prepared for each condition. On the next day, the appropriate wells were synchronized by using 1 mM dexamethasone for 1 h and then treated with TCDD (2 nM). Every 12 h, one of the plates was lysed and analyzed by using the protocol of the Dual-Luciferase® Reporter Assay System (Promega) kit. The promoter activity was determined by normalizing the measured firefly to the *Renilla* signal, and the data were analyzed using GraphPad® Prism (GraphPad Software).

Table 7: List of plasmids

Construct	Description	Vector backbone	Origin
CYP1A1-WT::LUC	Firefly luciferase reporter of *PER2* promoter (*PLB::LUC*)	pT81luc	[237]
CYP1A1-CDEF::LUC	Firefly luciferase reporter of mutated *CYP1A1 p*romoter that is not able to be induced	pT81luc	[237]
CYP1A1-3x C-DRE::LUC	Firefly luciferase reporter of mutated *CYP1A1* promoter that is constantly induced at a maximum	pT81luc	[237]
Renilla::LUC	Constantly active *CYP1A1 p*romoter	pRL	[237]

2.5 Protein biochemistry methods

2.5.1 Protein extraction from cells

Cells from a 6-well plate were washed twice with 1 mL of 1x PBS and lysed on ice by adding 100 µL Boehringer lysis buffer (Table 8) and using a cell scraper to detach them from the bottom of the well. The solution was immediately transferred to a 1.5 mL tube and incubated on ice for 20 min. Then, the tubes were centrifuged at 4°C for 20 min at 20,000 x g. The supernatant was transferred to a new 1.5 mL tube and immediately further processed to determine the protein concentration via DC protein assay.

Table 8: Boehringer lysis buffer

Reagent	**Final concentration**	**V= 500 mL**
Tris/ HCl, pH 7.4	50 mM	50 mL (500 mM Stock)
NaCl	150 mM	4.38 gr
EDTA ph 8.0	5 mM	50 mL (50 mM Stock)
EGTA	5 mM	0.95 gr
NP-40 Igepal	1 %	5 mL
Na-Desoxycholat	0.1 % (w/v)	0.5 gr
SDS	0.1 % (w/v)	0.5 gr

Add freshly:	
	for 2.5 mL
Protease inhibitor (25x stock) *	100 µL
Phosphatase inhibitor (10x stock) **	250 µL
Microcystin (stock 0.5 mM final 0.5 µM)	2.5 µL

*25x Stock: 1 Tablet cOmplete™ (protease inhibitor)/ 2 mL MilliQ H_2O
**10x Stock: 1 Tablet PhosSTOP™ (phosphatase inhibitor) in 1 mL MilliQ H_2O

→Keep the freshly prepared lysis buffer on ice

2.5.2 DC protein assay

The DC Protein assay is a technique for determining the protein concentration in samples, and it was performed according to the DC Protein Assay Kit II (Bio Rad), which is an improved version of the well-known Lowry assay. This assay is based on two steps: First, protein solutions are treated with a copper alkaline tartrate solution and subsequent mixed with a folin reagent. The copper treated proteins, mainly due to the amino acids, tyrosine and tryptophan, cause a reduction of the folin reagent by loss of 1, 2 or, 3 oxygen atoms leading to products with a characteristic blue color with a maximal absorbance of 750 nm.

This assay is better than the classic Lowry assay because the maximum color is produced in 15 min, and it stays stable for over 2 h.

The protein amount can be quantified by measuring the absorption spectra and comparing them with the ones of known protein concentration solutions, like BSA. The working reagent from the A/S Solution from the DC Protein Assay Kit from Bio Rad (50:1, Reagent A:S) was prepared according to the following formula to determine the total volume of reagents required:

(#standards + #unknowns) × (#replicates) (× 0.025 mL) = (5 + #unknowns) × (2) (× 0.025)

One 96-well plate was spotted in duplicate with the BSA standards according to Table 9 and with the diluted samples (1 µL sample and 9 µL ddH2O). Then, 25 µL of the premixed A/S working reagent was added to each well and subsequently 200 µL of solution B. The solution in the wells was mixed well by pipetting up and down, avoiding creating air bubbles, and the plate was covered with aluminum foil and incubated at RT for 10 min.

Table 9: Preparation of BSA standards

Final BSA Concentration	ddH_2O	BSA (1 µg/ µL)
0 µg/ µL (stock)	10 µL	-
2 µg/ µL	8 µL	2 µL
4 µg/ µL	6 µL	4 µL
6 µg/ µL	4 µL	6 µL
8 µg/ µL	2 µL	8 µL
10 µg/ µL	-	10 µL

Then, the absorption was measured at a wavelength of 750 nM. A regression line and a line equation were constituted with the absorbance values of the known concentration solutions to quantify the concentration of the protein in the samples. Once the protein concentrations were determined, all of the samples were adjusted to a protein amount of 30 µg or 50 µg. The adjusted lysates were mixed 1:3 with 4x Laemmli sample buffer/ β-mercaptoethanol. SDS in the sample buffer binds proteins, giving a uniform negative charge along the length of the polypeptide, and β-mercaptoethanol breaks the disulfide bonds between the cysteine of proteins. All the samples were boiled at 95 °C for 10 min.

2.5.3 SDS polyacrylamide gel electrophoresis

SDS-PAGE (sodium dodecyl sulfate-polyacrylamide gel electrophoresis) is a technique to separate denatured proteins according to their electrophoretic mobility. The negatively charged proteins migrate across the gel through the pores towards the positive electrode

(anode). The proteins migrate different distances according to their size, e.g. smaller proteins migrate faster than larger ones as they pass more easily through the pores of the gel. Moreover, the acrylamide concentration changes the size of the pores in the gel. The higher the percentage of the gels is (higher concentration of acrylamide), the more suitable it is for resolving smaller proteins (smaller pores in the gel).

The gel matrix consists of two different percentage gels: the stacking gel and the running gel. In the stacking gel, the proteins in the samples are aligned to the same level (interface between the stacking and the running gel) in order to start separate from the same level and according to their mass in the running gel. The gels and buffers for the SDS-PAGE were prepared according to Table 11 and Table 12. First, the appropriate percentage running gel solution was poured between two glass plates (1.5 mm) in the SDS gel caster (Mini-PROTEAN® Tetra Cell Casting Module, Bio-Rad) and poured over with approx. 1 mL of isopropanol. After the gel was polymerized, the isopropanol was removed by rinsing the gel between the glass plates with water, and the insert of the chamber was dried carefully without touching the gel using Whatman paper. The stacking gel solution was poured and a 10- or 15-well comp (1.5 mm thickness) was inserted, trying not to get bubbles stuck underneath. After the gel was polymerized, the electrophoresis apparatus was assembled (Mini-PROTEAN® Tetra hand-cast systems, Bio-Rad). Premixed 10x running buffer (Biorad, Tris/ glycine/ SDS) was diluted into 1x and poured into the space between the plates of the Mini-PROTEAN® Tetra Electrode Assembly to check for leakage. Once secure, the buffer was poured into the space surrounding the plate up to the line indicated on the apparatus.

Table 10: Premixed 10x running buffer (Tris/ glycine/ SDS buffer, pH 3, Biorad)

Components	**Final concentration**
Tris-base	25 mM
Glycine	192 mM
SDS	0.1%
→ Add MilliQ H_2O to appropriate volume. *To make 1 L of 1x Running Buffer, add 100 mL of 10x RB to 900 mL MilliQ H_2O	

Table 11: Composition of running gel solution (preparation of 2 gels, V_{final}= 20 mL).

Components	8%	10%	12%	15%
Tris-HCL, pH 8.8 (2 M)	5 mL	5 mL	4 mL	2.67 mL
37:5:1 Acrylamide/ Bis (Bio-Rad)	5.33 mL	6.67 mL	8 mL	10 mL
MilliQ H_2O	9.47 mL	8.13 mL	7.8 mL	7.13 mL
SDS (10%)	200 µL	200 µL	200 µL	200 µL
TEMED	20 µL	20 µL	20 µL	20 µL
APS (10%)	200 µL	200 µL	200 µL	200 µL

Table 12: Composition of stacking gel solution (5%, preparation for 2-4 gels, V_{final}= 20 mL)

Components	
Tris-HCL pH 6.8 (2 M)	3 mL
37:5:1 Acrylamide/ Bis (Bio-Rad)	3.33 mL
MilliQ H_2O	13.47 mL
SDS (10%)	200 µL
TEMED	20 µL
APS (10%)	200 µL

If the loading samples were frozen down, they were once again heated up for 10 min at 95 °C to be denatured and linearized before loaded onto the gel. Thermo Scientific™ PageRuler™ Plus Prestained 10- 250 kDa protein ladder (Thermo Scientific) was used as a molecular marker (Figure 7). After the samples and ladder were loaded, the electrophoresis was running for approx. 1-2 hours at 100- 110 V until the dye front ran off or near the bottom of the gel.

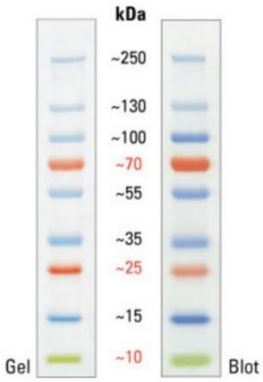

Figure 7: Thermo Scientific™ PageRuler™ Plus prestained 10- 250 kDa protein ladder
The PageRuler™ Plus Prestained Protein Ladder was used to estimate the molecular weight of the proteins which were separated by SDS-PAGE. The represented images are from SDS-PAGE gel (left) and its transfer to membrane (right). (www.thermoscientificbio.de).

2.5.4 Semidry Western blot

During Western blot analysis, the proteins were transferred from within the polyacrylamide gel of the SDS-PAGE onto a membrane made of nitrocellulose (0.2 µm pore–size nitrocellulose membrane, Bio-Rad) by using electric current. The proteins migrated from the cathode (gel) to the anode (nitrocellulose membrane), as they are negatively charged.

The Western blotting cassette (Trans-Blot® Turbo™ Transfer System, Biorad) was organized according to Figure 8. More specifically, a filter paper sandwich (8.5 x 13.5 cm) immersed in transfer buffer was placed on the down part of the cassette and the nitrocellulose membrane (0.2 µm, 8.5 x 13.5 cm, Bio-Rad) immersed also in transfer buffer, was placed on top of the filter paper sandwich. Next, the polyacrylamide gel was positioned on the membrane, and a second filter paper sandwich was placed on it. The air bubbles were removed by using a blot roller. Then, the blotting cassette was closed and placed into the blotting instrument (Mini Trans-Blot Central Core, Bio-Rad). The core was placed into the electrophoresis apparatus and run for 10 min at 2.5 A, up to 25 V (for transfer of two gels) or 10 min at 1.3 A, up to 25 V (for transfer of 1 gel).

Table 13: Composition of premixed 10x transfer buffer (Tris/ glycine, Biorad)

Components	Concentration
Tris-base	25 mM
Glycine	192 mM
For 1 L of 1x Transfer Buffer: Add 100 mL of premixed 10x transfer buffer and 100 mL ethanol in 800 mL MilliQ H_2O	

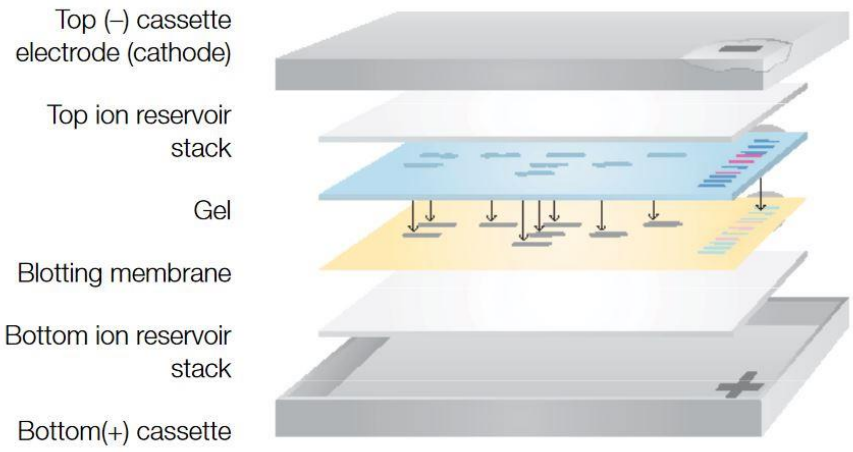

Figure 8: Schematic structure of the Western blot apparatus
A filter paper sandwich (8.5 x 13.5 cm) immersed in transfer buffer was placed on the downside of the cassette. The nitrocellulose membrane (0.2 µm) was put onto the sandwich and the polyacrylamide gel was placed on top of the membrane. The gel was covered with a further filter paper sandwich, and the assembled transfer pack was rolled to remove air bubbles. The cassette was closed and placed into the Western blot apparatus. (Figure adapted from www.bio-rad.com).

The membrane was washed in 1x washing buffer (TBS) for 5 min and blocked in Intercept (TBS) Blocking Buffer (LI-COR) while shaking for 1 h at room temperature. The membrane was washed with 1x TBST (diluted from premixed 20x TBST, Santa Cruz) three times for 10 min. The membrane was incubated with the appropriate primary antibody solution overnight at 4 °C on a rocking shaker. Primary antibodies were diluted in 3% w/v BSA/ 1x TBST (Table 14). All the used primary antibody solutions are listed in Table 15.

Table 14: Composition of 5% w/v BSA/ 1x PBST

Components	**3%**
Bovine serum albumin (BSA)	1.2 g
1x PBST	40 mL

Table 15: List of primary antibodies

Name	Manufacturer/ Cat. No.	Target	Size	WB Dilution	Species
Ah Receptor (B-11)	Santa Cruz/ sc-74571	AhR	105 kDa	1:500	mouse
AIP polyclonal antibody	Thermofisher/ PA5-29862	AIP	37 kDa	1:1,000	rabbit
AIP/ARA9 antibody (35-2)	NovusBio/ NB100-127	AIP/ARA9	37 kDa	1:1,000	mouse
Anti-AHRR antibody	Abcam/ ab108518	AHRR	76 kDa	1:1,000	rabbit
Anti-Aryl hydrocarbon Receptor antibody [EPR7119(N)(2)]	Abcam/ ab190797	AhR	105 kDa	1:1,000	rabbit
Anti-beta Actin antibody	Abcam/ ab8227	β-Actin	42 kDa	1:5,000	rabbit
BMAL1 (B-1)	Santa Cruz/ sc-365645	BMAL1	75-86 kDa	1:500	mouse
BMAL1 antibody	NovusBio/ NB100-2288	BMAL1	70 kDa	1:1,000	rabbit
CLOCK (D45B10), rabbit mAb	Cell Signaling/ #5157	CLOCK	100 kDa	1:1,000	rabbit
GAPDH (D16H11) XP®	Cell signaling/ #5174	GAPDH	37 kDa	1:1,000	rabbit
GSK-3β (D5C5Z) XP®	Cell signaling/ #12456	GSK3β	46 kDa	1:1,000	rabbit
HIF-1β/ARNT (C15A11)	Cell Signaling/ #3414	ARNT/ HIF-1β	87 kDa	1:1,000	rabbit
HSP90 (C45G5) rabbit mAb	Cell Signaling/ #4877	HSP90	90 kDa	1:1,000	rabbit
HSP90 mouse [AC88]	Abcam/ ab13492	HSP90	90 kDa	1:1,000	mouse
Lamin A/C (4C11)	Cell signaling/ #4777	Lαmin A/C	74/ 63 kDa	1:2,000	mouse
p23 monoclonal antibody (JJ3)	Invitrogen/ #MA3-414	p23	25 kDa	1:10,000	mouse
SP1 Antibody	NovusBio/ NB600-233	SP1	Ca. 90 kDa	1:2,000	rabbit
β-Actin (8H10D10) Mouse mAb	Cell Signaling/ #3700	β-Actin	42 kDa	1:10,000	mouse

The next day, all the non- or unspecific bound antibodies were washed away by a three-time 10 min washing with 1x TBST. The membrane was incubated for 1 h at RT with a diluted solution of the appropriate secondary antibody. All the secondary antibodies were diluted in 1x TBST/ 3 % w/v BSA and listed in Table 16. The secondary antibodies we used are labeled with IRDye near-infrared (NIR) fluorescent dyes. NIR fluorescent signals are stable for months, and no enzymes or substrates are needed to detect interacting proteins.

Table 16: List of secondary antibodies

Name	Manufactor/ Cat. No	Target	WB dilution	Species
Anti-mouse IgG (H+L) (DyLight ™ 680 Conjugate)	Cell signaling / #5470	mouse	1:15,000	Goat
Anti-rabbit IgG (H+L) (DyLight™ 800 4X PEG Conjugate)	Cell signaling/ #5151	rabbit	1:15,000	Goat

Finally, the membranes were washed three times for 10 min with 1x TBST and one time for 5 min with 1x TBS. The proteins were visualized using the Odyssey CLx Imaging System (Odyssey CLx, LI-COR). All pictures of the membranes were analyzed using the Image Studio™ Lite Software and the Empiria Studio Software by LI-COR Biosciences.

2.5.5 Immunoprecipitation assays

Immunoprecipitation (IP) assays are commonly used to identify protein-protein interactions. A specific antibody for the protein of interest bound to beads, e.g. sepharose beads, is used to isolate the protein of interest together with its interaction partner from protein lysates. In this study, this procedure was used to identify differences in protein-protein interactions between synchronized and non-synchronized cells treated or not with TCDD at different time points. The antibodies used to bind the proteins of interest on the beads are listed in Table 17.

Table 17: List of antibodies used for IP assay

Name	Manufacturer/ Cat. No.	Target	Size	Species	Volume for IP (1.5 µg antibody)
Anti-Aryl hydrocarbon Receptor antibody [EPR7119(N)(2)]	Abcam/ ab190797	AhR	105 kDA	rabbit	1 µL
p23 monoclonal antibody (JJ3)	Invitrogen/ #MA3-414	p23	25 kDA	mouse	1 µL
AIP polyclonal antibody	Thermofisher/ PA5-29862	AIP	37 kDa	rabbit	1.5 µL
BMAL1 antibody	NovusBio/ NB100-2288	BMAL1	70 kDA	rabbit	1.5 µL
SP1 antibody	NovusBio/ NB600-233	SP1	90 kDa	rabbit	2.7 µL

Big amounts of HME1_PLB cells (synchronized: min. 4 plates 15 cm/ per condition; non-synchronized: min. 8 plates 15 cm/ per condition) were harvested, re-suspended in 1 mL DPBS, transferred in a 1.5 mL tube and centrifuged for 5 min at 200 x g. The supernatant was aspired, and the pellet was re-suspended in 200- 400 µL ice cold IP lysis buffer (Table 18), depending on the size.

Table 18: Lysis buffer for IP

Reagent	Concentration	V= 50 mL
Tris/HCL ph 7.5	150 mM	2.5 mL (1 M)
NaCl	150 mM	1.5 mL (5 M)
Glycerin	10%	5 mL (100%)
EDTA ph 8.0	0.1 mM	10 µL (0.5 M)
NP-40, Igepal®	0.25%	1.25 mL (10%)
Add freshly	cOmplete™ protease inhibitor	2 tablets
	PhosSTOP™ phosphatase inhibitor	5 tablets
	0.5 µM Microcystin-LR	50 µL (0.5 mM)
	1mM DTT	50 µL (1M)

The cell lysates were sonicated 4-5 times, with in-between placement on ice, of 20 cycles at 0.5 kHz intensity, with 80% amplitude (Sonicator, G. Heinemann Ultraschall- und Labortechnik) and then centrifuged at 4° C for 15 min at 20,000 x g. The supernatant was transferred in a new 1.5 mL tube and 5 µL were diluted 1:10 in a new 0.5 mL tube to determine the protein concentration of the lysate via DC protein assay (2.5.2). 50 µg of the lysates was used as input control and 1 mg at a final concentration of 7 mg/ mL (adjusted with IP lysis buffer) as used to perform the IP. The IP lysates were incubated with 1.5 µg antibody (Table 17), in rotation at 4°C for 1.5 h. In the meantime, the required amount of 50% w/v suspension (50% slurry) of protein G sepharose beads (15 µL per lysate) was transferred in a new tube and the amount of the solution was marked with a line on the outside of the tube. The beads were washed twice with 1x PBS and once with IP lysis buffer by spinning them down for 20 sec at 2,000 x g between each step. Then, the beads were immersed in IP lysis buffer until the previously drawn line and mixed well until the solution was homogenous. In each protein-antibody lysate, 15 µL beads (50% slurry) was added and incubated for another 1.5 h in rotation at 4°C. Afterwards, the samples were centrifuged at 2,000 x g for 20 sec, the supernatant was carefully aspired, and the beads were washed 4 times with 0.5 mL IP lysis buffer. Finally, 15 µL 4x Laemmli buffer was added to the beads with the protein-protein interaction partners, boiled at 95° C for 2 min and stored at -20°C until further processing by Western blot analysis (2.5.3 and 2.5.4). For SDS-PAGE analysis, the samples were centrifuged at 2,000 x g for 20 sec, boiled at 95°C for 2 min and the supernatant was loaded to a gel avoiding pipetting the beads into the wells.

2.5.6 Cell fractionation for Western blot analysis

Cell content was separated into nucleolar and cytoplasmic fractions and analyzed via Western blot to identify changes in the translocation of AhR or other components of its signaling pathway upon synchronization and/or treatment with TCDD. Cells were trypsinized, centrifuged at 200 x g for 5 min, resuspended in 1 mL DPBS and transferred in a 1.5 mL tube. Then, the cell pellet was washed one more time with DPBS, resuspended in 200 µL lysis buffer A for cytoplasm (Table 19) and incubated for 3 min on ice. The suspension was transferred into a pre-chilled 0.5 mL dounce homogenizer, and the cells were broken open using 10 strokes of a tight pestle. Then the solution was retransferred in a 1.5 mL tube and centrifuged at 1,000 rpm for 5 min at 4°C. While the nuclei pellet was kept on ice until further processing, the supernatant, containing the cytosolic proteins was transferred in a fresh 1.5 mL tube and centrifuged briefly at full speed to remove any remaining nuclei. Then, it was transferred again into a fresh 1.5 mL tube and further processed for Western blot analysis. Then, the previously retained nuclei pellet was washed twice with 200 µL lysis buffer A, centrifuged at 100 rpm for 2 min at 4°C and finally

resuspended in 200 µL lysis buffer B for the nucleolar fraction (Table 20). The resuspended nuclei were sonicated 4-5 times, with in-between placement on ice, for 20 cycles at 0.5 kHz intensity, and 80% amplitude (Sonicator, G. Heinemann Ultraschall- und Labortechnik) and then centrifuged at 4°C for 15 min at 20,000 x g. The supernatant was transferred in a new 1.5 mL tube and further processed for Western blot analysis.

Table 19: Lysis buffer A for retaining proteins from the cytosolic fraction

Reagent	Final Concentration	V= 50 mL
Tris/HCL pH 7.5	150 mM	2.5 mL (1 M)
NaCl	150 mM	1.5 mL (5 M)
Glycerin	10%	5 mL (100%)
EDTA ph 8.0	0.1 mM	10 µL (0.5 M)
NP-40, Igepal™	0.05%	250 µL (10%)
Add freshly:	cOmplete™ protease inhibitor	2 tablets
	PhosSTOP™ phosphatase inhibitor	5 tablets
	1mM DTT	50 µL (1M)

Table 20: Lysis buffer B for retaining proteins from the nucleolar fraction

Reagent	Final Concentration	V= 50 mL
Tris/HCL pH 7.5	150 mM	2.5 mL (1 M)
NaCl	150 mM	1.5 mL (5 M)
Glycerin	10%	5 mL (100%)
EDTA ph 8.0	0.1 mM	10 µL (0.5 M)
NP-40, Igepal™	0.25%	1.25 mL (10%)
Add freshly:	cOmplete™ protease inhibitor	2 tablets
	PhosSTOP™ phosphatase inhibitor	5 tablets
	1mM DTT	50 µL (1M)

2.6 Molecular biological methods

2.6.1 RNA extraction and concentration determination

For RNA isolation, cells of a 6-well plate were washed twice with DPBS and the protocol of the *Rneasy Mini Kit* ® (Qiagen) was followed. In every step, RNase-free tubes and filter tips were used and all surfaces were cleaned with *RNase AWAY* ® decontamination solution. In detail, the DPBS was aspirated from the cells, 350 µL of RLT buffer was added directly to

the well, and the lysed cells were transferred in a 1.5 mL tube. Then, 350 µL of 70% ethanol was added to the tube and mixed well. The mixture was added to the columns of the kit and spun down at 12,000 rpm for 30 sec. The flow-through was discarded and a first washing step with 350 µL RW1-buffer and a spin down at 12,000 rpm for 30 sec was performed. The flow-through was discarded, and 80 µL DNAse/ RDD mix (10 µL DNAse + 70 µL RDD buffer) was directly added on the filter of the column and incubated for 15 min at RT to eliminate any DNA. Three more washing steps were performed, one with 350 µL RW1 buffer directly added on the DNase/RDD mix, and then two more with 500 µL RPE buffer, with discarding the flow-through between every washing step, and centrifuging at 12,000 rpm for 30 sec and 1 min, respectively. Last, the column was put in a new collection tube and centrifuged at full speed for 2 min to dry the membrane and remove any washing buffer. The column was placed on a 1.5 mL tube, and the RNA was isolated by adding 30 µL RNase-free water on the filter of the column and spun down for 1 min at 12,000 rpm. The extracted RNA was placed on ice and subsequently measured by using the Nanodrop 200 spectrophotometer. The ratio of the absorbance at 260 nm and 280 nm indicates the purity of the DNA and RNA. A ratio of approx. 1.8 is generally accepted as very pure DNA, and a ratio of approx. 2.0, as very pure RNA. Lower ratios indicate the presence of proteins or other contaminants. Blank and RNA concentration measurements were performed with 1.5 µL RNAse-free H_2O or RNA solution, respectively.

2.6.2 Reverse transcription

For analysis of gene expression via *Real-Time* Quantitative Reverse Transcription *PCR* (RT-qPCR), RNA needs to be reverse transcribed into complementary stranded DNA (cDNA). The same amount of RNA must be transcribed into cDNA in order to compare the gene expression between the different conditions in the qPCR analysis. RNA and short primers complementary to the 3´end of the RNA (random primers) are used for direct synthesis of the first strand of cDNA. These strands are used as templates for the Polymerase Chain Reaction (PCR) and amplification of the cDNA. cDNA synthesis was carried out with 1 µg RNA using the High-Capacity cDNA Reverse Transcription Kit (Thermo Fisher Scientific) according to the manufacturer's instructions. The mixture used for the reverser transcription is summarized in Table 21 and the program used in the thermal cycler is found in Table 22. The newly synthesized cDNA was either directly used for qPCR or stored at -20 °C.

Table 21: Reverse transcription reaction mixture

Components	Volume for one sample
RNA	10 µL (adjusted at 1 µg with RNAse-free H_2O)
RNAse-free H_2O	3.2 µL
10x RT-Puffer	2 µL
25x dNTP	0.8 µL
10x RT-Randomprimer	2 µL
RiboLock 20 U/ µL	1 µL
Reverse transcriptase	1 µL
Total Volume	200 µL

Table 22: Running program of the thermal cycler for the reverse transcription

Settings	Temperature	Time
Step 1	25 °C	10 min
Step 2	37 °C	120 min
Step 3	85 °C	5 min
Step 4	4 °C	hold

2.6.3 Reverse Transcriptase real-time quantitative PCR (RT-qPCR)

Reverse Transcriptase Real-time quantitative PCR (RT-qPCR) relies on the process of the polymerase chain reaction to amplify nucleic acids and is widely applied to analyze gene expression in a quantitative manner. For the RT-qPCR, the fluorescent dye SYBR-Green (Applied Biosystems) was used, which intercalates nonspecifically into dsDNA enabling the measurement of the amount of PCR product. In this thesis, the *CYP1A1* induction upon synchronization, TCDD treatment and the absence or enhancement of components of the AhR signaling pathway was analyzed via RT-qPCR as well as the gene expression of the different components upon synchronization and TCDD treatment in relation with time. Therefore, master mixes for the cDNA and primers, respectively, were prepared in tubes (Table 23) and combined by pipetting them on the 384-well plate. Triplicates were prepared for each combination of sample and primer. First, the cDNA master mix (6 µL/ per well) was pipetted at the bottom of the well, and then, the primer master mix (5 µL/ per well) on the side of the well. The 384-well plate was covered with foil to prevent evaporation. The plate was centrifuged for 1 min at 3,500 x g to remove any bubbles and analyzed by using the run method summarized in Table 24 and the QuantStudio Flex 7 qPCR machine. The data were analyzed with the QuantStudio software.

Table 23: Schematic overview of the RT-qPCR master mixes for one sample

cDNA master mix		**Primer master mix**	
Components	**Volume**	**Components**	**Volume**
PowerUp™ SYBR® Green Master Mix	5 µL	Forward primer	0.25 µL [10 µM Stock]
cDNA (1:10)	1 µL	Reverse primer	0.25 µL [10 µM Stock]
		RNAse- free H_2O	4.5 µL
Total	6 µL	Total	5 µL

Table 24: Running RT-qPCR program in QuantStudio Flex 7 qPCR machine

Settings	**Temperature**	**Time**
Holding stage	50 °C	2 min
	90 °C	10 min
Cycling stage (40 cycles)	95 °C	15 sec
	60 °C	1 min
Melt curve stage	95 °C	15 sec
	60 °C (continuous to 95 °C)	1 min
	95 °C	30 sec
	60 °C	15 sec

The primers used in the RT-qPCR analysis are listed in Table 25. *B2M* was chosen as a housekeeper gene, as its expression remained stable between the samples. All other genes were normalized according to the B2M expression. The Ct value (cycle of threshold), indicating the amount of amplified products, was automatically determined by the QuantStudio Software and the Ct mean was calculated by the Ct values of the triplicates. The Ct mean from the gene of interest was normalized to the Ct mean of the *B2M* housekeeper gene (ΔCt). Next, the ΔΔCt was calculated by subtracting the ΔCt of the control cells from the ΔCt of the treated cells. Last, the fold change was calculated by subtracting the relative RNA level ($2^{-\Delta\Delta Ct}$) of the control cells from the relative RNA level ($2^{-\Delta\Delta Ct}$) from the treated cells to draw conclusions about changes in the expression of the gene of interest upon treatment or no treatment. The formulas used to calculate the fold change are summarized as following:

$$\textbf{ΔCt} = \text{Ct mean}_{\text{gene of interest}} - \text{Ct mean}_{\text{Housekeeper}}$$

$$\textbf{ΔΔCt} = \Delta Ct_{treatment} - \Delta Ct_{control}$$

$$\textbf{Relative RNA level} = 2^{-\Delta\Delta Ct}$$

$$\textbf{Fold change} = \text{relative RNA level}_{treatment} - \text{relative RNA level}_{control}$$

Table 25: List of RT-qPCR primers

Primer		Sequence
B2M	Forward	5'-CTCCGTGGCCTTAGCTGTG-3'
	Reverse	5'-TTTGGAGTACGCTGGATAGCC-3'
CYP1A1	Forward	5'-TTTGAGAAGGGCCACATCCG-3'
	Reverse	5'-AGGCCTCCATATAGGGCAGAT-3'
AhR	Forward	5'-AACGGAGGCCAGGATAACTG-3'
	Reverse	5'-GACATCAGACTGCTGAAACCCT-3'
AHRR	Forward	5'-AGCGGAGATGAAAATGAGGA-3'
	Reverse	5'-AGTTCCGATTCGCACAGACT-3'
p23	Forward	5'-GATTCCAAGCATAAAAGAACGGAC-3'
	Reverse	5'-GAATCATCTTCCCAGTCTTTCCAA-3'
SP1	Forward	5'-TTGAAAAAGGAGTTGGTGGC-3'
	Reverse	5'-TGCTGGTTCTGTAAGTTGGG-3'
ALDH3A1	Forward	5'-TGTAGAGCTCGTCCTGCTGA-3'
	Reverse	5'-GCAGACCTGCACAAGAATGA-3'
BMAL1	Forward	5'-AGGATGGCTGTTCAGCACATGA-3'
	Reverse	5'-CAAAAATCCATCTGCTGCCCTG-3'
PER2	Forward	5'-TGAGAAGAAAGCTGTCCCTGCCAT-3'
	Reverse	5'-GACGTTTGCTGGGAACTCGCATTT-3'
REVERBα	Forward	5'-GAGCACCAGCAACATCACCAAG-3'
	Reverse	5'-TCTTGAAGCGACATTGCTGGCA-3'
ARNT	Forward	5'-CAAGCTAACCATCTTACGCATGGCAG -3'
	Reverse	5'-TGGACCACCACGAAGTGAGGTTC -3'
HSP90	Forward	5'CTTGGGTCTGGGTTTCCTC-3'
	Reverse	5'-GGGCAACACCTCTACAAGGA-3'
AIP	Forward	5'-GAGCTCATCATTGGCAAGAAGTT-3'
	Reverse	5'-TACAGGACCACATGCTGGATGTC-3'
CLOCK	Forward	5'-AAGTTAGGGCTGAAAGACGACGA-3'
	Reverse	5'-GAACTCCGAGAAGAGGCAGAAG-3'

2.6.4 *De novo* mRNA expression assays

The newly (*de novo*) synthesized and non-modified mRNA can be measured via RT-qPCR by designing primers specifically recognizing intron regions of the RNA before it's spliced and modified into mRNA ready to be translated into protein. Analyzing the *de novo* mRNA expression indirectly shows the promoter activity of the gene of interest. Primers were designed specifically for intron regions of *CYP1A1* to verify that the circadian expression pattern of *CYP1A1* mRNA measured previously by RT-qPCR is due to a circadian regulation of the *CYP1A1* promoter, i.e. the AhR pathway. A nucleus/cytoplasm fractionation was performed, and the RNA was isolated from both compartments (2.6.4.2). Subsequently, the RNA from the nucleus fraction was used to synthesize cDNA, which would serve as a template for the RT-qPCR analysis with the previously designed *CYP1A1 de novo* specific primers (Table 26).

2.6.4.1 Primer design for CYP1A1 *de novo* mRNA expression analysis

Primers targeting the *de novo* non-modified *CYP1A1* mRNA were designed and are listed in Table 26. More specific the sequence of the CYP1A1 before and after splicing was compared and primers were designed to target either only intron regions or both intron and exon regions, e.g. the first 7-8 bp were targeting the intron region and the other 7-8 bp the exon region. In this way, the primer would only recognize the newly non-spliced mRNA and enable its analysis via RT-qPCR. The efficiency of the primer pairs listed in Table 26 was successfully validated and the two primer pairs dn_CYP_2 and dn_CYP_4 were chosen to analyze the samples and indirectly determine the activity of the CYP1A1 promoter.

Table 26: List of primers used to analyze the *de novo* CYP1A1 expression

Primer		Sequence	Target region
dn_CYP_1	Forward	5´- CTTCCTGTGCTCAAGTGCC - 3´	Intron between exon 4 and 5
	Reverse	5´- CCACTACCTACCTAGCTCCTC - 3´	End of exon 5 and intro after
dn_CYP_2	Forward	5´- TACCCTGTCCAGGGTTTGACA - 3´	Intron before exon 5 and beginning of exon 5
	Reverse	5´- AATCACTGTGTCTGCAGAACAC - 3´	Beginning of Exon 6 and intron before exon 6
dn_CYP_3	Forward	5´- CTCTTTGGAGCTGGTATGGT - 3´	End of exon 4 and intron after
	Reverse	5´- CCACTACCTACCTAGCTCCTC - 3´	End of exon 5 and intro after
dn_CYP_4	Forward	5´- CTCTTTGGAGCTGGTATGGT - 3´	End of exon 4 and intron after
	Reverse	5´- CAATCACTGTGTCTGCAGAAC - 3´`	Beginning of Exon 6 and intron before exon 6
dn_CYP_6	Forward	5´- GCCTGCCTAACTTCTTCTGT - 3´	Intron between exon 4 and 5
	Reverse	5´- AGGCCTCCATATAGGGCAGAT- 3´`	Exon 6 und 7
dn_CYP_7	Forward	5´- TTTGAGAAGGGCCACATCC - 3´	Exon 3 and 4
	Reverse	5´- TGGACAGGGTAGAACAGAAGA - 3´	
dn_CYP_8	Forward	5´- CTTCCTGTGCTCAAGTGCC - 3´	Intron between exon 4 and 5
	Reverse	5´- CAGGGACAAGATGGATGCAGG - 3´	

2.6.4.2 Cell fractionation for RNA isolation

Intracellular compounds were separated into nucleolar and cytoplasmic fractions, and only the RNA from the nuclei was used to synthesize cDNA, as the newly synthesized, non-modified mRNA is more concentrated inside the nucleus. Cells of one well and two wells of a 6-well plate of synchronized and non-synchronized, respectively, were trypsinized, collected in a 50 mL Falcon tube, and spun down at 200 x g for 5 min. The cell pellet was resuspended in 1 mL DPBS and transferred in a 1.5 mL tube. Then, it was washed one more time with 1 mL DPBS and centrifuged at 200 x g for 2 min. The cells were lysed with 100 µL Ipegal lysis buffer (Table 28) incubating for 5 min on ice. In the meantime, 250 µL cold sucrose buffer (Table 29) was added to a 1.5 mL tube. Next, the cell lysate was carefully pipetted to the wall of this tube on top of the sucrose buffer, so that two phases were visible, and centrifuged at 3,500 x g for 10 min. At this point, the pellet and the supernatant contained the intracellular compounds of the nucleolar and cytosolic fractions, respectively. The supernatant, i.e. cytosolic fraction, was transferred into a new 1.5 mL tube, centrifuged at 14,000 x g for 1 min and again collected into a new 1.5 mL tube until further

processing (2.6.4.3). The pellet, i.e. nucleolar fraction, was briefly rinsed with 1 mL ice cold DPBS and in case of disturbance of the pellet, a centrifugation step at 3,500 x g for 5 sec was performed. The pellet from the nucleic fraction was further processed according to chapter 2.6.4.3.

Table 27: Essential solutions for preparing the Igepal™ lysis buffer and sucrose buffer

Solution	Amount	Recipe
NaCl (1 M)	100 mL	5.84 g NaCl + 100 mL RNAse-free H_2O
Igepal™ (10%)	100 mL	10 mL Igepal +90 mL RNAse-free H_2O

Table 28: Igepal™ lysis buffer

Reagent	Final concentration	V= 200 mL
NaCl	150 mM	30 mL (1 M)
Tris pH 7.4	10 mM	2 mL (1 M)
Igepal™	0.15%	3 mL (10 %)
RNAse- free H_2O		165 mL
➔ Filter the solution through a 0.22 µM filter		

Table 29: Sucrose buffer

Reagent	Final Concentration	V= 200 mL
NaCl	150 mM	30 mL (1 M)
Tris, pH 7. 4	10 mM	2 mL (1 M)
Sucrose		48 gr
RNAse- free H_2O		add to 200 mL
➔ Filter the solution through a 0.22 µM filter		

2.6.4.3 RNA isolation, cDNA synthesis and analysis via RT-qPCR

The RNA from the cytoplasmic fraction was extracted using the Direct-zol RNA MiniPrep (Zymo Research). The cytosolic fraction, with a volume of approx. 250 µL, was resuspended in 750 µL Trizol (3x the volume of the lysate) and the solution was transferred in a 2 mL tube. An equal volume of 95%- 100% ethanol (1 mL) was added to the mixture, and all of it passed through the same column in 700 µL amounts by centrifuging in-between at 12,000 x g for 30 sec. The next steps of the RNA purification process were executed according to the protocol of the kit. In the end, the RNA was eluted in 30 µL RNAse-free H_2O and stored at -80 °C for further analysis. The nucleolar RNA was isolated by adding 350 µL RLT puffer

to the pellet and following the protocol from the *Rneasy Mini Kit* ® (Qiagen) and as described in chapter 2.6.1. Then, the RNA extracted from the nuclei was reverse transcripted to cDNA according to the protocol in chapter 2.6.2. In this case, as the nucleolar RNA is much lower concentrated than the RNA extracted from the whole cell, only 350 ng in a volume of 10 µL diluted with RNase free H_2O were used to synthesize the cDNA. Finally, RT-qPCR analysis was performed according to chapter 2.6.3, with the cDNA of the nucleolar RNA and the primer pairs listed in Table 26 to determine the *de novo CYP1A1* expression and *CYP1A1* promoter activity. The cDNA was used for the qPCR analysis undiluted, in comparison to the 1:10 dilution applied when the RNA was extracted from the whole cell.

2.7 Microscopy

2.7.1 Immunofluorescent staining

Cells were immunostained with various antibodies (Table 30) to analyze the localization of different components of the AhR signaling pathway upon synchronization and treatment with TCDD. Coverslips (10 cm X 10 cm) were disinfected with 70% ethanol, dried overnight under the cell culture hood, and placed into a 24-well plate (one coverslip per well). The wells with the coverslip were washed twice with 1X PBS and seeded with cells (HME-1 or M13SV1: UE= 4 x 10^4 cells/ well, E= 2.1 x 10^5 cells/ well). On the next day, the cells were washed twice with 0.5 mL 1x PBS and fixed in 0.5 mL 4% paraformaldehyde for 15 min at RT. Next, the fixative was aspired, and the cells were washed twice with 0.5 mL 1x PBS. Cells were permeabilized with 0.5 mL of 0.3% Triton X-100/ 1x PBS for 30 min and then washed twice with 1x PBS. To prevent non-specific antibody binding, the cells were immersed with 0.5 mL 5% BSA/ 1x PBS solution for 1 h and then washed twice with 1x PBS. The 24-well plate with the cells in 1x PBS (0.5 mL) was shielded with parafilm and stored until further processing at 4°C.

On the day of immunofluorescent staining, one Whatman paper was placed in a black box (LI-COR), wetted with H_2O and a piece of parafilm was placed on top (wet chamber). The primary antibodies were diluted according to Table 30 in 5% FCS/ 1x PBS and for each coverslip, a drop (20 µL) of antibody solution was placed on the parafilm. The coverslip with the fixed cells was taken out of the well by using tweezers or a syringe needle and placed on the antibody drop with the cells facing the solution. The coverslips were incubated in the primary antibody solution for 2 h at RT and with the box closed, away from light, and keeping the humidity to prevent the coverslips from drying out. Hence, the slips were placed again in a clean 24-well plate and washed 3 times with 0.5 mL 1x PBS. A new parafilm was placed in the wet chamber and drops (20 µL) of the secondary antibody solution were distributed on top of it. The coverslips were placed again on the drops and incubated for 1 h in the

secondary antibody (Table 31) away from light and with the box closed to preserve the humidity. The coverslips were washed by dipping them in a PBS glass and placed back in the 24-well plate. DAPI (0.5 mL, 1:10,000 in 1x PBS) was added to the wells and incubated for 5 min. The coverslip with the stained cells was washed 3 times with 0.5 mL 1x PBS and carefully taken out of the well by using tweezers, dipped first in 1x PBS, then in millipore H_2O and placed on a Whatman paper to air dry. The air-dried coverslip was placed (avoiding air bubbles) on the previously added drop of Aqua-Poly/ Mount (Polysciences) on a glass slide. The slides were dried overnight, and the cells were visualized using a confocal microscope.

Table 30: List of primary antibodies for immunofluorescent staining

Name	Manufacturer/ Cat. No.	Target	Size	IF Dilution	Species
Anti-Aryl hydrocarbon Receptor antibody [EPR7119(N)(2)]	Abcam/ ab190797	AhR	105 kDA	1:1,000	rabbit
α-Tubulin antibody	Cell Signaling/ #2144S	a-Tubulin	45 kDA	1:100	rabbit
HIF-1β/ARNT (C15A11)	Cell Signaling/ #3414	ARNT/ HIF-1β	87 kDa	1:400	rabbit
Recombinant Anti-p23 antibody	Abcam/ ab92503	p23	25 kDA	1:100	mouse
p23 monoclonal antibody (JJ3)	Invitrogen/ #MA3-414	p23	25 kDA	1:100	mouse
HSP90 mouse [AC88]	Abcam/ ab13492	HSP90	90 kDA	1:100	mouse
HSP90 (C45G5) rabbit mAb	Cell Signaling/ #4877	HSP90	90 kDA	1:100	rabbit
a-Tubulin antibody (B-5-12-)	Santa Cruz/ SC2394	a-Tubulin	45 kDA	1:650	mouse
AIP polyclonal antibody	Thermo Fisher scientifc/ PA5-29862	AIP	37 kDa	1:500	rabbit
AHRR (5G11) monoclonal antibody	Santa cruz/ sc-293297	AHRR	60-80 kDa	1:100	mouse
Anti-AHRR antibody	Abcam/ ab108518	AHRR	76 kDa	1:100	rabbit
SP1 antibody	NovusBio/ NB600-233	SP1	90 kDa	1:100	rabbit

Table 31: List of secondary antibodies for immunofluorescent staining

Name	Manufacturer/ Cat. No.	Target	IF Dilution	Species
Goat anti-Mouse IgG (H+L) Alexa Fluor™ 488	Thermo Fisher scientifc / A-11001	mouse	1:1,000	goat
Goat anti-Rabbit IgG (H+L) Alexa Fluor™ 594	Thermo Fisher scientifc / A-11012	rabbit	1:1,000	goat

2.7.2 Visualisation of cells

Cells were imaged by using the confocal microscope, LSM 880 AiryScan (Zeiss) and an 20x or 40x air objective, as well as a 63x oil objective. Lasers with a wavelength of 488 nm (GFP), 561 nm (TxRed) and 406 nm (DAPI) were used as light sources (LU-N4 laser unit, 15 mW). The images were acquired with LSM Image Browser software (Zeiss) and Zen software (Zeiss). At least four positions of each condition were scanned in Z-stacks at 1-µm intervals and 512 x 512 pixel resolution. Fiji Image J software was used for all image processing and analysis [238].

2.8 Statistical analysis

Calculations for the different experiments were conducted either with Microsoft Excel or GraphPad Prism 9. Statistical analysis and data visualization were performed using GraphPad Prism 9. Statistical significance was determined using an unpaired, one- tailed, moderated Student's *t*-test. Statistical significance was accepted at $P \leq 0.05$ and the P-values as well as non-significance ($P \geq 0.05$), denoted with “ns”, were complemented in the figures. The qPCR statistical analysis was performed after advising Dr. Matthias Steinfath (BfR) and the literature, especially the paper published by Goni et al. [239]. Last, figures were further edited with Adobe Illustrator.

2.9 List of chemicals, equipment and working reagents

2.9.1 Chemicals

Table 32: List of chemicals

Name	Manufacturer	Order number
10x Tris/Glycine transfer buffer	Bio-Rad	1610734
10x Tris/Glycine/SDS premixed running buffer	Bio-Rad	1610772
1kb DNA Ladder	New England Biolabs	N3232s
2,3,7,8-tetrachloridibenzodioxin	LGC Standards	CIL-ED-901-B
20x TBST	Santaa Cruz	sc-281695
30 % Acrylamide: Bisacrylamide 37.5:1	Bio-Rad	161-0158
4 % Paraformaldehyde	Thermo Fisher Scientific	15670799
4x Laemmli Puffer	Bio-Rad	1610747
50x TAE-Puffer	Thermo Fisher Scientific	B49
6X DNA Loadbuffer	Thermo Fisher Scientific	R0611
Acetic acid 100 %	Roth	6755.1
Actinomycin D	Merck	114666
Agarose (universal)	VWR	732-2789
Ammonium persulfate (APS)	Roth	9592.3
Benzo[a]pyrene	Sigma-Aldrich	B1760
Bovine Serum Albumin (BSA), Fraction V	Roth	8076.1
Bromophenol blue	Roth	A512.1
cOmplete™ Protease Inhibitor Cocktail	Sigma	4693124001
Dexamethasone	Sigma-Aldrich	D2915
Dimethylsulfoxid	Sigma-Aldrich	D2650
Dithiothreitol (DTT)	biomol	04010.5
D-Luciferin	PJK	102111
Dulbecco's phosphate buffered saline (PBS)	Sigma	D5652
EGTA	Roth	3054.1
Ethylenediaminetetraacetic acid (EDTA)	Roth	X986.1
Fetal bovine serum	PAN	P30-3702
Forskolin	Sigma-Aldrich	F6886
Gel green nucleic Acid Stain	Biotium	41005
Glycin	Sigma-Aldrich	G8898
Glycine	Sigma	G8898
Hydrogen chloride	Roth	4625.1
Igepal CA630	Sigma	I8896
Intercept® (TBS) Blocking Buffer	LI-COR	927-60003
Kaempferol	Sigma-Aldrich	K0133
Leptomycin B	Sigma-Aldrich	L291
Methanol	Merk	1.060.092.511
NewBlot™ Nitro Stripping Buffer(5X)	LI-COR	928-40030
Non Fat dry milk	Roth	T145.3
PageRuler Plus prestained Protein ladder	Thermo Fisher Scientific	26619
PhosSTOP Phosphatase Inhibitor Cocktail	Sigma	4906845001
Pierce SuperSignal West Femto	Thermo Fisher Scientific	34095

Pierce Western Blotting Substrate	Thermo Fisher Scientific	32109
PlusOne Coomassie Tablets, PhastGel Blue R-350	GE Healthcare life science	17-0518-01
Ponceau S	Roth	5938.1
Power UP SYBR Green PCR Master Mix	Thermo Fisher Scientific	15310939
Sodium azide	Sigma	S8302
Sodium chloride	Roth	HNOO.3
Sodium deoxycholate	Roth	3484.1
Sodium dodecyl sulfate (SDS)	Bio-Rad	161-0301
SR8278	Tocris	S9576
Sucrose		
Tetramethylenediamine (TEMED)	SERVA	35930
Tris	Roth	5429.2
Triton X-100	Sigma	T8787
Tween-20	Roth	9127.1
VectaShield	VectorLabs	H-1000
β-Mercaptoethanol	Sigma	M7154

2.9.2 Equipment

Table 33: List of equipment and machines

Equipment	Manufacturer
Apotome.2	Zeiss
Axio Observer.Z1	Zeiss
Biofuge Primo R230V	Heraeus
Centrifuge 5430 R	Eppendorf
Centrifuge Mini Spin Plus	Eppendorf
Centrifuge Z 400 K	Hermle
CKX41 inverted microscope	Olympus life science
CO_2 incubator HERACELL® 150i / 240i GP	Thermo Fisher Scientific
CO_2 incubator Heraeus BBD 6220	Thermo Fisher scientific
CO_2 incubator. Memmert Ico50	Memmert
Countess II FL Automated Cell Counter	Invitrogen
EcoVac vacuum pump	schuett-biotec
Fusion Solo 6S	Licor
GenePulser Xcell™	Bio-Rad
GENios	Tecan
Heraeus Labofuge 400	Thermo Fisher Scientific
Herasafe TM KSP 12	Thermo Fisher Scientific
Mastercycler nexus gradient	Eppendorf
Megafuge 16	Heraeus
Micro-centrifuge	Neo Lab
Mini-PROTEAN® Tetra Vertical electrophoresis Cell	Bio-Rad
Nanodrop 2000 spectrophotometer	Thermo Fisher Scientific
Odyssey DLx Imager	Licor
Opera Phenix High Content screening system	Perkin Elmer
PowerPac200	Bio-Rad
QuantStudio 7 Flex	Applied Biosystems
Roller mixer SRT6	Stuart
Synergy neo2 Multi-mode Reader	Biotek

THERMOstar	BMG Labtech
Thermostar	BMG Labtech
Thermostat 5320	Eppendorf
Thermostat 5320	Eppendorf
Trans-Blot Turbo Transfer System	Biorad
Vortex Genie™ 2	Scientific Industries
Vortex Genie™ 2	Scientific Industries
Vortexer Reax	Heidolph
VWR®, Tube Rotator	Avantor
Waterbath Precission TSGP20	ThermoFisher S
Xplorer plus electronic multichannel pipette	Eppendorf
Xplorer plus electronic singlechannel pipette	Eppendorf
Zeiss LSM 880 AiryScan Confocal Microscope	Zeiss
ZOE Fluorescent Cell Imager	Bio-Rad

2.9.3 Software

Table 34:List of Software

Software	Manufacturer
Adobe Illustrator	Adobe Systems
Chronalyzer	Dr. N. Violet, FG9, BfR
Microsoft office (Word, Excel, Powerpoint)	Microsoft
GraphPad Prism	GraphPad Software
Fiji: ImageJ	Fiji (Open source)
ImageJ	Open source
Magellan™	Tecan
NanoDrop™ Software	Thermo Fisher Scientic
Photoshop	Adobe Systems
QuanttStudio ® Software	Thermo Fisher Scientific
Image Studio™ Software	LI-COR
Empiria Studio® Software	LI-COR
LI-COR® Acquisition Software	LI-COR

2.9.4 Working material

Table 35: List of working materials

Materials	Manufacturer	Catalog number
Cell scraper	TPP	99002 (240 mm) 99003 (300 mm) 99004 (362 mm)
Centrifuge tubes (conical)	TPP	91050 (50 mL) 91015 (15 mL)
Electroporation cuvettes	Peqlab	71-2030
MicroAmp™ Optical Adhesive Film	Thermo Fisher Scientific	4311971
Microplates	PerkinElmer	6005060
Microplates	Greiner	655098
Nitrocellulose Membrane, Precut, 0.2 µm, 7 x 8.4 cm	Bio-Rad	1620147

Nitrocellulose/ Filter Paper Sandwiches 1620233	Bio-Rad	1620233
PCR strips ROTILABO® 8 with single lids, Flat caps	Roth	CEN5.1
Pipette tips (ep-Dualfilter T.I.P.S)	Eppendorf	0030073363 (0.1 -10 µL) 0030073428 (2- 200 µL) 0030073460 (50- 1000 µL) 0030078594 (1250 µL) 0030078624 (200- 5000 µL)
Pipette tips (epT.I.P.S. Reload)	Eppendorf	4.662 357 (50- 1000 µL) 4.662 355 (2- 200 µL) 4.662 352 (0.1 -10 µL)
qPCR plates (384-wells)	Thermo Fisher Scientific	10505035
Serological Pipettes	NeoLab	7-4029 (5 mL) 7-4034 (10 mL) 4-0134 (25 mL) 4-0135 (50 mL)
Tissue Culture Dish	TPP	93040 (9.2 cm^2) 93060 (22.1 cm^2) 93100 (60.1 cm^2) 93150 (147.8 cm^2)
Tissue Culture Test Plates	TPP	92406 (6-well) 92412 (12-well) 92696 (96-well)
Tubes	Eppendorf	30121708 (0.5 mL) 30120086 (1.5 mL) 30120094 (2 mL) 30119401 (5 mL)

2.9.5 Cell culture reagents

Table 36: List of cell culture reagents

Reagent	Manufacturer	Catalog number
BioFreeze	Biochrom/Merck	F2270
Trypsin Neutralizing Solution	Lonza	CC-5002
Trypsin/ EDTA	Lonza	CC-5012
MSU-1 Medium	PAN biotech	SO-03800
Dulbecco´s Phosphate-Buffered Saline	PAN biotech	P04-36500
Fetal bovine serum		
HEPES Buffer 1 M	PAN biotech	P05-01100
Opti-MEM	Gibco	5198503
MEMB™	Lonza	CC-3153
MEGM™ Single Quot Kit Suppl. & Growth Factors	Lonza	CC-4136
Penicillin-Streptomycin, 10,000 U/ml Penicillin, 10 mg/ mL Streptomycin	PAN biotech	P06-07100
Trypsin 0.05 %/EDTA 0.02 % in DPBS, w/o: Ca and Mg	PAN biotech	P10-023100

2.9.6 Kits

Table 37: List of kits

Kits	Manufacturer	Catalog number
CellTiter-BLUE® Cell Viability Assay	Promega	G9681
Dual-Glo® Luciferase Assay System	Promega	E2920
High-Capacity cDNA Reverse Transcription Kit	Applied Biosystems™	4368814
DC™ Protein Assay	Bio-Rad	5000112
Powe UP SYBR® Green PCR Master Mix	Applied Biosystems™	4367659
RNase-Free DNase Set	Qiagen	79254
RNeasy Mini kit	Qiagen	74106
SuperSignal™ West Femto Maximum Sensitivity Substrate	Thermo Fisher Scientific	34095
Direct-zol RNA Miniprep Kits	Zymo Research	R2050
NucleoBond Xtra Midi kit for transfection-grade plasmid DNA	Macherey-Nagel	740410.50

3 Results

3.1 Cell lines suitable for circadian rhythm studies

In this thesis, the two human breast epithelial cell lines, M13SV1 and HME1, were primarily used to conduct experiments. Specifically, the stable HME1 cell line (HME1_PLB) expressing a firefly luciferase reporter of the *PER2* promoter was used to visualize the PER2 oscillation as an indicator of the circadian synchronized cell populations. Figure 9 shows representative fitted curves of the circadian reporter. Bioluminescence was recorded every 30 min over at least 72 h. In a non-synchronized cell culture, every cell exhibits its own circadian rhythm, i.e. the rhythm of each cell has its own phase, and these are not aligned in a uniform pattern, making the visualization of an oscillating luciferase activity impossible. On the other hand, monitoring confluent HME1_PLB cells, which were synchronized using 1 µM dexamethasone for 1 h, allowed the detection of an oscillating luciferase activity with a 24 h period that remains stable for at least 72 h (Figure 9). This verifies the successful circadian synchronization, i.e. the oscillation in a uniform circadian phase, of the cells and supports the data published by Ndikung *et al.* [201]. Importantly, these previous studies already showed that treatment with DMSO or TCDD did not alter circadian synchrony in HME1_PLB cells, whereas the REVERBα antagonist SR8278 disrupted circadian oscillation, as shown in both *PER2* and *BMAL1* reporter cell lines [201, 203]. Most importantly, Ndikung *et al.* were the first to describe that synchronized HME1_PLB cells show a more sensitive cell response to TCDD and higher induction of AhR target genes, in particular *CYP1A1*, and that *CYP1A1* mRNA is circadian regulated upon TCDD-mediated activation of the AhR signaling [201]. All these data provide sufficient evidence that HME1_PLB is a suitable cell line to study the mechanism behind the circadian regulation of the AhR signaling pathway.

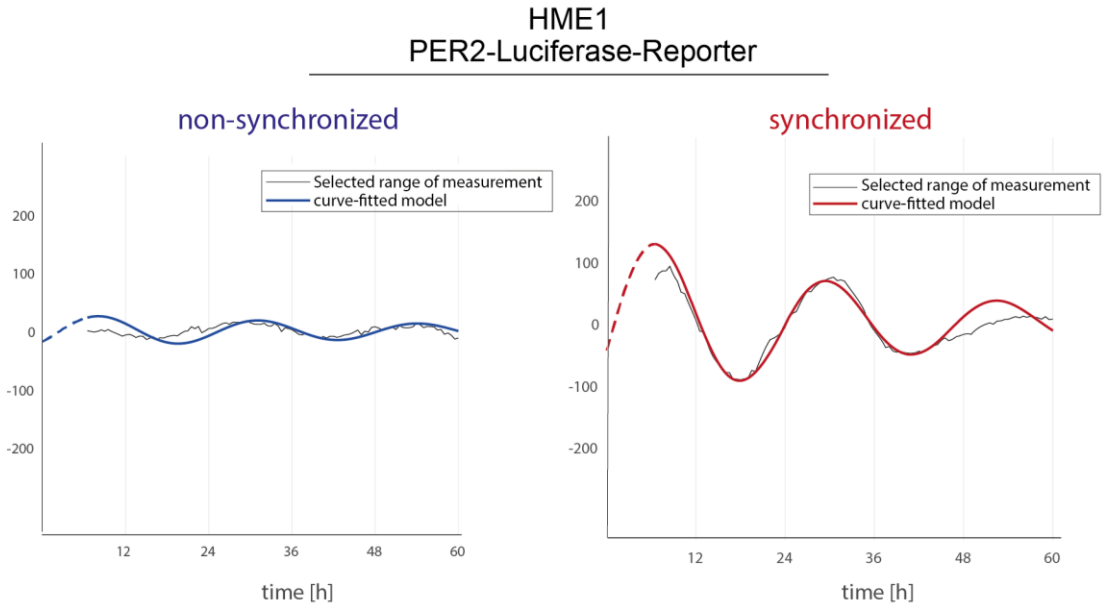

Figure 9: Visualization of the circadian rhythm in *PER2* luciferase reporter HME1 cells
Representative curves of fitted bioluminescence measurements of non-synchronized and synchronized *PER2*-luciferase reporter HME1 cells. For the synchronized condition, the confluent cells were treated with 1 µM dexamethasone for 1 h to achieve synchronization. The cells were monitored for at least 72 h and the bioluminescence was recorded every 30 min. The non-synchronized cells (left) exhibit non-circadian activation of the *Per2* promoter and luciferase bioluminescence expression, i.e. non circadian rhythmicity, in comparison to the synchronized cells (right), which show a circadian oscillation with a period of approximately 24 h.

The only disadvantage of the HME1_PLB cell line is that it is almost impossible to transfect, which makes mechanistic studies very difficult, as it is often necessary to upregulate (overexpression) or downregulate (knockdown or knockout) genes to understand their function in the pathway of interest. Therefore, M13SV1 cells were used as an alternative to perform gene editing since these can be easily transfected with different reagents for overexpression and knockdown experiments. To ensure that M13SV1 cells are suitable for studying circadian rhythms, they were transiently transfected with the firefly luciferase reporters of *PER2 or BMAL1,* and the circadian rhythm was monitored for 48 h in synchronized cells (Figure 10). In addition, as previously reported by Ndikung *et al.*, M13SV1 cells show a more sensitive cell response to TCDD through higher induction of AhR target genes, e.g. *CYP1A1*, upon synchronization, indicating that it is a proper cell line to study the mechanism behind the circadian regulation of the AhR signaling pathway [201].

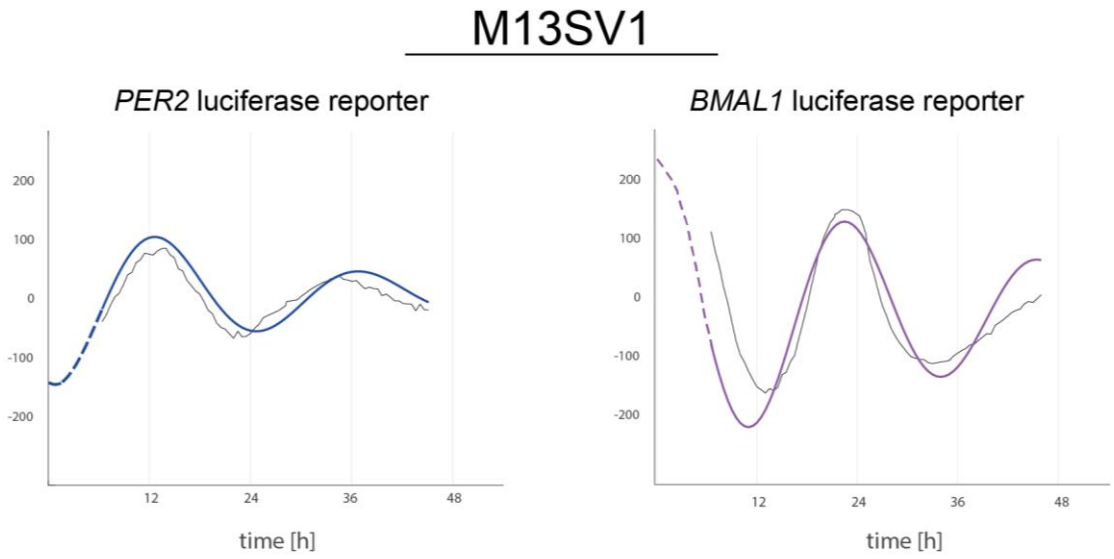

Figure 10: Visualization of the circadian rhythm in transient transfected M13SV1 cells with a *PER2* or *BMAL1* luciferase reporter plasmid
M13SV1 cells were transfected with a *PER2* or *BMAL1* luciferase reporter plasmid and then synchronized for 1 h with 1µM dexamethasone to visualize the circadian rhythm by measuring the luciferase activity every 30 min for 48 h. Here, representative curves of fitted bioluminescence recordings of synchronized cells are displayed.

3.2 Increased AhR target gene induction in circadian synchronized cells

HME1_PLB cells were analyzed for enhanced TCDD-mediated induction of AhR target genes upon synchronization to first verify data published by Ndikung *et al*. that support an induced *CYP1A1* and *ALDH3A1* expression upon synchronization, and second to identify further circadian regulated AhR target genes that could be used as an additional marker for circadian synchrony [201]. HME1_PLB cells were synchronized and treated with 2 µM TCDD for 24 h before being analyzed by RT-qPCR. Further, the REVERBα antagonist SR8278 (10 µM) was applied for 24 h to disturb synchronization by interfering with the proper function of BMAL1, as REVERBα forms a feedback loop with RORα that plays a major role in *BMAL1* transcription. The mRNA expression was normalized to endogenous *B2M* and the fold change for the DMSO plus SR8278, TCDD, and TCDD plus SR8278 treated cells was calculated compared to the control DMSO treated cells. *B2M* was chosen as a housekeeper gene, as its expression remained stable between the conditions, i.e. was not regulated by either synchronization or treatment with any of the applied substances. In non-synchronized cells, TCDD induced a 28-fold change in *CYP1A1* expression, whereas treatment with SR8278 had no effect on the TCDD-induced *CYP1A1* expression. In comparison, a 111-fold induction of *CYP1A1* expression was observed in TCDD-treated

synchronized cells, and the presence of SR8278 suppressed this induction by approx. 50% (Figure 11A). Similar, a second AhR target gene, *ALDH3A1,* showed a 2.9-fold induction in non-synchronized TCDD-treated cells and a 4-fold induction in the synchronized cells. Also, TCDD-induced expression of *ALDH3A1* could be suppressed via SR8278 treatment, verifying the dependence of the enhanced stimulation of these genes on circadian synchronization (Figure 11B).

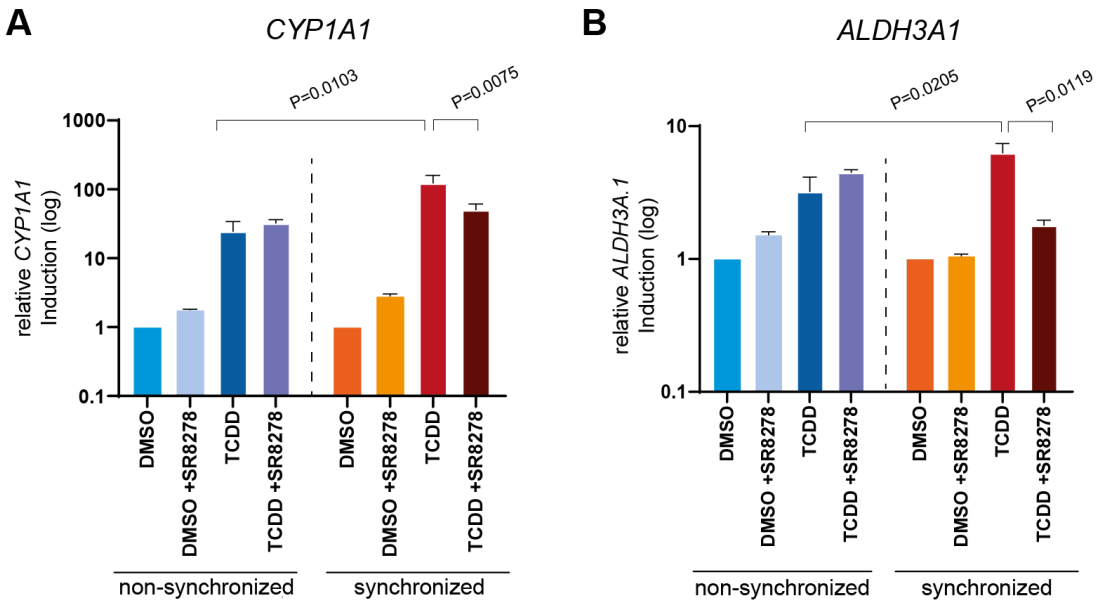

Figure 11: Enhanced *CYP1A1* and *ALDH3A1* induction after TCDD exposure in synchronized cells
CYP1A1 (A) and *ALDH3A1* (B) induction of non-synchronized and synchronized HME_PLB cells after 24 h treatment with TCDD (0.5 nM) and with or without the circadian synchrony disruptor, SR8278 (10 µM). The mRNA expression was determined by RT-qPCR and normalized to the endogenous control *B2M*. The *CYP1A1 or ALDH3A1* fold change for DMSO plus SR8278, TCDD, and TCDD plus SR8278 treated cells was calculated based on the respective DMSO (control) treated cells. Statistical significance of the fold change of the *CYP1A1* or *ALDH3A1* expression was determined by using an unpaired, one-tailed, t-test between TCDD treated synchronized and non-synchronized cells, and the P-values are displayed in the graph. Statistical significance was accepted at $P \leq 0.05$. (mean ± SD, n=3).

Further analysis of genes involved in the AhR pathway identified *AHRR* as an additional AhR target gene with an TCDD-mediated induced expression upon 24 h of synchronization. In Figure 12, the mRNA expression of *AHRR*, is shown in non-synchronized and synchronized cells treated with DMSO, DMSO plus SR8278, TCDD, and TCDD plus SR8278. The *AHRR* mRNA expression was normalized to *B2M* and the fold change for the DMSO plus SR8278, TCDD, and TCDD plus SR8278 treated cells was determined based on the control DMSO treated cells. Non-synchronized and synchronized cells were exposed to SR8278 without TCDD to identify possible SR8278 side effects. The synchronized cells

exposed to TCDD exhibit a 4.6-fold change in *AHRR* expression in contrast to the non-synchronized, which showed only a 3-fold change (Figure 12). In the synchronized cells, the TCDD-mediated *AHRR* induction was reduced by disrupting the circadian synchrony with SR8278 treatment. This remained undisturbed in non-synchronized cells treated with SR8278.

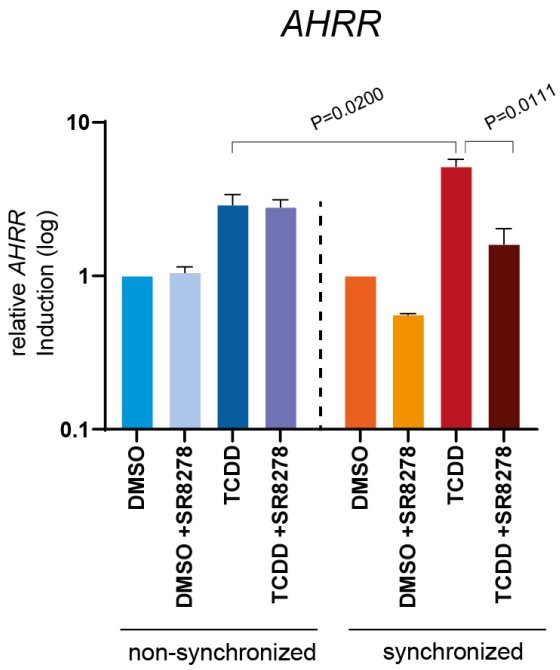

Figure 12: Enhanced *AHRR* induction after TCDD treatment in synchronized cells
AHRR induction of non-synchronized and synchronized HME_PLB cells after 24 h treatment with TCDD (0.5 nM) and with or without the circadian synchrony disruptor, SR8278 (10 µM). The mRNA expression was determined by RT-qPCR and normalized to the endogenous control *B2M*. The *AHRR* fold change after DMSO plus SR8278, TCDD, and TCDD plus SR8278 treatment was calculated based on the respective DMSO (control) treated cells. Statistical significance of the fold change of the *AHRR* expression was determined by using an unpaired, one-tailed, t-test between TCDD treated synchronized and non-synchronized cells, and the P-values are displayed in the graph. Statistical significance was accepted at $P \leq 0.05$. (mean ± SD, n=3).

3.3 Circadian oscillation of AhR target genes

The mRNA expression of AhR target genes was observed over time to examine the circadian, time-dependent response and verify that the AhR pathway is circadian regulated. The *CYP1A1*, *ALDH3A1,* and *AHRR* induction was examined in non-synchronized and synchronized cells after 12 h, 24 h, 36 h, and 48 h of TCDD (0.5 nM) exposure by RT-qPCR. The data from each timepoint were normalized to the endogenous *B2M* and then to the DMSO control of the same timepoint. Figure 13 shows the time-dependent mRNA induction of *CYP1A1* and *ALDH3A1* after TCDD treatment. The synchronized cells show a clear time-dependent circadian *CYP1A1* and *ALDH3A1* induction, with weaker responses after 12 h

and 36 h and stronger responses after 24 h and 48 h. In comparison, non-synchronized cells show significant increase in *CYP1A1* induction from 12 h to 24 h and from 36 h to 48 h, but no significant circadian pattern was observed. On the other hand, in non-synchronized cells, no significant increase or decrease as well as no circadian pattern was observed in *ALDH3A1* induction. In general, the *CYP1A1* induction is higher than the induction of *ALDH3A1*.

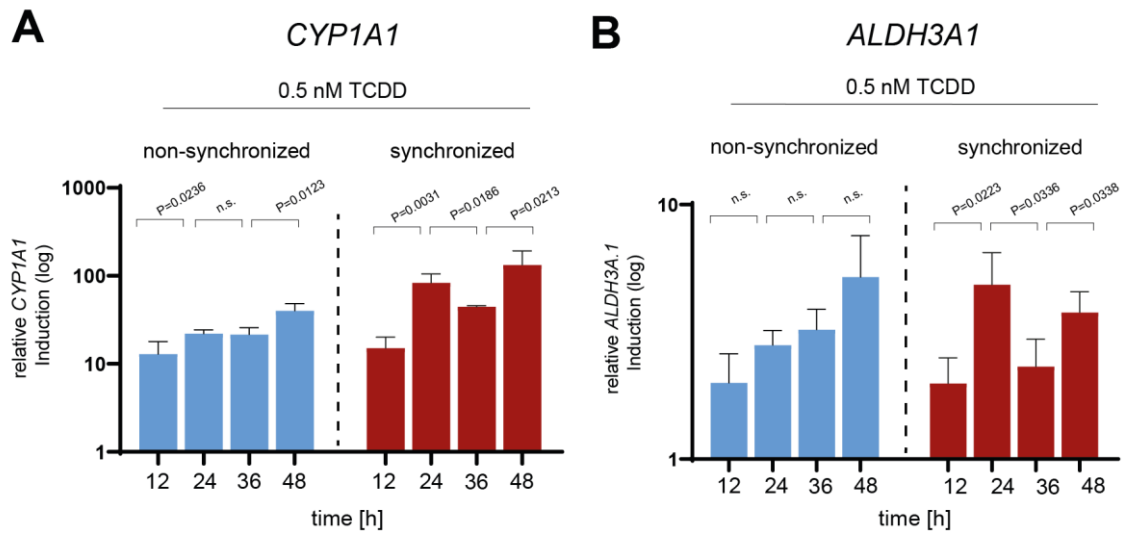

Figure 13: Circadian expression of TCDD-induced *CYP1A1* and *ALDH3A1* mRNA expression in synchronized cells
CYP1A1 (A) and *ALDH3A1* (B) fold induction at different timepoints in non-synchronized and synchronized cells after TCDD (0.5 nM) treatment. The mRNA expression was analyzed by RT-qPCR and normalized to the endogenous control *B2M*. The fold change of *CYP1A1* expression upon TCDD treatment for each timepoint was calculated based on the control DMSO treatment of the respective timepoint. The fold induction shows a circadian pattern, peaking at 24 h and 48 h in synchronized cells. Statistical significance of the fold change of the *CYP1A1 and ALDH3A1* expressions was determined by using an unpaired, one-tailed, t-test in synchronized cells between the timepoints 12 h and 24 h, 24 h and 36 h, as well as 36 h and 48 h and the P-values are displayed in the graph. Statistical significance was accepted at $P \leq 0.05$. (mean±SD, n=3).

Similarly, analyzing over time the expression of the newly identified circadian regulated target gene, *AHRR,* showed a circadian rhythmicity in TCDD-mediated expression upon synchronization (Figure 14). The highest induction was at 24 h (83-fold) and 48 h (132-fold), and the lowest at 12 h (14-fold) and 36 h (44-fold). In contrast, the *AHRR* induction in non-synchronized cells is significant higher from 12 h to 24 h and from 36 h to 48 h, but no significant circadian pattern could be identified. Summarizing, a circadian expression of all three AhR-target genes upon TCDD treatment and synchronization could be observed, strongly indicating a circadian regulation of the AhR pathway.

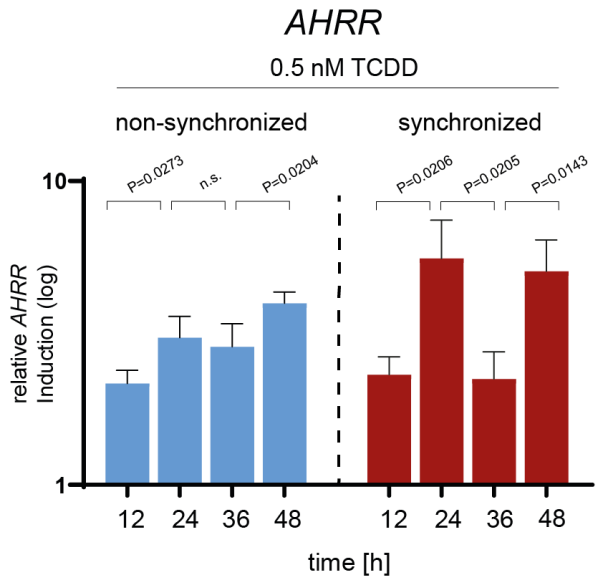

Figure 14: Circadian expression of the AhR target gene, *AHRR*, upon synchronization and after TCDD treatment
AHRR fold induction at different timepoints in non-synchronized and synchronized cells upon TCDD (0.5 nM) treatment. The mRNA expression was analyzed by RT-qPCR and normalized to the endogenous control *B2M*. The fold change of *CYP1A1* expression after TCDD treatment for each timepoint was calculated based on the control DMSO of the respective timepoint. The fold induction shows a circadian pattern, peaking at 24 h and 48 h in synchronized cells. Statistical significance of the fold change of the *AHRR* expression was determined by using an unpaired, one-tailed, t-test in synchronized cells between the timepoints 12 h and 24 h, 24 h and 36 h, as well as 36 h and 48 h and the P-values are displayed in the graph. Statistical significance was accepted at $P \leq 0.05$. (mean±SD, n=3).

3.4 AhR gene and protein expression in synchronized cells

After showing a correlation between the circadian rhythm and the AhR pathway through the circadian regulation of AhR target genes, further studies were carried out to analyze *AhR* expression itself at protein and mRNA levels. This would determine whether this oscillating AhR target gene expression is due to a circadian expression of AhR itself and help us unravel the mechanism of the circadian-dependent AhR signaling. First, the *AhR* mRNA expression upon TCDD treatment after synchronization was compared to that of non-synchronized cells to possibly explain the induction of AhR target genes upon synchronization by identifying an induced AHR expression upon synchronization. Therefore, non-synchronized and synchronized HME1_PLB cells were treated with DMSO, DMSO plus SR8278, TCDD, and TCDD plus SR8278, and subsequently, the *AhR* mRNA levels were analyzed with RT-qPCR. Figure 15A shows the fold change of the *AHR* expression for DMSO plus SR8278, TCDD, and TCDD plus SR8278 treated cells, which was determined based on the DMSO (control) treated cells. The *AhR* expression is not induced by TCDD, neither in the non-synchronized nor in the synchronized cells. Also, the

REVERBα antagonist, SR82878, could not alter the *AhR* expression by disrupting the circadian synchrony. Next, the TCDD-mediated induction of AhR upon time of synchronization was analyzed to possibly explain the circadian pattern in the time-dependent TCDD-mediated expression of AhR target genes. Figure 15B displays the fold change of the *AhR* expression after 12 h, 24 h, 36 h, and 48 h of cell synchronization (or not) and treatment with TCDD (0.5 nM). This fold change was determined based on the DMSO control treatment of the respective timepoint. The *AhR* expression shows no significant change over time, as the fold change remains constant at 1-fold, and no circadian expression pattern is observed.

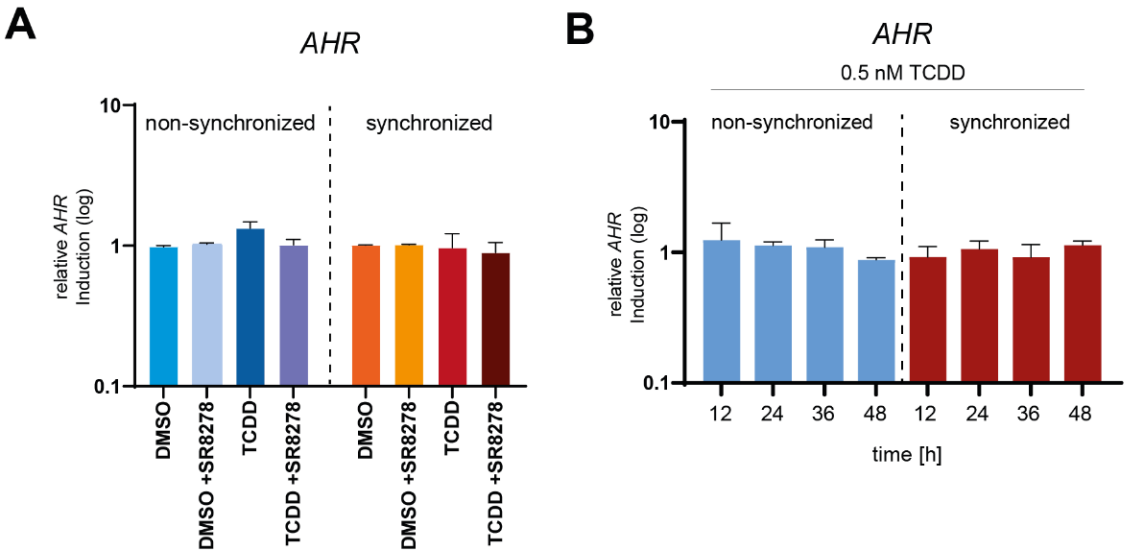

Figure 15: *AhR* mRNA expression displays no induction or circadian synchrony upon TCDD-treated synchronized cells
A) AHR induction of non-synchronized and synchronized HME_PLB cells after 24 h treatment with TCDD (0.5 nM) and with or without the circadian synchrony disruptor, SR8278 (10 µM). The mRNA expression was determined by RT-qPCR and normalized to the endogenous control *B2M*. The *AHR* fold change after DMSO plus SR8278, TCDD, and TCDD plus SR8278 treatment was calculated based on the according DMSO (control) treated cells. B) TCDD-mediated *AhR* fold induction after 12 h, 24 h, 36 h, and 48 h of synchronization or not. The *AHR* mRNA expression was analyzed by RT-qPCR, normalized to the endogenous control *B2M,* and the fold change of the *AHR* expression after TCDD exposure for each timepoint was calculated based on the control DMSO of the respective timepoint. (mean±SD, n=3).

To cover the full transcriptional process, the protein levels were determined by Western blot analysis. HME1_PLB cell samples were collected every 12 h after synchronization and treatment with DMSO (control) or TCDD (0.5 nM). Then, AhR was detected with an appropriate antibody on the Western blots to identify whether it is circadian regulated in protein level. Figure 16 shows a representative Western blot of synchronized HME1_PLB cells treated with DMSO or TCDD over a 48 h period of time. The protein levels of AhR in

synchronized cells were reduced after the treatment with TCDD compared to the DMSO control of the same timepoint. This matches the literature, that supports TCDD-induced degradation of AhR by the ubiquitin-proteasome pathway [240]. Also, in the DMSO control cells, the protein levels of AhR remained constant between 12 h, 24 h, 36 h, and 48 h after synchronization, and no circadian pattern in the AhR expression could be observed either in DMSO or TCDD treated synchronized cells. All in all, these data suggest that the AhR target gene induction is not driven either by a circadian dependent mRNA expression of *AhR* or a circadian regulation of the AhR protein, but probably is mediated by circadian binding of AhR and its cofactors on the *XRE* promoter, initiating its circadian activation.

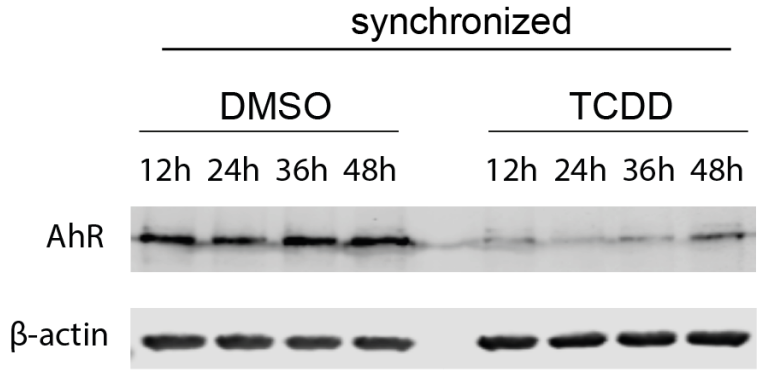

Figure 16: TCDD reduces the AhR protein levels but no circadian rhythmicity in the AhR protein expression
Representative Western blot membrane of synchronized cells treated with DMSO or TCDD (0.5 nM). Protein lysates were extracted from HME1_PLB cells synchronized and treated with DMSO or TCDD for 12 h, 24 h, 36 h, and 48 h. Then, the proteins were separated through SDS-PAGE and analyzed via Western blot. AhR antibody revealed bands specific for AhR at approx. 100 kDa. β-Actin was detected, at ~ 42 kDa, as loading control. (n=4).

3.5 Circadian regulation of *CYP1A1* promoter activity

The data demonstrated that the circadian regulation of AhR target gene induction could not be explained through the direct circadian regulation of the AhR gene itself. Ndikung *et al.* published data that showed enhanced *CYP1A1* promoter activity in synchronized M13SV1 cells upon 24 h TCDD treatment [201]. Therefore, further studies analyzing the promoter activity over time were performed to first verify the already published data, and second to identify a possible circadian regulation of the promoter activity.

As the necessary tools were already available, M13SV1 cells were co-transfected with a *Renilla* luciferase construct as a control for transfection efficiency and either with a human wildtype *CYP1A1* promoter or a non-inducible mutant construct as a control transfection. These constructs were firefly luciferase reporter plasmids of the human *CYP1A1* promoter, and the firefly luciferase signal served as a direct indicator of the promoter activity. The firefly and *Renilla* luciferase signals were measured in non-synchronized and synchronized

cells after 12 h, 24 h, and 36 h of TCDD treatment, and the firefly signal was normalized to the *Renilla* signal for each condition. Figure 17 depicts the normalized firefly luciferase signal of TCDD-treated cells in relation to DMSO-treated cells and is a direct indication of the *CYP1A1* promoter activity. In non-synchronized TCDD-treated cells, the promoter activity was constantly approx. 2.5-fold induced over time. In comparison, synchronization of the cells revealed a 3-fold, 3.5-fold, and 4-fold induction after 12 h, 24 h, and 36 h of synchronization and TCDD treatment, respectively. The M13SV1 cells transfected with the non-inducible mutant (control transfection) showed no difference in the relative *CYP1A1* promoter activity over time. Unfortunately, no circadian regulation of the promoter activity could be identified in M13SV1 cells, but the enhanced promoter activity at each timepoint in synchronized TCDD-treated cells supports the theory that the induced AhR-target gene expression upon synchronization is due to elevated promoter activity. The artificial promoters seem not to be an appropriate tool to study circadian effects over time, as not all regulatory aspects of the endogenous gene are considered. Also, the results seem to be tampered by changes during the experiment in various factors, such as cell density and transfection efficiency, as no stable cell lines were used. Identifying that this system is not fully suitable for these promoter activity studies, *de novo* expression experiments measuring the newly synthesized *CYP1A1* expression, reflecting the *CYP1A1* promoter activity, were performed next.

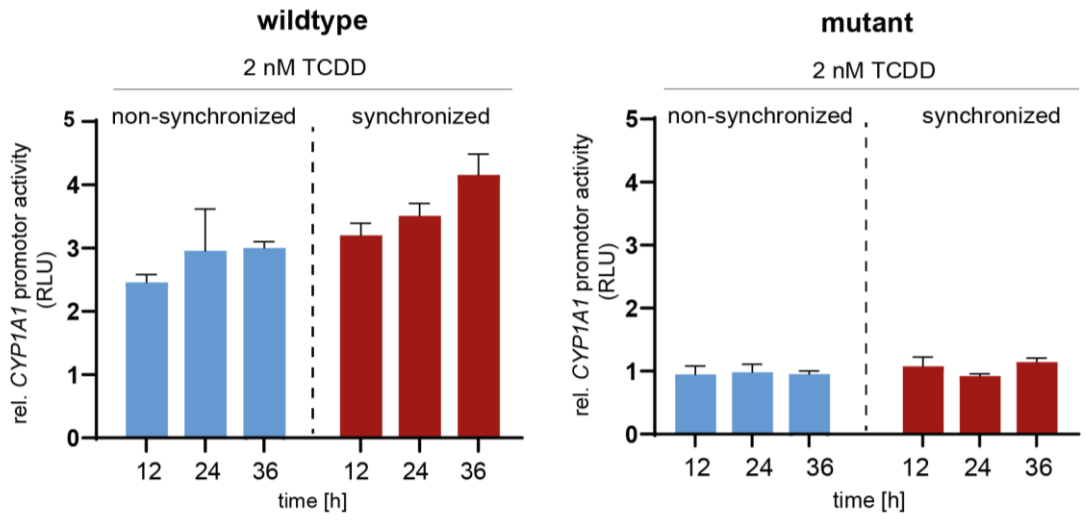

Figure 17: Enhanced TCDD-mediated activity of the *CYP1A1* promoter in synchronized cells
Normalized firefly luciferase signal of TCDD in relation to DMSO treated non-synchronized or synchronized M13SV1 cells for 12 h, 24 h, or 36 h, indirectly reflecting the *CYP1A1* promoter activity. These cells were co-transfected with a firefly luciferase reporter plasmid containing either a human wildtype *CYP1A1* promoter construct (wildtype) or a non-inducible mutant (mutant). These were also co-transfected with a constitutive active *Renilla* luciferase plasmid as control. After 24 h of transfection, the cells were synchronized or not and treated with 2 nM TCDD for an additional 12 h, 24 h, and 36 h. The dual luciferase assay was conducted with the Dual-Glo® Luciferase Assay System (Promega) according to the manufacturer´s protocol. (n=3).

As the artificial promoter constructs seem less appropriate to analyze circadian effects upon time, the *de novo CYP1A1* expression by RT-qPCR in HME1_PLB cells was analyzed to confirm the circadian activity of the *CYP1A1* promoter. Primers were designed to target intron regions of the *CYP1A1* mRNA, and thus the unprocessed, newly synthesized (*de novo*) *CYP1A1* mRNA. The determination of the *de novo CYP1A1* expression is an indirect measurement of the promoter activity, as it shows the mRNA that was immediately synthesized after activation of the promoter. Figure 18 shows the *de novo CYP1A1* induction of non-synchronized and synchronized cells treated with 0.5 nM TCDD over time. The *de novo CYP1A1* expression in synchronized cells treated with TCDD exhibits a circadian pattern, with the highest induction after 24 h (16-fold) and 48 h (15.3-fold), and the lowest after 12 h (4.4-fold) and 36 h (4.8-fold) of synchronization. On the contrary, the expression remains constant in the non-synchronized cells. This aligns with the previous data showing a circadian regulation of the AhR-target gene expression and indicates that the circadian regulation of *CYP1A1* is modulated through a circadian activation of the *CYP1A1* promoter. All in all, the TCDD-induced *CYP1A1* promoter activity is not only enhanced in synchronized cells, but it is also circadian activated over time.

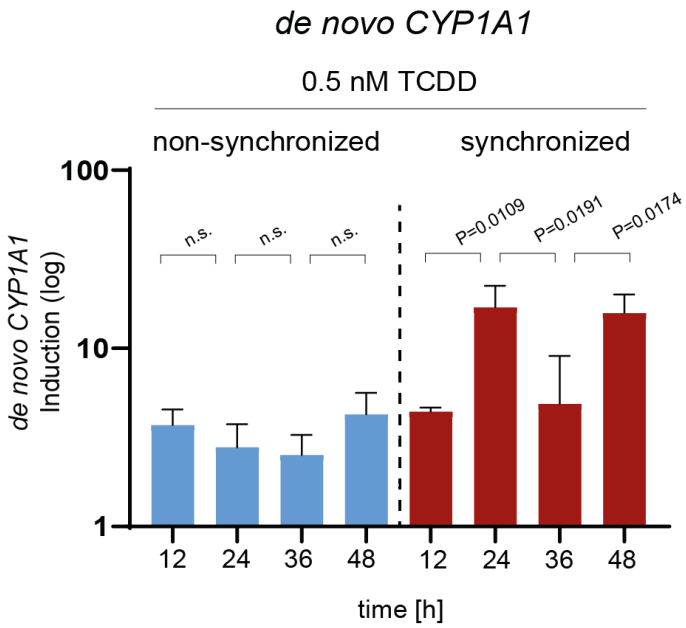

Figure 18: Circadian *de novo* mRNA expression of *CYP1A1* after TCDD exposure
Non-synchronized and synchronized HME1_PLB cells were treated with DMSO or 0.5 nM TCDD for 24 h and fractionated into cytoplasm and nucleus. The mRNA was isolated only from the nucleus, and the expression of the newly synthesized, unprocessed (*de novo*) *CYP1A1* mRNA was analyzed by RT-qPCR, using primers that identify intron regions. The *de novo CYP1A1* mRNA was normalized to the endogenous control *B2M*. For each timepoint, the fold change of the *de novo CYP1A1* expression after TCDD exposure was calculated based on the DMSO control of the respective timepoint. The TCDD-mediated *de novo CYP1A1* expression exhibits a circadian pattern only in synchronized cells. Statistical significance of the fold change of the *de novo CYP1A1* expression was determined by using an unpaired, one-tailed, t-test in synchronized cells between the timepoints 12 h and 24 h, 24 h and 36 h, as well as 36 h and 48 h, and the P-values are depicted in the graph. Statistical significance was accepted at $P \leq 0.05$. (mean±SD, n=3).

3.6 Analysis of AhR signaling components at mRNA and protein level for identification of circadian regulations

Since the *CYP1A1* promoter is circadian regulated, the next step was to identify whether AhR signaling components are induced in synchronized TCDD-treated cells (3.6.1), or they exhibit a circadian pattern at mRNA (3.6.2) or protein level (3.6.3). Identifying any circadian regulation of these AhR signaling components could possibly provide a hint of the mechanism behind the circadian regulation of the *CYP1A1* promoter activity.

3.6.1 Identification of AhR signaling components with induced gene expression upon synchronization

To identify enhanced TCDD-mediated expression of AhR cofactors upon synchronization, non-synchronized and synchronized HME1_PLB cells were treated for 24 h with 0.5 nM TCDD to activate the AhR pathway, and with SR8278 to disturb circadian synchrony. Then, the gene expression of the AhR components *AIP*, *SP1*, *ARNT*, *HSP90,* and *p23* was determined by RT-qPCR, normalized to the endogenous *B2M,* and the fold change of synchronized (or not) cells treated with DMSO plus SR8278, TCDD, and TCDD plus SR8278 was calculated based on the control DMSO treated cells. Figure 19A shows the fold change of the expression of the different AhR cofactors upon circadian disturbance with no TCDD-mediated activation of the AhR signaling, as a control. The inhibitor SR8278, as circadian disruptor, had no effect on the gene expression of the AhR cofactors. Next, the components *AIP, p23,* and *HSP90*, which maintain AhR in an inactive state, showed no difference in the fold change (1-fold) upon synchronization (or not) and after TCDD treatment. No increased TCDD-mediated induction of these genes upon synchronization was observed, which would explain the enhanced TCDD-mediated *CYP1A1* induction after synchronization (Figure 19B). Similarly, no alterations were identified in the TCDD-mediated gene expression of the AhR cofactor *ARNT*, which is required for *CYP1A1* promoter activation, upon synchronization. Indeed, in both non-synchronized and synchronized TCDD exposed conditions, the fold change of *ARNT* remained stable at approx. 1-fold (Figure 19B). *SP1*, described in the literature to cooperate with AhR and ARNT for drug-induced *CYP1A1* expression, was also not induced by TCDD treatment either in non-synchronized or synchronized cells (Figure 19B) [241]. Last, Figure 19C shows that disturbance of the circadian rhythmicity with SR8278, had no effect on the fold change of the TCDD-mediated expression of AhR cofactors.

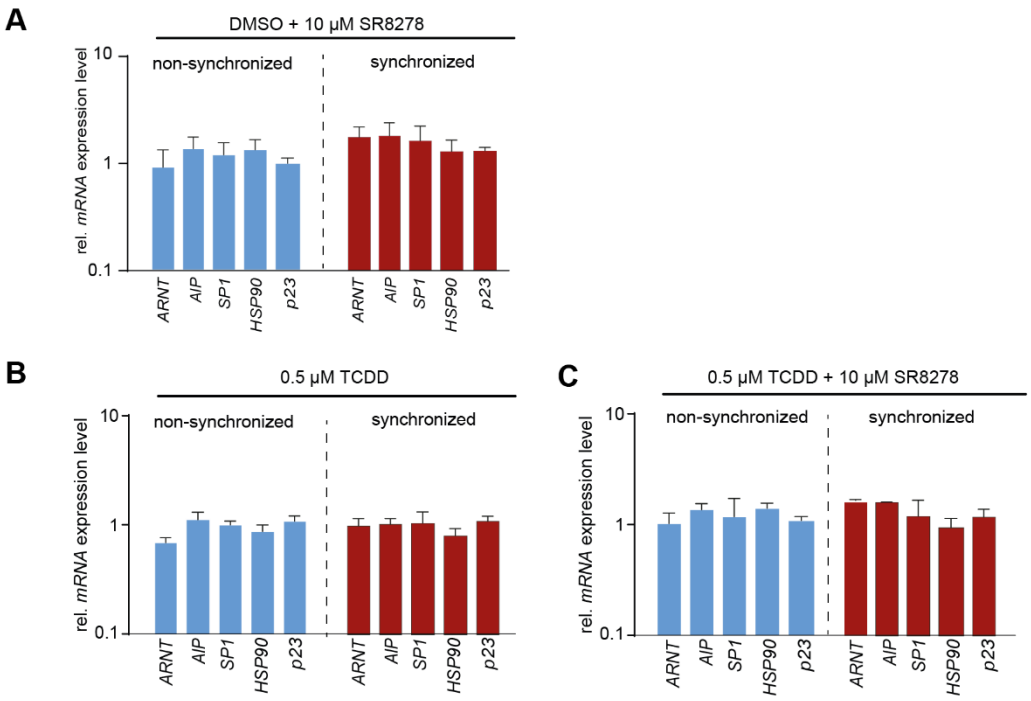

Figure 19: TCDD-mediated gene expression of AhR cofactors is not enhanced upon synchronization
A), B), and C) HME1_PLB cells were treated after synchronization (or not) with 1µM dexamethasone for 24 h with DMSO, DMSO plus SR8278 (10µM), TCDD (0.5 nM), and TCDD (0.5 nM) plus SR8278 (10 µM), and the mRNA expression of AhR cofactors was analyzed by RT-qPCR. The mRNA expression of *AIP*, *SP1*, *ARNT*, *HSP90,* and *p23* was normalized to the endogenous control *B2M,* and the fold change of the AhR cofactors mRNA expression for DMSO plus SR8278 (A), TCDD (B), and TCDD plus SR8278 (C) treated cells was calculated based on the respective control DMSO treated cells. No difference in the TCDD-mediated gene expression of the AhR cofactors was observed upon synchronization. (mean±SD, n=3).

3.6.2 Identification of AhR signaling components displaying a circadian mRNA expression

To investigate if the AhR cofactors in the presence of an AhR ligand are expressed in a circadian manner, the expression of *p23*, *AIP*, *SP1*, *HSP90,* and *ARNT* in non-synchronized and synchronized TCDD-treated cells was analyzed by RT-qPCR over time. Therefore, non-synchronized and synchronized HME1_PLB cells were treated with 0.5 nM TCDD over time. Cell samples were collected every 12 h for a time span of 48 h, and the *p23*, *AIP*, *SP1*, *HSP90,* and *ARNT* expression was determined by RT-qPCR analysis. The gene expression was normalized to endogenous *B2M* and the fold change for the TCDD-treated cell was calculated in comparison to control DMSO-treated cells, for each individual timepoint. Figure 20A, B, and C show no alterations in the fold change of the gene expression of the AhR cofactors, *p23*, *AIP,* and *HSP90,* in both non-synchronized and synchronized conditions. Similarly, the fold change of *SP1* and *ARNT* expression at 12 h, 24 h, 36 h, and

48 h after synchronization remains constant (Figure 20D, E). Taken together, the circadian expression of AhR target genes is not caused by circadian mRNA expression of the AhR cofactors *p23*, *AIP*, *ARNT*, *HSP90,* or *SP1,* supporting the hypothesis that circadian regulation of the AhR pathway is due to a circadian binding of AhR to the promoter modulated by AhR cofactor or clock genes.

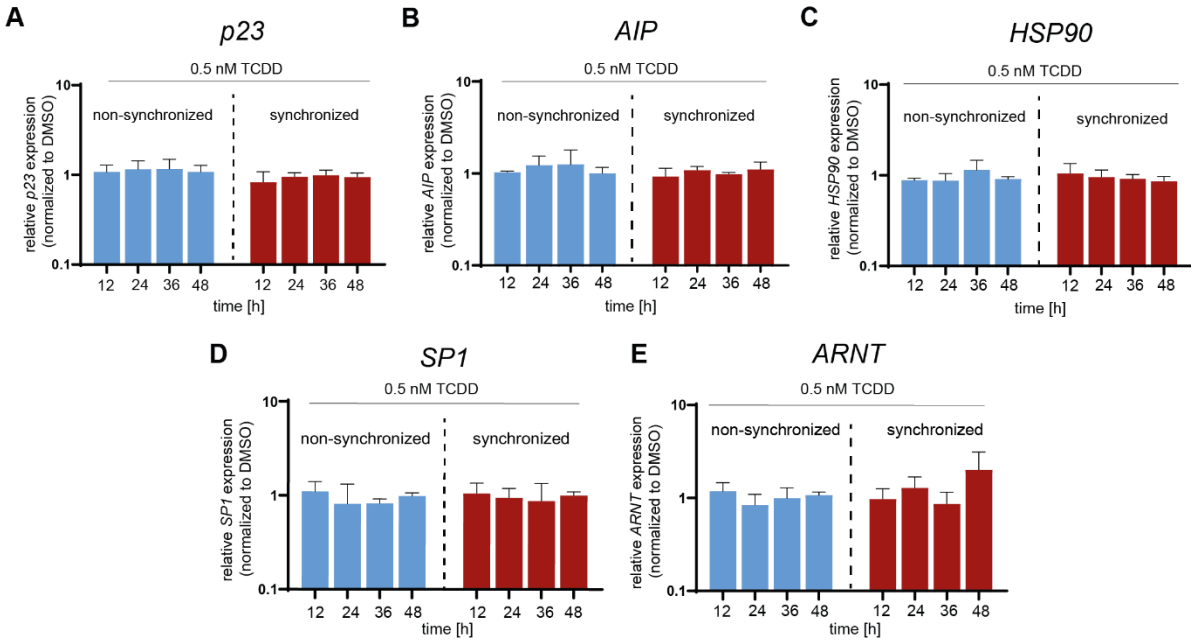

Figure 20: No circadian regulation of the TCDD-mediated gene expression of AhR cofactors
Non-synchronized and synchronized cells were treated with DMSO and TCDD (0.5 nM), and the mRNA expression of *p23*, *AIP*, *SP1, HSP90,* and *ARNT* was analyzed by RT-qPCR at different timepoints. Normalized to the endogenous control *B2M,* and the fold change of the mRNA expression after TCDD treatment for each timepoint was calculated based to the control DMSO of the respective timepoint. In synchronized cells, none of the fold induction of the AhR cofactors shows a circadian pattern. (mean±SD, n=3).

3.6.3 Identification of AhR signaling components displaying a circadian protein expression

Since the mRNA expression of AhR cofactors did not show any circadian regulation, the protein levels over time of synchronized cells upon activated or not AhR signaling were analyzed to identify a potential circadian pattern in the protein expression of AhR components, which would explain the mechanism behind the circadian activation of the *CYP1A1* promoter. Figure 21 shows representative Western blot analysis of synchronized HME1_PLB cells treated with DMSO (control) or TCDD (0.5 nM) for 12 h, 24 h, 36 h, and 48 h. First, AIP is equally expressed at a protein level over a time-period of 48 h upon control DMSO or TCDD exposure in synchronized cells, showing no circadian protein expression. Similarly, HSP90 and p23 protein levels did not show any circadian pattern. However, in

DMSO synchronized cells, SP1 protein levels were reduced after 12 h and 36 h compared to after 24 h and 48 h of synchronization, indicating a circadian oscillation of the SP1 protein level. After exposure to TCDD, the protein levels were reduced at 12 h and 48 h compared to 24 h and 36 h with no circadian pattern. Thus, SP1 could be identified as the first AhR cofactor that shows circadian regulation at protein level. As SP1 has also been described in the literature to influence drug induced *CYP1A1* expression, it represents a good candidate to mediate circadian regulation of *CYP1A1* expression. Its role in the circadian regulation of the AhR pathway was further analyzed and described in the following chapters.

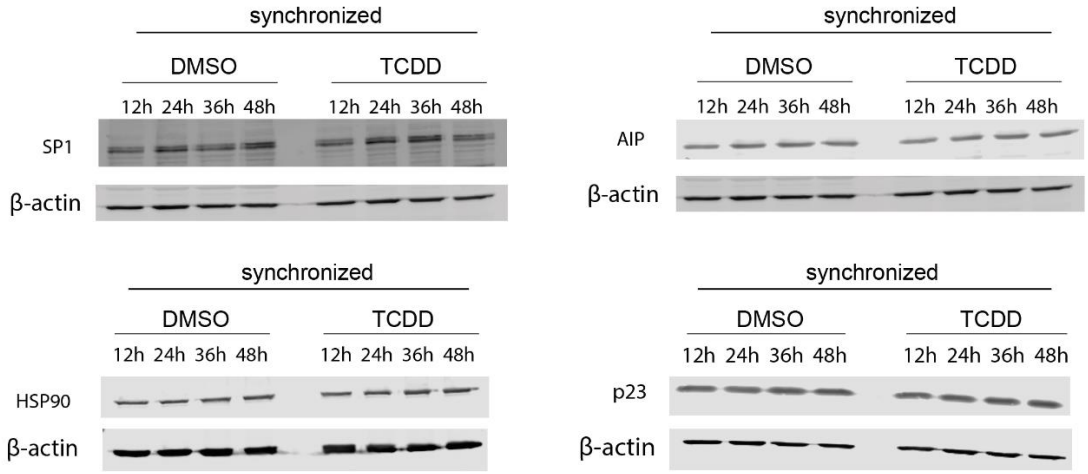

Figure 21: Identification of SP1 as an AhR cofactor with a circadian expression pattern in protein level
Representative Western blots of synchronized cells treated with DMSO or TCDD (0.5 nM). Protein lysates were extracted from synchronized HME1_PLB cells and treated with DMSO (control) or TCDD for 12 h, 24 h, 36 h, and 48 h. Then, the proteins were separated through SDS-PAGE and analyzed by Western blot. The AhR cofactors, SP1 (~90 kDa), AIP (~38 kDa), HSP90 (~90 kDa), and p23 (~25 kDa), were detected with specific antibodies. β-Actin was detected, at ~42 kDa, as loading control and showed an equal expression between the loading samples, enabling a direct comparison of the other proteins of interest between them. No circadian pattern in protein expression was identified for p23, AIP, and HSP90, whereas SP1 showed a circadian rhythmicity upon DMSO with the highest protein levels after 24 h and 48 h of synchronization. (n=4).

3.7 The effect of AhR signaling components on TCDD-induced *CYP1A1* expression in synchronized cells

After the transcription and translation of AhR cofactors were analyzed for circadian regulation, the next step was to investigate the role of AhR cofactors on the circadian regulation of *CYP1A1*. Therefore, AhR cofactors were downregulated by siRNA knockdown in M13SV1 cells, and the *CYP1A1* expression was determined after 24 h of synchronization with or without TCDD treatment. The cells were transfected with siRNA targeting the following AhR cofactors: AhR, ARNT, p23, AHRR, AIP, HSP90, and SP1. After

synchronization of the cells, a treatment with 0.5 nM or 2 nM TCDD was performed, and 24 h later, the cells were subjected to RNA isolation and analysis by RT-qPCR. Figure 22A shows the dependence of *CYP1A1* induction by TCDD in non-synchronized and synchronized cells of AhR cofactor knockdown cells to control scrambled siRNA (SCR) transfected cells. In addition, Figure 22B shows the analysis of the siRNA knockdown efficiency. For analysis of the *CYP1A1* induction after downregulation of genes, first the *CYP1A1* gene expression was normalized to endogenous *B2M,* and then the *CYP1A1* induction by TCDD was calculated based on the DMSO control. Subsequently, the dependence of the *CYP1A1* induction by TCDD on different AhR components was determined by calculating the fold change of the *CYP1A1* induction between cells with downregulated genes and the control cells transfected with scrambled siRNA (SCR) (Figure 22A). In non-synchronized cells, siRNA-mediated knockdown of *AhR*, *ARNT*, and *AIP* showed an approx. 40% decrease in *CYP1A1* induction by TCDD. Similarly, in synchronized cells, *AhR*, *ARNT,* and *AIP* siRNA achieved an approx. 60% decrease in the TCDD-mediated *CYP1A1* induction. These data correlate with the literature supporting that a downregulation of these genes results in reduced activation of the *CYP1A1* promoter, despite the circadian synchrony [165, 242, 243]. However, *HSP90* downregulation appeared to have no effect on TCDD-mediated *CYP1A1* induction in either non-synchronized or synchronized conditions. AHRR repression showed a decrease (0.7-fold) in TCDD-mediated *CYP1A1* induction only in non-synchronized cells. Further, downregulation of *SP1* exhibits a tendency toward a decrease in *CYP1A1* induction by TCDD in contrast to SCR control in both synchronized and non-synchronized cells (0.75-fold, and 0.82-fold change, respectively). Most interestingly, in non-synchronized cells, a *p23* knockdown caused a possible decrease in the *CYP1A1* induction by TCDD (0.74-fold), but in synchronized cells, its knockdown achieved an almost 2.5-fold increase. These data indicate that p23 might play an important role in the *CYP1A1* induction by TCDD in synchronized cells compared to non-synchronized cells, and may negatively regulates the circadian modulation of the AhR-target gene expression.

Figure 22B shows the knockdown efficiency of each gene using the respective siRNA and ensures that the effects observed are a result of downregulation of the corresponding gene. Each bar in the graph shows the fold change in expression of the gene downregulated by siRNA in transfected cells compared to the fold change in expression of that gene in SCR control cells. In non-synchronized cells, more than 40% downregulation was achieved for *AhR*, *ARNT*, *p23*, *AIP,* and *SP1,* as well as only 20% for *AHRR* and *HSP90*. Although, in synchronized cells, a downregulation of over 30% could be achieved through *AhR*, *ARNT*, *AIP*, *SP1*, *HSP90*, *p23*, and *AHRR* siRNA for each corresponding gene. These data verify

that the effects on the *CYP1A1* induction are a result of alterations in the expression of the AhR cofactors themselves. However, weak effects, as observed for *HSP90* and *AHRR* siRNA, might also be due to an ineffective reduction of the protein level. In future studies, stable knockdown or knockout cell lines should be generated to get a more comprehensive picture of the cofactor dependence of this regulation. For now, the subsequent work was focused on further characterization of the *p23* and *SP1* knockdown effects.

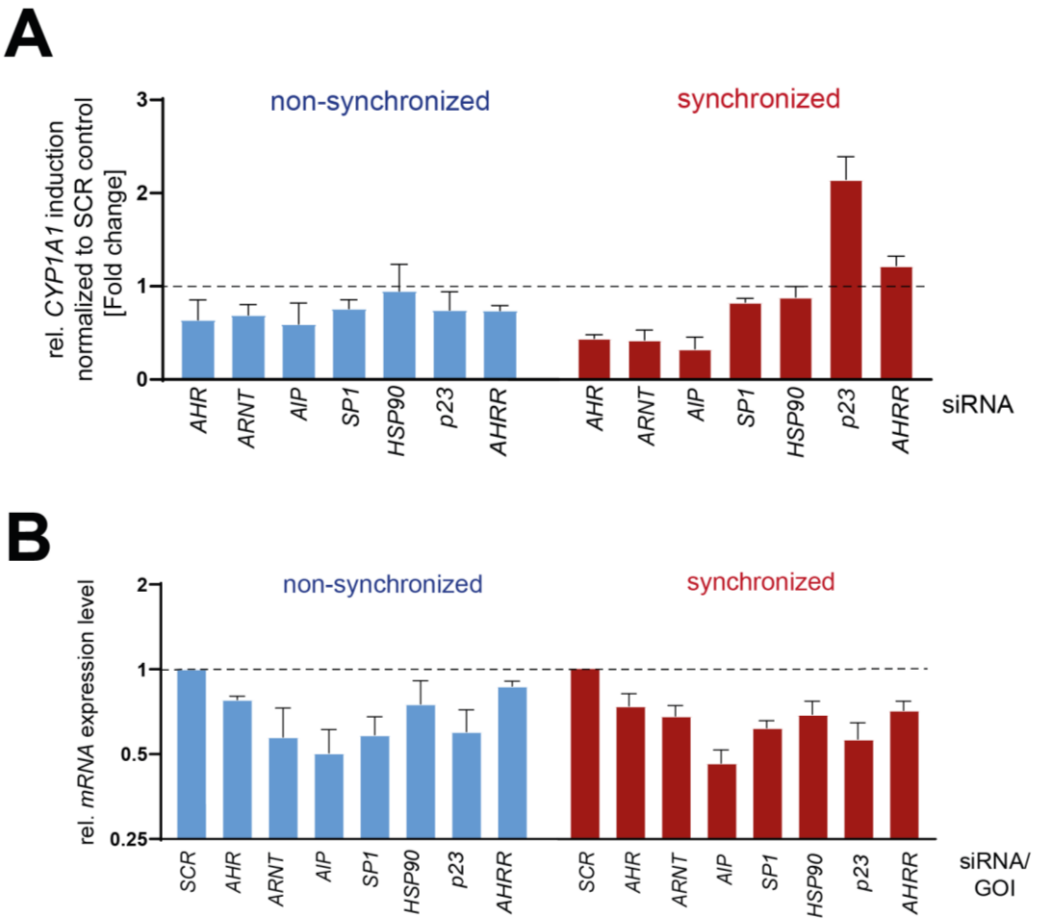

Figure 22: Identification of AhR cofactors, modulating the TCDD-mediated CYP1A1 induction
M13SV1 cells were transfected with siRNAs of the following AhR signaling components: AhR, ARNT, AIP, SP1, HSP90, p23, and AHRR. Transfection of scrambled (SCR) siRNA served as control. After 48 h of transfection, the cells were synchronized or not and treated with two different concentrations of TCDD (0.5 nM or 2 nM) for 24 h. The *CYP1A1* (A) and AhR cofactors (B) mRNA expression were analyzed by RT-qPCR, and normalized to the endogenous control *B2M*. A) The fold change of the *CYP1A1* expression after TCDD treatment was calculated based on the respective DMSO treatment, and then the TCDD-mediated *CYP1A1* induction of the siRNA condition was normalized in relation to the respective SCR control condition. B) The efficiency of each siRNA to achieve a knockdown was calculated by normalizing the AhR cofactor mRNA expression of the corresponding siRNA transfected cells to the expression of the SCR control transfected cells, upon DMSO. The siRNAs could achieve, at least in the synchronized cells, a knockdown of at least 0.7-fold change, i.e. 30% knockdown. (mean±SD, n=3).

3.8 The AhR cofactor p23 regulates induction of AhR target genes

The AhR cofactor p23 was identified as a possible, additional to SP1, candidate playing an important role in the mechanism behind the circadian regulation of the AhR pathway. Further studies were conducted to unravel its exact role in this regulation. First, the effect of both p23 suppression and overexpression on the TCDD-mediated CYP1A1 induction at different timepoints of synchronization was analyzed by RT-qPCR to identify time-dependent changes. Additionally, this would show whether a *p23* overexpression represses TCDD-mediated *CYP1A1* induction, leading to a reverse effect of the p23 suppression that enhances TCDD-mediated CYP1A1 induction (3.8.1). Second, the TCDD-dose response *CYP1A1* induction was analyzed in *p23* downregulated or upregulated synchronized cells and compared to synchronized SCR or empty vector control cells (3.8.2). This would elucidate the effect of p23 on the circadian induction of *CYP1A1* after treatment with different TCDD concentrations.

3.8.1 Overexpression or downregulation of p23 alters the TCDD-mediated *CYP1A1* induction in synchronized cells

To identify the role of p23 on the enhanced TCDD-mediated *CYP1A1* induction upon synchronization, the *p23* expression in M13SV1 cells was either downregulated by *p23* siRNA or upregulated via transfection with a *p23-GFP* overexpression plasmid before the cells were synchronized (or not) and treated with TCDD (0.5 nM). Subsequently, the *CYP1A1* expression was analyzed by RT-qPCR. First, the fold change of *CYP1A1* induction by TCDD was calculated to the induction by DMSO of non-synchronized and synchronized control SCR cells and compared to p23 suppressed or overexpressed cells after 12 h and 24 h of synchronization. Figure 25A shows the fold change of the TCDD-mediated *CYP1A1* induction of non-synchronized and synchronized *p23* suppressed cells normalized to the control (SCR) cells. In addition, Figure 25B shows the corresponding TCDD-mediated *CYP1A1* induction of *p23* overexpressed cells normalized to the control (*empty vector*) cells. In non-synchronized cells, the downregulation of *p23* had no effect on the fold change of the TCDD-mediated *CYP1A1* induction. Thus, in synchronized *p23* knockdown cells, there was an approx. 1.7-fold change in TCDD-induced *CYP1A1* expression after 24 h of synchronization compared to the control (SCR) cells (Figure 25A). Figure 25B shows that *p23* overexpression in non-synchronized cells resulted in a slight reduction in TCDD-mediated *CYP1A1* expression compared to control cells, i.e. approx. 40% and 30% reduction upon 12 h and 24 h after synchronization, respectively. However, the fold change of the TCDD-mediated *CYP1A1* expression normalized to control (SCR) cells was much more decreased upon synchronization, where the reduction was 50% and 70% at 12 h and

24 h after synchronization, respectively. These data indicate that p23 is a negative regulator of the circadian-dependent *CYP1A1* induction.

Figure 25B and Figure 25C show the efficiency of *p23* siRNA and the *p23 GFP* overexpression plasmid to suppress and overexpress *p23*, respectively. In non-synchronized and synchronized cells of both timepoints (12 h and 24 h after synchronization), an approx. 60% downregulation was achieved compared to the control transfected with SCR siRNA (Figure 25C). Similar, Figure 25D shows that a successful overexpression of *p23* was achieved in both non-synchronized and synchronized cells. These data verify that p23-mediated changes in the *CYP1A1* induction are due to a successful manipulation of the p23 expression.

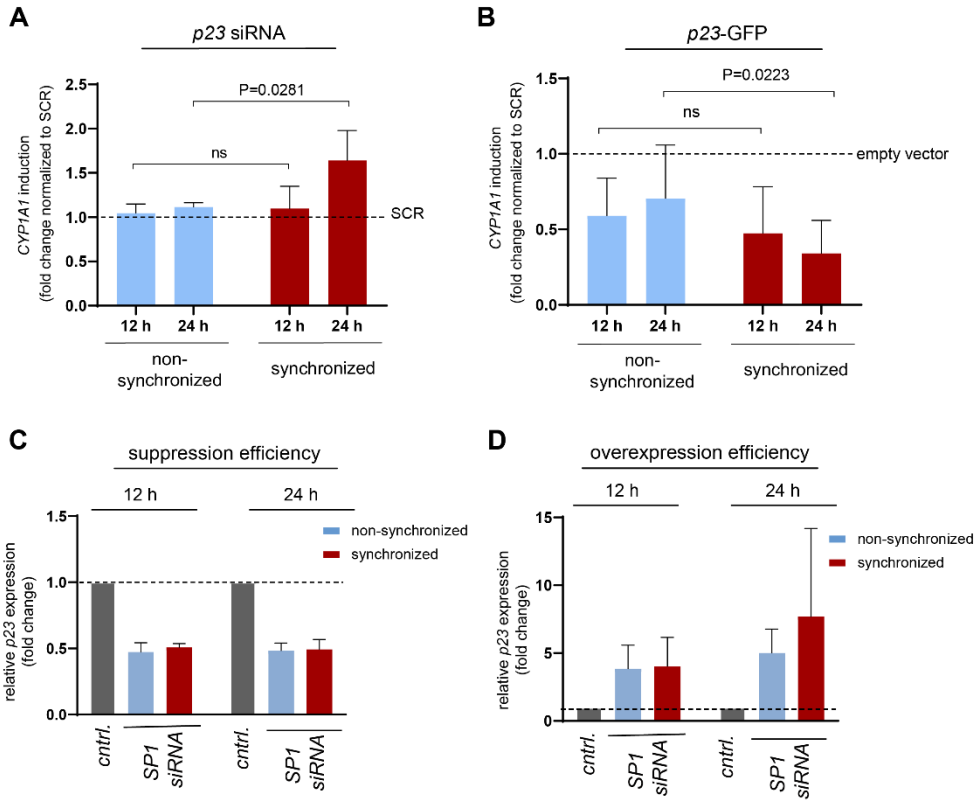

Figure 23: Alterations in p23 expression change TCDD-mediated *CYP1A1* induction upon synchronization
A), B), C), and D) After 48 h of transfection with *p23* siRNA or *p23 GFP* overexpression plasmid, M13SV1 cells were synchronized (or not) and treated with TCDD (0.5 nM) for 12 h and 24 h. The *CYP1A1* (A and B) and the *p23* expression (C and D) were analyzed by RT-qPCR and normalized to the endogenous control *B2M*. A) and B) The fold change of the *CYP1A1* expression after TCDD treatment was calculated based on the according DMSO treatment for each condition, and then the TCDD-mediated *CYP1A1* induction of the *p23* knockdown (A) or overexpression (B) cells was normalized in relation to the control cells (SCR (A) or *empty vector* (B)). Statistical analysis was performed between non-synchronized and synchronized conditions of each timepoint by using an one-tailed, unpaired t-test. Statistical significance was accepted at $P \leq 0.05$. C) and D) For each timepoint (12 h and 24 h after synchronization), the efficiency of the *p23* siRNA to achieve a *p23* suppression (C) and the *p23-GFP* plasmid to achieve a *p23* overexpression (D) was calculated by normalizing the *p23* mRNA expression of the *p23* gene-modified cells to the control (SCR (C) or empty vector (D)) cells after DMSO treatment. (mean±SD, n=3).

3.8.2 Manipulation of the p23 expression alters dose response curves of *CYP1A1* expression after TCDD treatment

To analyze the effect of p23 on the TCDD dose response of *CYP1A1* induction, M13SV1 cells were transient-transfected with control (SCR for siRNA transfection or *empty vector* for plasmid transfection), *p23* siRNA, or *p23-GFP* overexpression plasmid, and 48 h after transfection, the cells were synchronized and treated with 0.1 nM, 0.25 nM, 0.5 nM, 1 nM, or 2 nM TCDD for 24 h. Additionally, non-synchronized and synchronized cells treated with the different TCDD concentrations were analyzed as control for the synchronized ones. Figure 24A and B show dose response curves of *CYP1A1* induction in control and p23 suppressed or overexpressed M13SV1 cells after 24 h of exposure to TCDD. The fold change of *CYP1A1* induction at different TCDD concentrations was determined based on the DMSO of the corresponding condition. As expected, the induction of *CYP1A1* after a TCDD dose dependent treatment was enhanced in control synchronized cells compared to the non-synchronized and synchronized treated with SR8278 cells, confirming that the synchronization of the cells was successful. Disrupting the circadian rhythm with SR8278 reduced the enhanced *CYP1A1* induction to the level of the non-synchronized cells. The TCDD dose response curve of *CYP1A1* was increased in synchronized p23 knockdown cells compared to the control synchronized, and the curves had a difference of approx. 1.6-fold in the lower TCDD concentrations (0.25 nM and 0.5 nM) and 1.9-fold in the higher TCDD concentrations (1 nM and 2 nM) (Figure 24A). The *p23* overexpressed and synchronized cells exhibit a slight decrease in *CYP1A1* induction after TCDD dose dependent treatment compared to the control synchronized cells (Figure 24B).

Figure 24C shows the fold change of the *p23* expression in the *p23* downregulated or upregulated cells normalized to the control cells (SCR or *empty vector*) depicted in Figure 24A and B to determine the transfection efficiency of the *p23* siRNA and *p23-GFP* overexpression plasmid. Both could successfully suppress or overexpress *p23* gene expression, indicating that the effects observed on the TCDD dose dependent *CYP1A1* induction reflect alterations in p23 expression. All in all, these findings support the involvement of p23 in the circadian regulation of the AhR signaling.

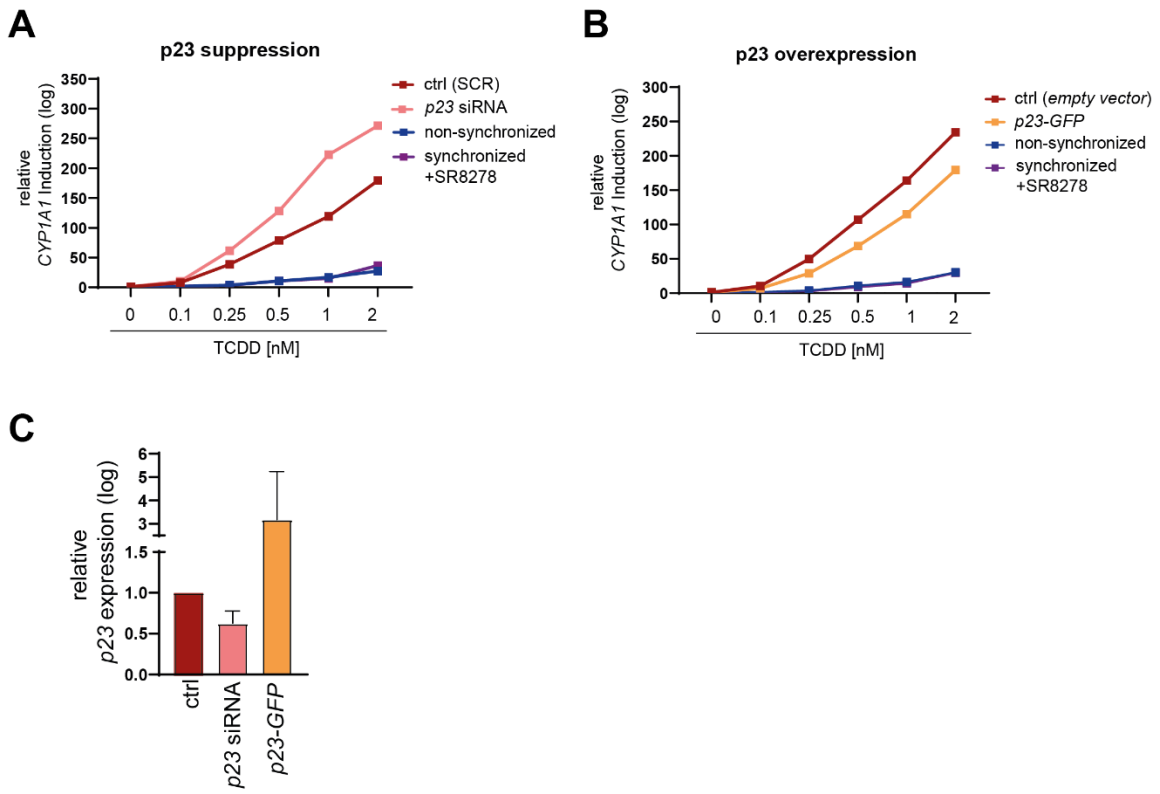

Figure 24: p23 negatively regulates the TCDD-mediated *CYP1A1* induction
A) and B) Dose response curves of *CYP1A1* gene expression in non-synchronized, synchronized with disturbed circadian rhythm through SR8278, and synchronized transfected with scrambled siRNA (SCR), control plasmid (*empty vector*), *p23* siRNA or *p23* overexpression plasmid (*p23-GFP*) M13SV1 cells. The cells were transfected with *p23* siRNA, or *p23-GFP* overexpression plasmid to suppress or overexpress p23. As a control, cells were transfected with scramble (SCR) siRNA for the p23 downregulation and with *empty vector* plasmid for the p23 overexpression. Then, these cells were synchronized with 1 µM dexamethasone for 1 h and treated with different TCDD concentrations (0.1 nM, 0.25 nM, 0.5 nM, 1 nM, and 2 nM). Also, non-synchronized cells and synchronized cells treated with SR8278 (10 µM) to interfere with the circadian synchrony were treated with the same TCDD concentration for 24 h. The *CYP1A1* mRNA expression was analyzed by RT-qPCR and normalized to the endogenous control *B2M*. The fold change of the *CYP1A1* expression after TCDD treatment was calculated based on the respective DMSO for each condition. B) The efficiency of the *p23* siRNA and the *p23-GFP* overexpression plasmid to achieve a p23 downregulation and upregulation, respectively, was calculated by normalizing the *p23* expression of the *p23* downregulated or upregulated cells to the expression of the control SCR or *empty vector* cells after DMSO treatment. (mean±SD, n=3).

3.9 SP1 modulates the circadian regulation of the AhR pathway

SP1 showed a circadian regulation in protein level (Figure 21) implying in general that this gene plays a part in circadian rhythmicity, and more specifically, potentially in the circadian regulation of the AhR pathway, as data support that it is an AhR signaling cofactor. To better understand its role in circadian regulation of the AhR signaling and specific modulating *CYP1A1* expression, experiments altering the SP1 expression and analyzing the TCDD-mediated *CYP1A1* induction were performed. First, the effect of SP1 suppression on the

CYP1A1 induction by TCDD in non-synchronized and synchronized M13SV1 cells was investigated at two different time-points (3.9.1). Second, the TCDD-dose response *CYP1A1* induction was analyzed for SP1 suppressed and overexpressed synchronized cells and compared to synchronized (SCR or *empty vector*), non-synchronized, and synchronized treated with SR8278 cells (3.9.2).

3.9.1 Effect of SP1 suppression on TCDD-mediated *CYP1A1* induction

Experiments were performed in which SP1 was silenced by siRNA in synchronized or non-synchronized M13SV1 cells treated with 0.5 nM TCDD, and the *CYP1A1* expression was determined by RT-qPCR. First, the fold change of *CYP1A1* induction by TCDD was calculated to the induction by DMSO of non-synchronized and synchronized control SCR cells and compared to SP1 suppressed cells, after 12 h and 24 h of synchronization. Figure 25A shows the fold change of the TCDD-mediated *CYP1A1* induction of non-synchronized and synchronized SP1 suppressed cells normalized to the control (SCR). In non-synchronized cells, the downregulation of *SP1* has no effect on the fold change of the TCDD-mediated *CYP1A1* induction. In contrast, in synchronized *SP1* knockdown cells, there is a 50% decrease in TCDD-induced *CYP1A1* expression after 12 h of synchronization and a 30% decrease after 24 h of synchronization compared to the control (SCR) cells. The fold change of the TCDD-mediated *CYP1A1* expression in *SP1* knockdown cells is lower after 12 h of synchronization in contrast to the one after 24 h.

Figure 25B shows the knockdown efficiency of the *SP1* siRNA. In non-synchronized cells at both timepoints (12 h and 24 h after synchronization), an approx. 40% downregulation was achieved compared to the control transfected with scrambled siRNA (SCR). Similarly, for the cells synchronized for 12 h and 24 h, a downregulation of approx. 30% was observed compared to control cells. These data show that the *SP1* siRNA successfully downregulated SP1 for a timespan of over 72 h and the changes on the circadian-dependent *CYP1A1* induction are due to the *SP1* suppression. Summarizing, SP1 plays an important role in the induction of AhR target genes (e.g. *CYP1A1*) and possibly in the modulation of the circadian regulation of the AhR pathway.

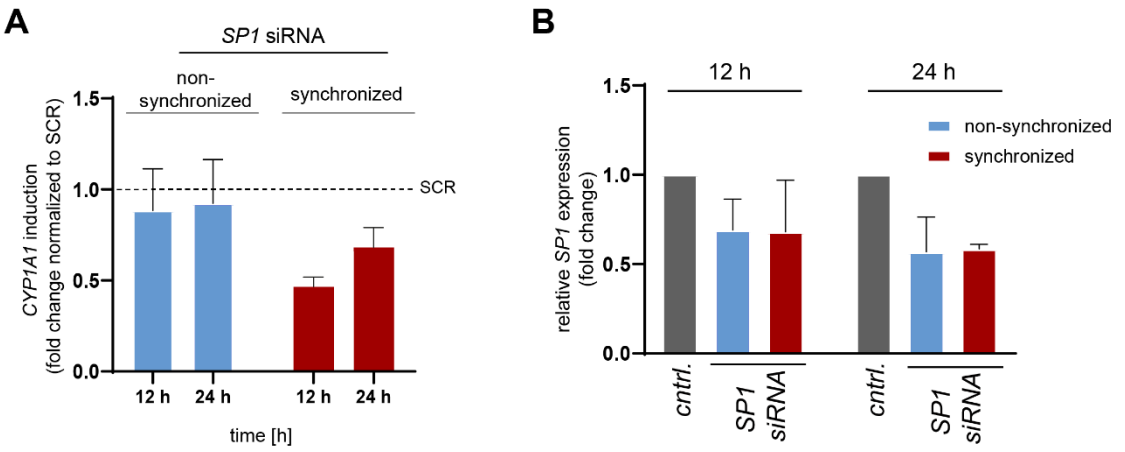

Figure 25: Suppression of SP1 decreases the TCDD-mediated *CYP1A1* induction upon synchronization
After 48 h of transfection of M13SV1 cells with *SP1* siRNA, the cells were synchronized or not with 1 µM dexamethasone for 1 h and treated with TCDD (0.5 nM) for 12 h and 24 h. The *CYP1A1* (A) and *SP1* (B) expression was analyzed by RT-qPCR and normalized to the endogenous control *B2M*. A) The fold change of the *CYP1A1* expression after TCDD treatment was calculated based on the respective DMSO for each condition, and then the TCDD-mediated *CYP1A1* induction of the *SP1* knockdown cells was normalized in relation to the SCR control cells. B) The efficiency of the *SP1* siRNA to achieve a *SP1* downregulation was calculated by normalizing the *SP1* expression of the *SP1* knockdown cells to the expression of the SCR control cells after DMSO treatment. (mean±SD, n=2).

3.9.2 Manipulation of the SP1 expression alters dose response curves of *CYP1A1* expression after TCDD treatment

To analyze the impact of SP1 on the dose response of *CYP1A1* induction after treatment with TCDD in circadian synchronized cells, M13SV1 cells were transfected with control (SCR for siRNA transfection or *empty vector* for plasmid transfection), *SP1* siRNA, or *SP1* overexpression plasmid, and 48 h after transfection, the cells were synchronized and treated with 0.1 nM, 0.25 nM, 0.5 nM, 1 nM, or 2 nM TCDD for 24 h. Additionally, non-synchronized and synchronized cells treated with the different TCDD concentrations were analyzed as control to the synchronized ones. Figure 26A and B show dose response curves of *CYP1A1* induction in control and SP1 suppressed or overexpressed M13SV1 cells after 24 h of exposure to TCDD. The fold change of *CYP1A1* induction at different TCDD concentrations was determined based on the DMSO of the corresponding condition. Again, as expected, the induction of *CYP1A1* after a TCDD dose dependent treatment was enhanced in control synchronized cells compared to the non-synchronized and synchronized treated with SR8278 cells, confirming that the synchronization of the cells was successful. The *SP1* suppressed and synchronized cells exhibit a slight decrease in *CYP1A1* induction after TCDD dose dependent treatment compared to the control synchronized cells. These data support the observations shown in Figure 26A and B,

indicating that SP1 modulates the *CYP1A1* induction in synchronized cells. Vice versa, the TCDD dose response curve of *CYP1A1* was increased in synchronized cells overexpressing SP1 compared to the control synchronized cells,and the curves had a difference of approx. 1.4-fold for each TCDD concentration.

Figure 26C shows the fold change of the *SP1* gene expression in SP1 suppressed or overexpressed cells normalized to the control cells (SCR or empty vector), which were used to perform the experiments shown in Figure 26A and B. The *SP1* siRNA could successfully suppress *SP1* mRNA expression, as the expression of *SP1* was 50% reduced in SP1 siRNA transfected cells. However, analyzing the SP1 overexpressed cells, no upregulation of *SP1* could be verified at mRNA level. The *SP1* upregulation at mRNA level could not be detected with RT-qPCR analysis, possibly because the primer was not suitable to identify and amplify the overexpression plasmid. Therefore, Western blot analysis of the samples was performed to verify the suppression and overexpression at protein level (Figure 26D). Detection of SP1 on the blots revealed two bands in the SP1 overexpressed cells indicating the success of the *SP1* overexpression plasmid in increasing the SP1 protein level. Additionally, the SP1 protein level of SP1 suppressed cells was reduced compared to control cells, verifying that the suppression was successful also in protein level. All this indicates that the effects observed on the TCDD dose-dependent *CYP1A1* induction reflects alterations in the SP1 expression. All in all, SP1 seems to have a pivotal role in the circadian regulation of the AhR signaling.

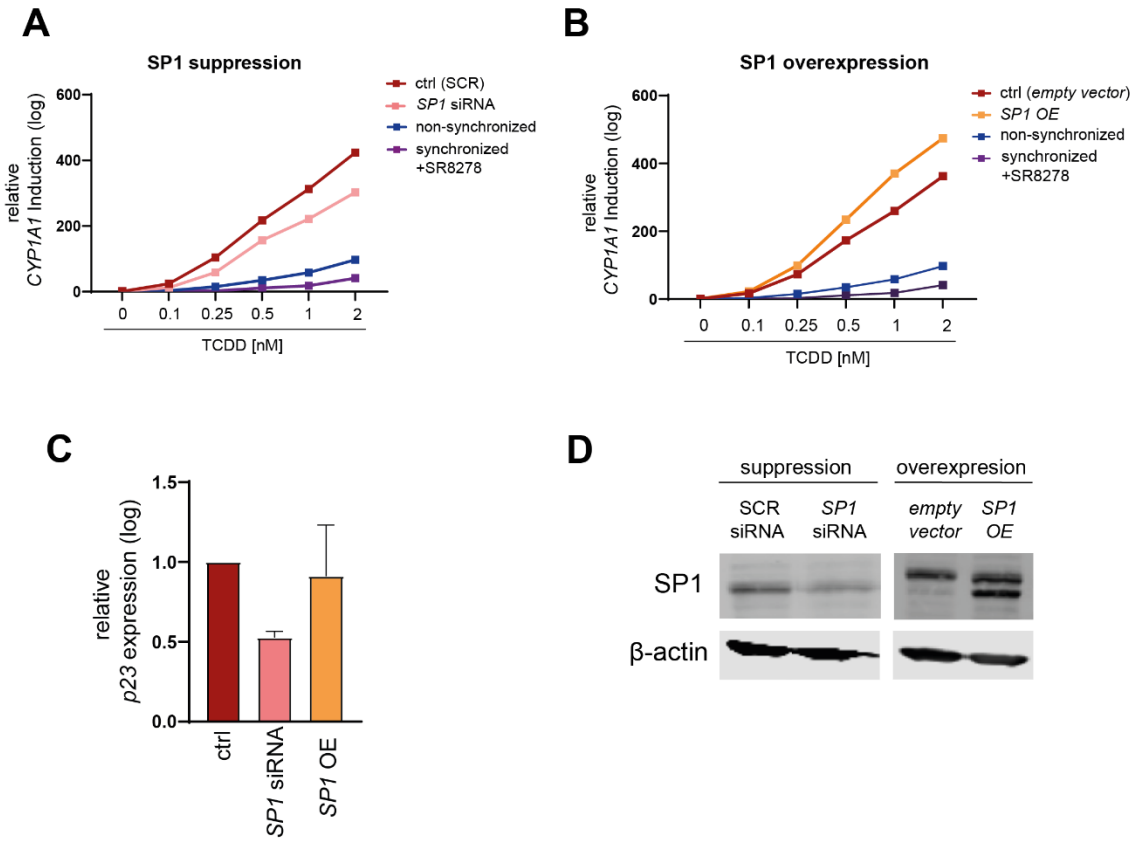

.

Figure 26: SP1 promotes the TCDD-mediated *CYP1A1* expression upon synchronization
A) and B) TCDD-dose response curves of *CYP1A1* expression in non-synchronized, synchronized with disturbed circadian rhythm through SR8278, and synchronized transfected with control (SCR or *empty vector*), *SP1* siRNA, or SP1 overexpression plasmid M13SV1 cells. The cells were transfected with *SP1* siRNA or *SP1* overexpression plasmid to downregulate or upregulate SP1 expression. As control, cells were transfected with scramble (SCR) siRNA for the *SP1* downregulation and with an *empty vector* plasmid for the upregulation. Then, these cells were synchronized with 1 µM dexamethasone and treated with different TCDD concentrations (0.1 nM, 0.25 nM, 0.5 nM, 1 nM, and 2 nM). Non-synchronized and synchronized cells treated with SR8278 (10 µM) to disrupt circadian synchrony were also treated with the same concentration of TCDD for 24h. The *CYP1A1* expression was analyzed by RT-qPCR and normalized to the endogenous control *B2M*. The fold change of the *CYP1A1* expression after TCDD treatment was calculated based on the respective DMSO for each condition. C) The efficiency of the *SP1* siRNA and the *SP1* overexpression plasmid to achieve a *SP1* downregulation and upregulation, respectively, at mRNA level was calculated by normalizing the *SP1* mRNA expression of the SP1 suppressed or overexpressed cells to the expression of the control cells after DMSO treatment. D) Representative Western blot stained for SP1 to identify whether transfection with *SP1* siRNA or *SP1* overexpression plasmid could achieve SP1 downregulation or upregulation in protein level. Bands specific for SP1 were identified at ~90 kDa and β-actin was detected, at ~ 42 kDa, as loading control. (mean±SD, n=3).

3.10 Comparison of the translocation of AhR cofactors between non-synchronized and synchronized TCDD-treated cells

AhR and several of its signaling cofactors are translocated into the nucleus after ligand exposure. Translocation experiments were performed to analyze the localization of AhR and its cofactors, with a specific focus on p23, which was already identified to play an important role in the circadian regulation of the AhR pathway. At this point, it is important to mention that SP1 was not further analyzed in the translocalization studies, as it is located only in the nucleus and has no relation to the translocation mechanism of the AhR from the cytoplasma to the nucleus [244, 245]. Cell fractionation (3.10.1) and immunofluorescent experiments (3.10.2) were conducted to identify whether there is a difference in localization (nuclear or cytoplasmic) of AhR signaling components between non-synchronized and synchronized cells that could explain the enhanced induction of the AhR target genes upon synchronization. For example, if the localization of a component was enhanced or reduced in the nucleus of synchronized cells in comparison to non-synchronized cells, it would imply that it enhances or represses AhR signaling and the expression of the target genes. This could be supportive evidence of the involvement of this component in the circadian regulation of the AhR signaling pathway.

3.10.1 Analysis of nucleolar and cytoplasmic protein levels of AhR signaling components upon TCDD exposure and synchronization

Next, the focus was laid on analyzing and comparing p23 localization in the nucleus and cytoplasm of the cells to better understand its role in the circadian regulation of the AhR signaling. In addition, the localization of AhR itself, AIP, and HSP90 were analyzed, as these last two, together with p23, form the AhR inactivating complex in the cytoplasm and contribute to the AhR translocation in the nucleus after AhR ligand exposure. HME1_PLB cells were first synchronized (or not) with 1 µM dexamethasone for 1 h and after 24 h of synchronization, cells were treated for 1 h with DMSO (control) or TCDD (2 nM). Subsequently, the cell material was divided into cytoplasmic and nuclear fractions, and the proteins of each fraction were isolated and analyzed by Western blot. In both Figure 27 and Figure 28, representative Western blots are shown. As controls for a successful fractionation, Lamin A/C, which should only be detected in the nuclear fraction, and GAPDH, which is only located in the cytoplasm, were used.

Figure 27 shows the protein levels of AhR, HSP90, and AIP in the cytosolic and nuclear fractions of synchronized and non-synchronized cells treated with TCDD (2 nM). More in

detail, TCDD treatment in both non-synchronized and synchronized cells decreased the AhR protein level in the cytoplasm, indicating either its translocation into the nucleus or a rapid degradation after ligand exposure. However, in the nuclear fraction, no bands or very faint ones were detected for AhR, suggesting that probably AhR translocates in the nucleus, activates *the CYP1A1* promoter, and is being degraded very rapidly in the cytoplasm [240]. Thus, the amount of AhR in the nucleus may have been too low to be detected by our Western blot protocol. No difference was observed at the AhR protein level after DMSO or TCDD treatment in the cytoplasm between non-synchronized and synchronized cells. The protein levels of HSP90 in the cytoplasm were the same in all conditions. However, in the nucleus, TCDD exposure decreased the protein levels in both non-synchronized and synchronized cells. The decreased HSP90 protein level was the same between non-synchronized and synchronized cells. On the other hand, in the cytoplasm, AIP protein level was slightly decreased in both non-synchronized and synchronized cells after TCDD treatment. Interestingly, AIP was detected in the nucleus, contradicting the literature, which describes AIP only located in the cytoplasm. Additionally, the AIP protein levels in the nucleus were increased in both DMSO and TCDD-treated synchronized cells but not in non-synchronized cells.

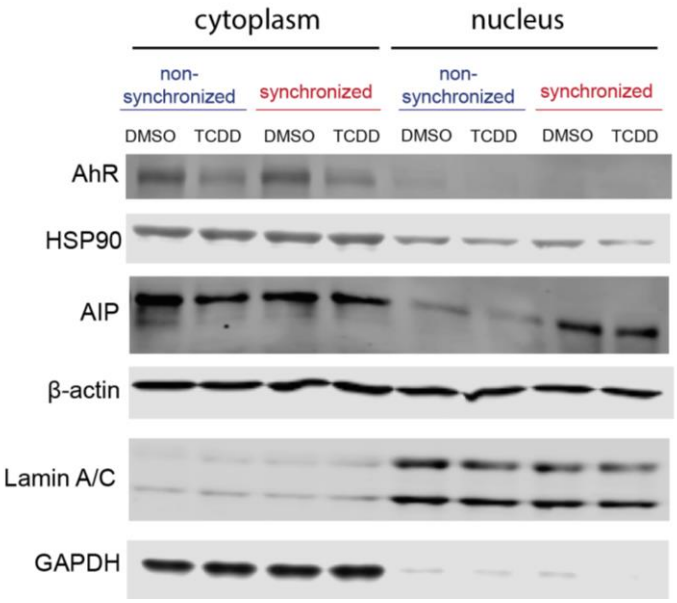

Figure 27: TCDD or synchronization changes the localization of AhR, HSP90 and AIP
Representative Western blot of nuclear and cytoplasmic fractions of HME1_PLB cells upon synchronization or not and after treatment with DMSO (control) or TCDD. After 23 h of synchronization (or not), the cells were treated for 1 h with DMSO or TCDD (2 nM), and subsequently lysed for cell fractionation. Specific protein bands for AhR (~100 kDa), AIP (~38 kDa), and HSP90 (~90 kDa) were detected on the blots by using specific antibodies. In the nucleus, AIP protein levels were increased upon synchronization in both control and TCDD-treated cells. HSP90 protein levels were decreased in the nucleus after TCDD treatment, whereas AhR levels were decreased after TCDD treatment in the cytoplasm. Lamin A/C (~70 kDa) and GAPDH (~37 kDa) were detected to verify the success of the fractionation, as Laminin A/C and GAPDH are localized only in the nucleus and cytoplasm, respectively. β-Actin (~42 kDa) was detected, as loading control. (n=2).

Figure 28 shows the p23 protein levels in non-synchronized or synchronized cells after 1 h of TCDD or DMSO (control) exposure. In the cytoplasm, the bands specific for the p23 protein have approx. the same signal intensity, indicating no influence of TCDD on the p23 protein level. Interestingly, the p23 protein levels in the control DMSO condition are higher in the synchronized cells compared to the non-synchronized. Nonetheless, in the nucleus, TCDD exposure decreases the localization of p23 in both non-synchronized and synchronized cells. This indicates that p23 after TCDD treatment is either less translocated into the nucleus from the cytoplasm or that more and less amount is degraded and expressed, respectively.

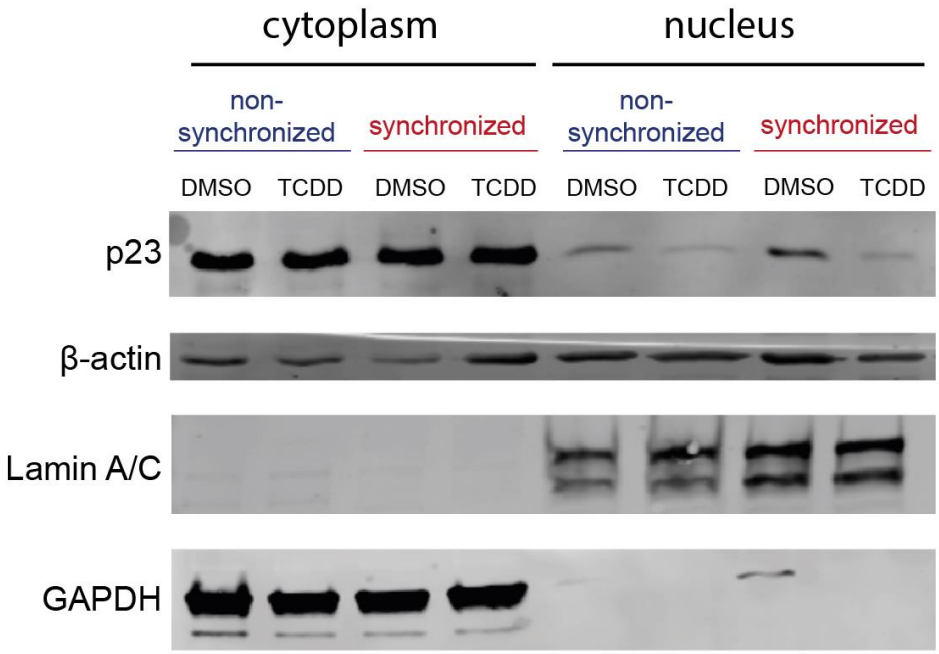

Figure 28: Localization of p23 in the nucleus is altered after TCDD treatment upon synchronization
Representative Western blot of nuclear and cytoplasmic fractions of HME1_PLB cells upon synchronization or not and treatment with DMSO (control) or TCDD (2 nM). After 23 h of synchronization (or not), the cells were treated for 1 h with DMSO or TCDD (2 nM), and subsequently lysed for cell fractionation. Specific protein bands for p23 were detected at ~23 kDa. In the nucleus, p23 protein levels were decreased after TCDD exposure in both non-synchronized and synchronized cells. Lamin A/C (~70 kDa) and GAPDH (~37 kDa) were detected to verify the success of the fractionation, as Laminin A/C and GAPDH are localized only in the nucleus and cytoplasm, respectively. β-Actin (~42 kDa) was detected, as loading control. (n=2).

3.10.2 Effects of synchronization and TCDD treatment on immunofluorescence staining of AhR signaling components

In parallel to the cell fractionation, immunofluorescence staining was performed on HME1_PLB cells to verify the differences in the localization of AhR and the AhR signaling components AIP and p23, which showed some interesting data in the cell fractionation experiments (3.10.1). HME1_PLB cells were synchronized for 24 h and treated with TCDD for 1 h before fixation. Non-synchronized cells treated with DMSO were used as control. Figure 29, Figure 30, and Figure 31 show representative confocal microscopy pictures of the immunofluorescent staining with antibodies specific for AhR, p23, and AIP, respectively. AhR was localized more in the cytoplasm in non-synchronized and synchronized cells treated with DMSO compared to the TCDD-treated cells, supporting the data of the cell fractionation shown in Figure 27. However, in contrast to the lack of detection of nuclear AhR protein by cell fractionation analysis, AhR was localized to the nucleus by immunofluorescence after TCDD treatment. This aligns with the data described in the literature that AhR translocates to the nucleus after ligand binding, and supports the reduction of the AhR protein in the cytoplasm after TCDD exposure, as shown in Figure 27. No difference in AhR localization was identified between non-synchronized and synchronized cells.

Immunostaining for p23, showed that in non-synchronized cells, p23 is localized rather in the nucleus than the cytoplasm, compared to the synchronized cells. The p23 localization was identical between the DMSO and TCDD conditions. These data contradict the cell fractionation experiments (Figure 28) that showed a higher amount of p23 protein in the nucleus of synchronized cells compared to non-synchronized cells upon DMSO and the same amount of protein in the cytoplasm between these two conditions. On the other hand, AIP is described to be localized, independently of ligand exposure, rather in the cytoplasm, but the data shown in Figure 31 identify AIP in both cytoplasm and nucleus regardless of synchronization or TCDD treatment. This matches with the data of the cell fractionation shown in Figure 27, that indicate general AIP localization in both the nucleus and cytoplasm. No difference in AIP localization was observed between non-synchronized and synchronized cells treated with DMSO or TCDD, contradicting the data from the cell fractionation that showed a higher nuclear localization in synchronized cells. However, an exact quantification of p23 and AIP localization in the nucleus compared to the cytoplasm by further analysis of the already existing microscopy pictures with an appropriate program is necessary. This would give more accurate data about the exact localization of p23 and AIP in synchronized and non-synchronized cells. Unfortunately, prioritizing other experiments together with time limitations and technical issues did not enable the

quantification of these data, but it would be of highest interest to further analyze and quantify these microscopy pictures in the future. Summarizing, the difference in p23 localization upon synchronization identified by both immunofluorescence and cell fractionation analysis further support the previous data that p23 plays an important role in the circadian regulation of the AhR signaling.

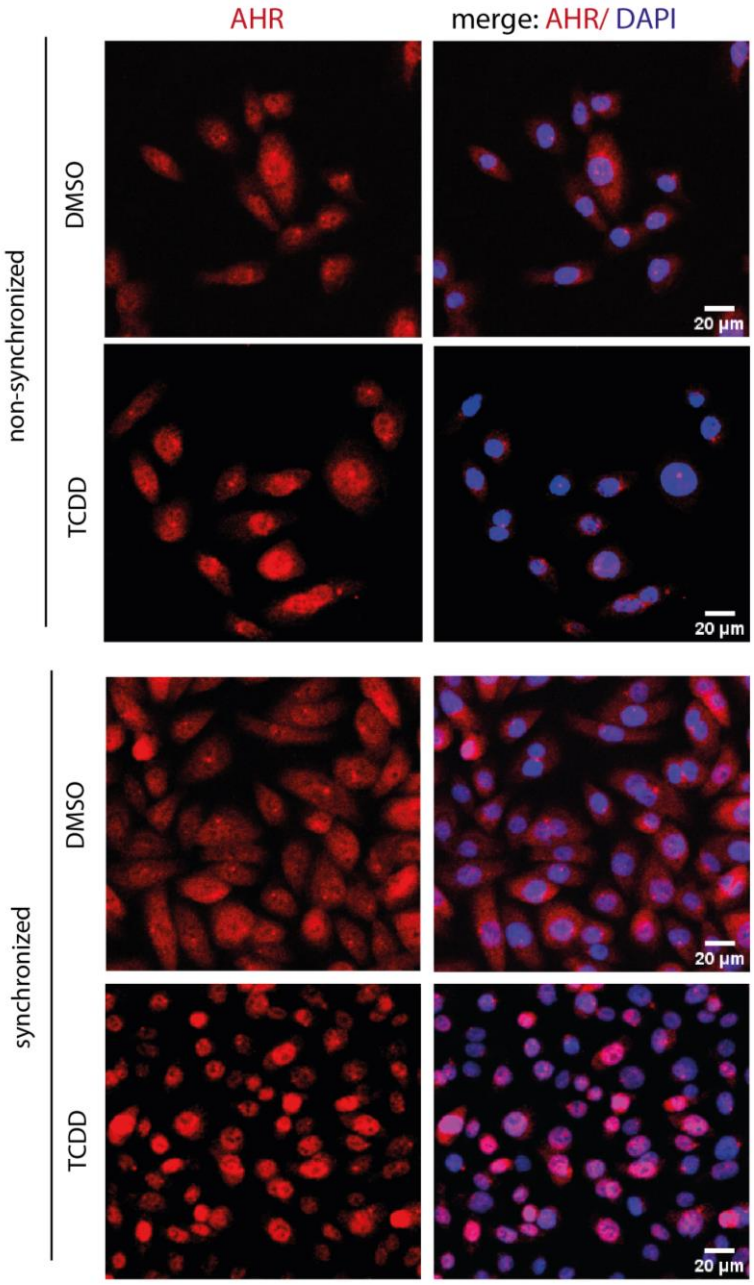

Figure 29: TCDD treatment increased AhR localization in the nucleus in both non-synchronized and synchronized cells
Representative images of non-synchronized and synchronized HME1_PLB cells in the presence or absence of TCDD treatment stained for AhR. After 23 h of synchronization, the cells were treated for 1 h with DMSO or TCDD (2 nM), and subsequently fixated. The localization of AhR is shown in red, and DAPI, staining the nuclei, in blue. Images (Z-stacks) of at least 4 different positions on the slide were taken for each condition by using the confocal microscope, Zeiss LSM 880 AiryScan, and a 40x air objective. Scale bar: 20 µM. (n=3).

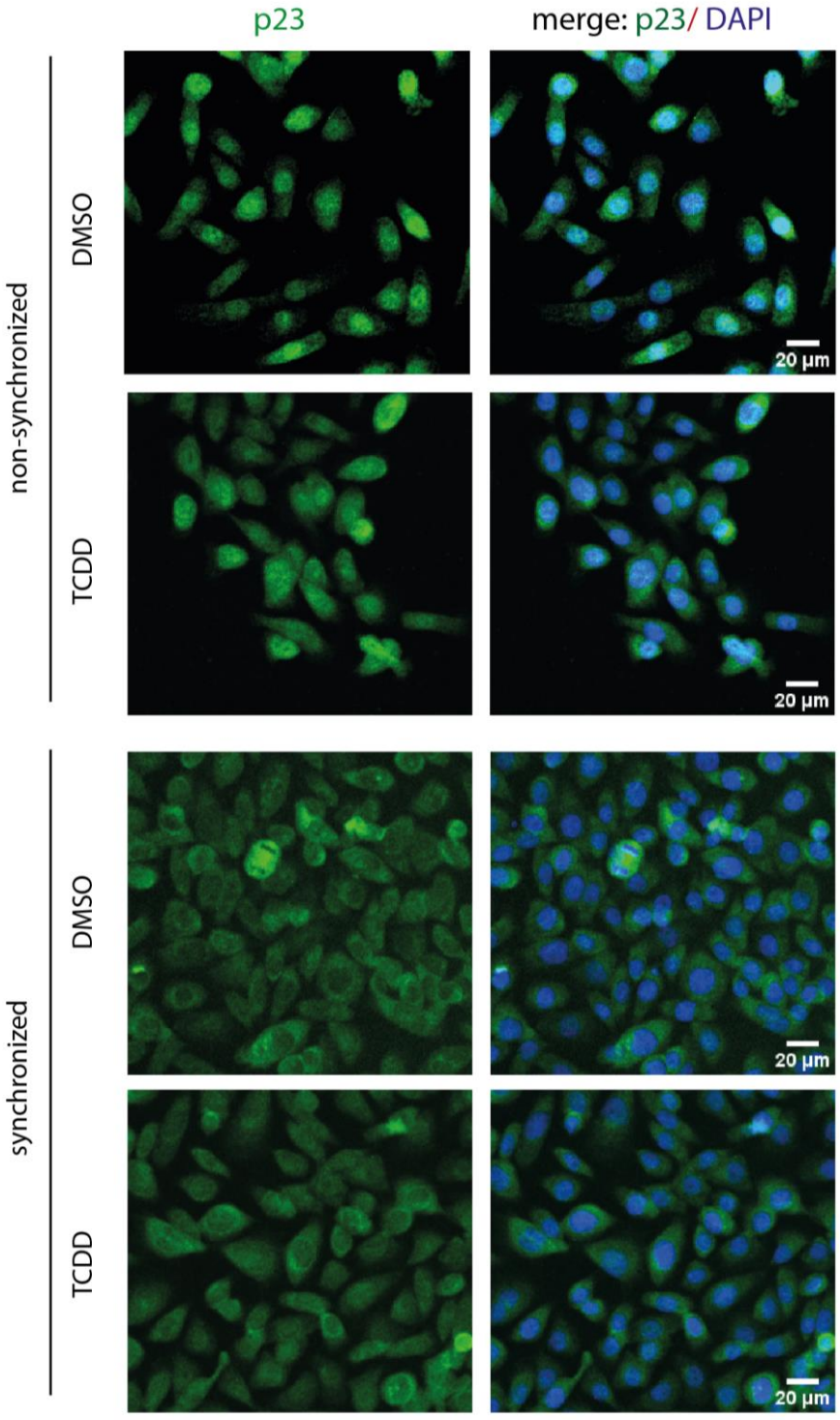

Figure 30: p23 is rather localized in the cytoplasm than the nucleus upon synchronization
Representative images of non-synchronized and synchronized HME1_PLB cells in the presence or absence of TCDD treatment stained for p23. After 23 h of synchronization, the cells were treated for 1 h with DMSO or TCDD (2 nM) and subsequently fixated. The localization of p23 is shown in green, and DAPI, staining the nuclei, in blue. Images (Z-stacks) of minimum 4 different positions on the slide were taken for each condition by using the confocal microscope, Zeiss LSM 880 AiryScan, and a 40x air objective. Scale bar: 20 µM. (n=3).

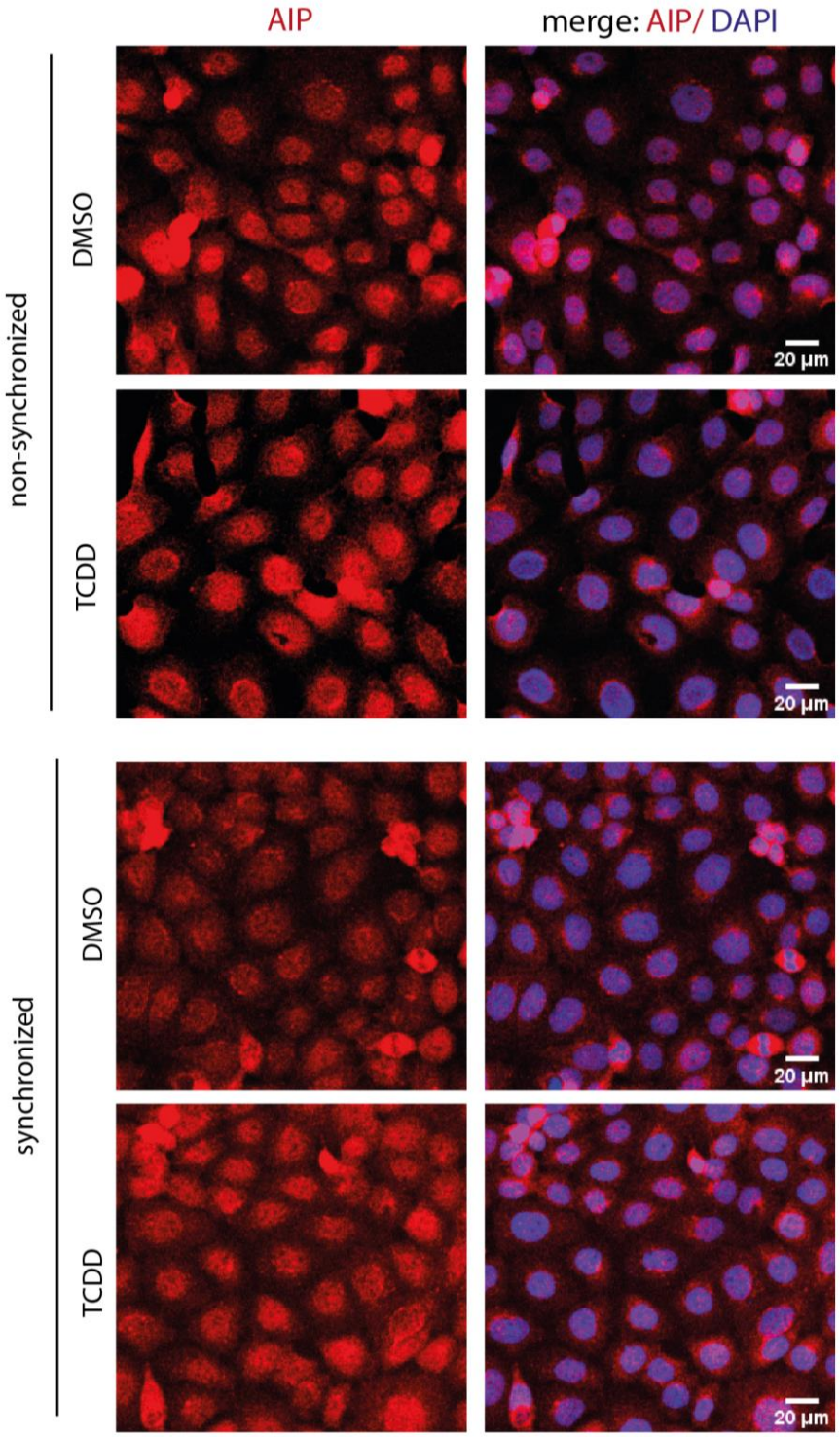

Figure 31:No changes in AIP localization upon synchronization and treatment with TCDD
Representative images of non-synchronized and synchronized HME1_PLB cells in the presence or absence of TCDD treatment stained for AIP. After 23 h of synchronization, the cells were treated for 1 h with DMSO or TCDD (2 nM) and subsequently fixated. The localization of AIP is shown in red, and DAPI, staining the nuclei, in blue. Images (Z-stacks) of at least 4 different positions on the slide were taken for each condition by using the confocal microscope, Zeiss LSM 880 AiryScan, and a 40x air objective. Scale bar: 20 µM. (n=3).

3.11 Characterization of interactions between AhR signaling components or with clock proteins

Immunoprecipitation assays were performed to characterize the interaction of AhR with its cofactors, e.g p23 and SP1 (3.11.1), or clock proteins, e.g. BMAL1, (3.11.2) at different timepoints of synchronization. This would provide information about a possible circadian regulation of the AhR interaction with its cofactors or the direct interaction with clock genes, indicating a circadian regulation of the AhR binding on the *CYP1A1* promoter and the circadian expression of AhR target genes.

3.11.1 AhR interacts with p23 and SP1

The AhR signaling components SP1 and p23 might be involved in the circadian regulation of the *CYP1A1* induction. Therefore, the interaction of these two with AhR was further analyzed by immunoprecipitation assays. First, HME1_PLB cells were synchronized for 24 h and 36 h before being treated with DMSO (control) or TCDD (2 nM) for 1 h. Then, the protein lysates of these cells were immunoprecipitated using an SP1 specific antibody. Figure 32 shows a representative Western blot of the immunoprecipitation assay performed with a SP1 specific antibody and immunoblotted for AhR, SP1, p23, and GAPDH. The immunoprecipitation assay was successful, as no GAPDH or increased SP1 protein levels were detected in the immunoprecipitants. Further, the SP1 protein amount was the same between the immunoprecipitants, enabling the direct comparison of the amounts of interaction with the other proteins. AhR was identified in the SP1 immunoprecipitants, suggesting an interaction between these two components. Interestingly, the interaction between AhR and SP1 was increased after TCDD exposure compared to DMSO, as well as possibly more enhanced after 36 h of synchronization compared to 24 h. However, after DMSO treatment, the interaction of AhR and SP1 seems also to be increased after 36 h compared to 24 h of synchronization. Last, p23 shows no interaction with SP1, as no band specific for p23 was identified in the SP1 immunoprecipitants on the membrane.

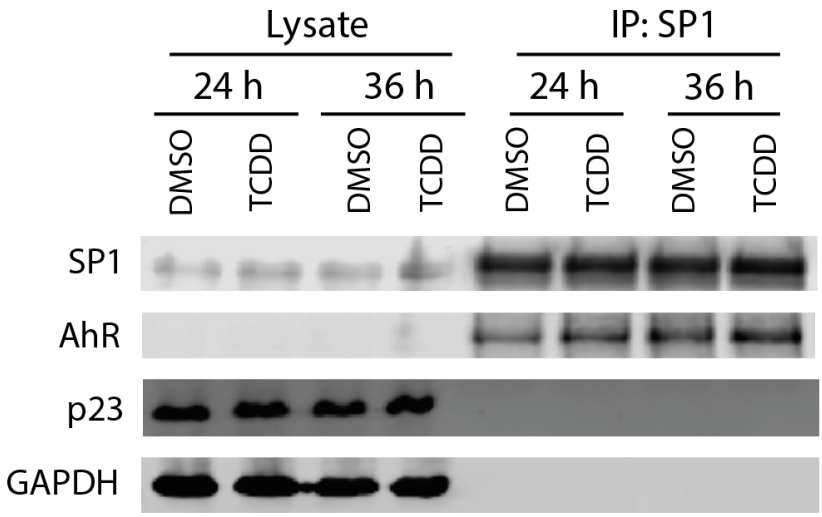

Figure 32: Interaction of SP1 and AhR upon synchronization and TCDD treatment
Representative Western blot of the SP1 immunoprecipitation assay. After 24 h and 36 h of synchronization, HME1_PLB cells were treated with DMSO (control) or TCDD (2 nM) for 1 h and subjected to immunoprecipitation with an SP1 specific antibody attached to sepharose beads. Whole cell lysates (Lysate) and immunoprecipitants (IP:SP1) were analyzed by Western blot. SP1 (~90 kDA), p23 (~25 kDA), and AhR (~100 kDa) were immunoblotted on the membrane. GAPDH (~36 kDA) was detected as a loading control for the lysates and as a marker for a successful immunoprecipitation assay, as it is not interacting with SP1. (n=3).

Immunoprecipitation assay using a p23 antibody revealed an interaction between AhR and p23 in HME1_PLB cells, which were synchronized for 24 h, 36 h, and 48 h, and exposed to TCDD (2 nM) for 1 h. Figure 33 shows a representative Western blot of p23 immunoprecipitated protein samples of 24 h, 36 h, and 48 h synchronized and 1 h TCDD-treated HME_PLB cells. Aligning with the literature, upon TCDD exposure, the interaction between p23 and AhR is decreased, as AhR is being released from the HSP90/ p23/ AIP complex and translocated into the nucleus for activation of the AhR target gene expression. In the control DMSO treated cells, the immunoprecipitation assay revealed a decreased interaction of AhR and p23 during 24 h and 48 h of synchronization compared to 36 h. However, before performing the immunoprecipitation assay, the AhR protein levels were already decreased after 24 h of synchronization, compared to 36 h and 48 h in both DMSO and TCDD lysates. The p23 immunoprecipitation was successful, as GAPDH is absent and p23 protein is increased in the p23 immunoprecipitants compared to the lysates. Thus, SP1 as well as p23 show interactions with AhR, in particular possibly stronger at 36 h after synchronization, but whereas the interaction of SP1 and AhR is rather stimulated by TCDD, the interaction of p23 and AhR is blocked, possibly explaining the positive and negative effects of SP1 and p23 on the *CYP1A1* induction shown in the previous overexpression and knockdown experiments.

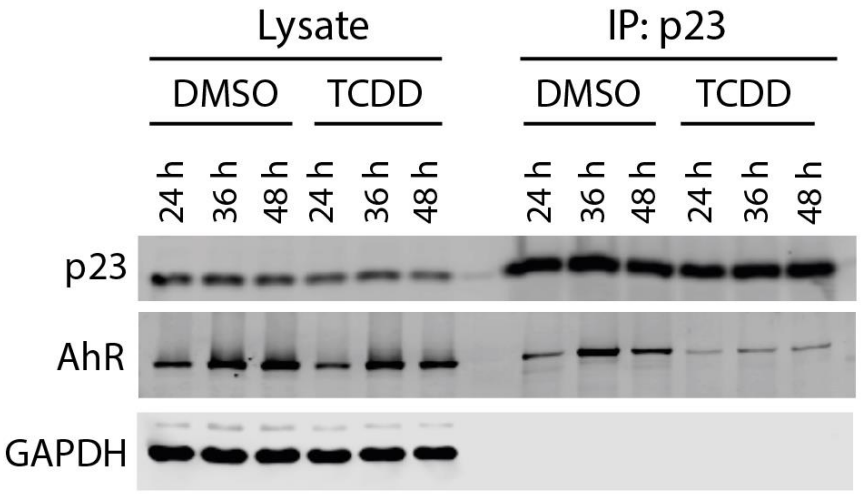

Figure 33: TCDD reduces the interaction between AhR and p23 upon synchronization
Representative Western blot of SP1 immunoprecipitation assay. After 24 h and 36 h of synchronization, HME1_PLB cells were treated with DMSO (control) or TCDD (2 nM) for 1 h and subjected to immunoprecipitation with a p23-specific antibody attached to sepharose beads. Whole cell lysates (Lysate) and immunoprecipitants (IP: p23) were analyzed by Western blot. p23 (~25 kDA) and AhR (~100 kDa) were detected on the blot by using specific antibodies to analyze their interaction. GAPDH (~36 kDA) was detected as a loading control for the lysates and as a marker for a successful immunoprecipitation assay because it is not interacting with p23. (n=3).

3.11.2 Analysis of ARNT and BMAL1 interaction with AhR by immunoprecipitation assay

After ligand binding, AhR forms a complex with ARNT to bind to the DNA of the *CYP1A1* promoter, mediating target gene transcription. Immunoprecipitation assays were performed to identify the amount of AhR::ARNT complex at different timepoints of synchronization, which could indicate a possible circadian regulation of the interaction between AhR and ARNT. HME1_PLB cells were synchronized for 24 h and 36 h and treated with TCDD for 1 h. Then, the protein lysates of these cells were immunoprecipitated by using an AhR specific antibody bound to sepharose beads, and further analyzed by Western blot. Development of the Western blot showed that the AhR immunoprecipitation was successful, as the AhR protein level was increased in the AhR immunoprecipitants, and no GAPDH was identified in these (Figure 34). In the lysates, no bands for AhR were observed, possibly because the exposure was not long enough during the development. As expected, an interaction between AhR and ARNT was identified after TCDD treatment, but interestingly, it was increased after 36 h of synchronization compared to the 24 h. This indicates a possible circadian-regulated interaction between AhR and ARNT.

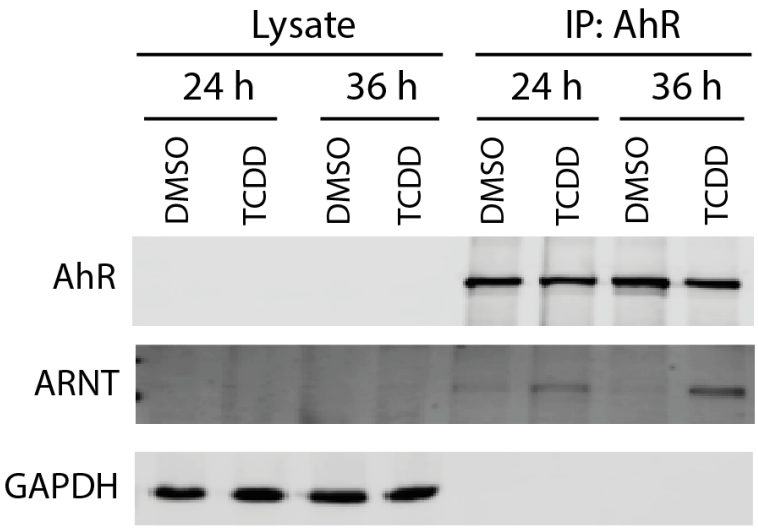

Figure 34: Time-dependent TCDD-mediated AhR and ARNT interaction upon synchronization Representative Western blot of AhR immunoprecipitation assay. After 24 h, and 36 h of synchronization, HME1_PLB cells were treated with DMSO (control) or TCDD (2 nM) for 1 h and subjected to immunoprecipitation with an AhR specific antibody attached to sepharose beads. Whole cell lysates (Lysate) and immunoprecipitants (IP: AhR) were analyzed by Western blot. AhR (~100 kDa) and ARNT (~85 kDA) were detected on the membrane by using specific antibodies to analyze their interaction. AhR interacts with ARNT only after TCDD treatment, and the interaction is increased after 36 h of synchronization compared to 24 h. GAPDH was detected as a loading control for the lysates and as a marker for a successful immunoprecipitation assay, as it is not interacting with AhR. (n=3).

Similarly, to identify whether AhR interacts with BMAL1, an AhR immunoprecipitation was performed with synchronized (16 h or 24 h) and 1 h TCDD-treated HME1_PLB cells. Then, the AhR immunoprecipitants and the lysates were Western blotted for BMAL1, and a representative Western blot is shown in Figure 35. BMAL1 was identified in all different conditions of the AhR immunoprecipitants, suggesting an interaction between AhR and BMAL1. This signifies a possible interaction of AhR with the circadian rhythm regulator BMAL1 and could also explain the circadian expression of AhR target genes.

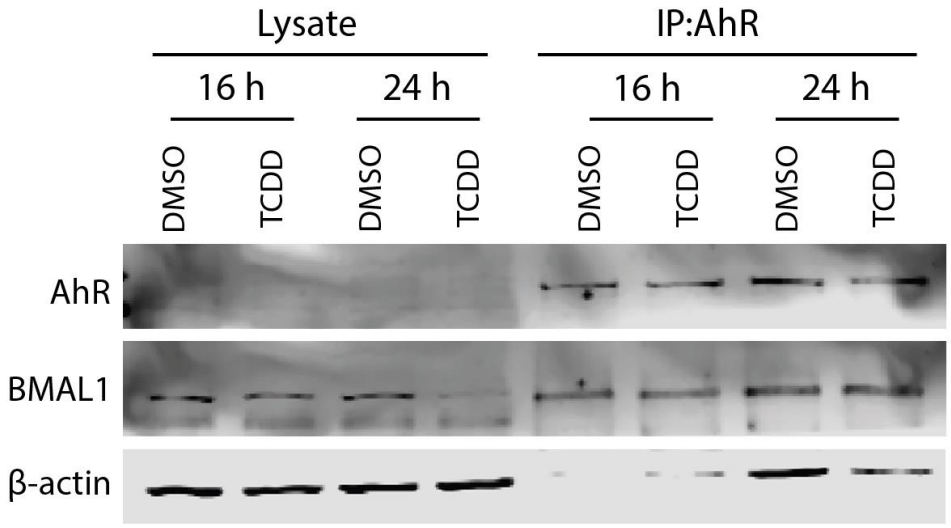

Figure 35: AhR interacts with BMAL1 upon synchronization
Representative Western blot of AhR immunoprecipitation assay. After 16 h and 24 h of synchronization, HME1_PLB cells were treated with DMSO (control) or TCDD (2 nM) for 1 h and subjected to immunoprecipitation with an AhR specific antibody attached to sepharose beads. Whole cell lysates (Lysate) and immunoprecipitants (IP: AhR) were analyzed by Western blot. AhR (~100 kDa) and BMAL1 (~80 kDA) protein bands were detected on the membrane by using specific antibodies to analyze their interaction. AhR interacts with BMAL1 upon synchronization and the interaction seems to be increased after 24 h of synchronization compared to after 16 h, independently of the TCDD treatment. β-Actin was detected as loading control for the lysates. (n=3).

BMAL1 immunoprecipitation and Western blotting for AhR were performed with protein lysates extracted from 1 h TCDD-treated non-synchronized and synchronized (16 h and 24 h) HME1_PLB cells to verify the specificity of the AhR and BMAL1 interaction (Figure 36). Additionally, CLOCK was detected on the Western blot membrane to verify the success of the immunoprecipitation assay, as it has been proven in several studies that BMAL1 and CLOCK are interaction partners regulating the circadian rhythm in cells. Indeed, interaction between those two components was verified, as well as no GAPDH was identified in the BMAL1 immunoprecipitants, suggesting a successful immunoprecipitation assay. AhR detection in the BMAL1 immunoprecipitants strongly supports the interaction of these two components. Summarizing, all these data suggest an interaction between AhR and BMAL1 that could also possibly be regulated in a circadian manner.

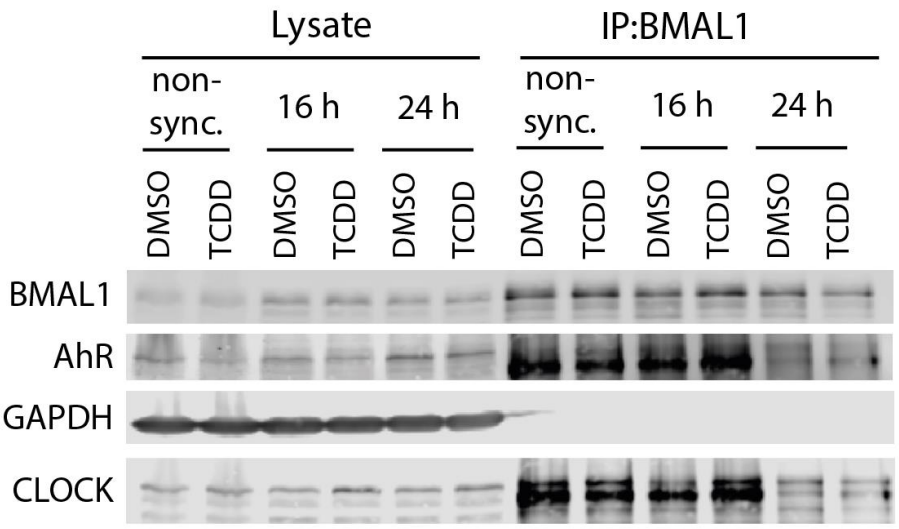

Figure 36: BMAL1 interaction with AhR and CLOCK upon different timeponints of synchronization
Representative Western blot of BMAL1 immunoprecipitation assay. After 16 h and 24 h of synchronization, HME1_PLB cells were treated with DMSO (control) or TCDD (2 nM) for 1 h, and subjected to immunoprecipitation with an BMAL1 specific antibody attached to sepharose beads. Whole cell lysates (Lysate) and immunoprecipitants (IP: BMAL1) were analyzed by Western blot. AhR (~100 kDa), CLOCK (~100 kDa), and BMAL1 (~80 kDA) were detected on the membrane by using specific antibodies to analyze their interaction. Both, CLOCK and AhR interact in different amounts with BMAL1, depending on the time of synchronization. GAPDH was detected as a loading control for the lysates and as a marker for a successful immunoprecipitation assay because it is not interacting with BMAL1. (n=2).

Last, both Figure 35 and Figure 36 showed first evidence that there is possibly a time-dependent interaction between AhR and BMAL1 upon synchronization. Indeed, Figure 35 shows that the interaction of AhR and BMAL1 seems to be increased 24 h after synchronization compared to 16 h, although there was still some β-actin identified in the immunoprecipitants of the 24 h after synchronization samples. In contrast, Figure 36 shows exactly the opposite, i.e. the interaction of AhR and BMAL1 is rather decreased 24 h after synchronization compared to 16 h after synchronization. Further experiments optimizing the immunoprecipitation protocol or subjecting the samples to a more precise proteomic analysis need to be performed to understand the time-dependent interplay between AhR and BMAL1.

3.12 Inhibition of GSK3β influences circadian rhythmicity and the circadian TCDD-mediated *CYP1A1* induction

Considering the previous data that p23 plays a role in the enhanced induction of *CYP1A1* upon synchronization but is not itself circadian regulated led to the hypothesis that another circadian regulated mediator may be the key link to this interplay. In the literature, GSK3β has been proposed as a potential candidate connecting these two components. Yang *et al*. demonstrated that AhR is phosphorylated in a p23-dependent manner for a canonical activation of ligand-dependent AhR target gene transcription [157, 246]. Additional studies described a circadian pattern in the phosphorylated form of GSK3β or a crosstalk between GSK3β and clock genes [157, 247]. Since SP1 displayed a circadian regulation at protein level and the literature predicts SP1 as a phosphorylation target of GSK3β, these data indicate a possible interplay between p23, SP1, and GSK3β in the circadian regulation of the AhR signaling. Therefore, further experiments were performed by inhibiting GSK3β with the inhibitor CHIR99021 to elucidate the role of GSK3β in the circadian regulation of AhR target gene induction (3.12.1 and 3.12.2). Besides that, protein levels of AhR, and AhR signaling components were examined after GSK3β inactivation via the inhibitor CHIR99021 (3.12.3) to understand the effect of GSK3β on the circadian regulation of the AhR pathway.

3.12.1 Inhibition of GSK3β alters the period of the circadian rhythm

After synchronization, HME1_PLB cells were treated with different concentrations of CHIR99021 to inhibit GSK3β, and their circadian rhythmic, i.e. rhythmic expression of *PER2*, was monitored for 72 h by measuring the luciferase activity every 30 min to identify the role of GSK3β on the circadian synchrony. Non-synchronized and synchronized cells treated with DMSO were used as control. Figure 37A shows representative bioluminescence curves of non-synchronized and synchronized HME1_PLB cells treated with CHIR99021 (1 µM, 5 µM, and 10 µM). The control synchronized cells displayed an oscillating luciferase activity with a period of 24 h, that was stable for at least 48 h. Cells treated with CHIR99021 of various concentrations also showed a 48 h stable oscillation, but the period was shortened. Treatment with 1 µM CHIR99021 caused a reduction of approx. 8 h, i.e. was approx. 16 h long, whereas treatment with 10 µM CHIR99021 caused a shortening of approx. 4 hours, i.e. was approx. 20 h long. Accordingly, exposure to 5 µM CHIR99021 displayed oscillating luciferase activity with a period of 18 h. Finally, the CellTiter-Blue® cell viability assay was performed after 72 h of incubation with CHIR990221 to ensure that the period shift observed in the cells was not due to cell death. The recorded fluorescence shown in Figure 37C was approx. the same between DMSO and CHIR99021 treated cells, indicating no cell death. Summarizing inhibition of GSK3β with CHIR99021

results in changes in the length of circadian rhythm in HME1_PLB cells, which supports a role of GSK3β in the regulation of the circadian clock machinery.

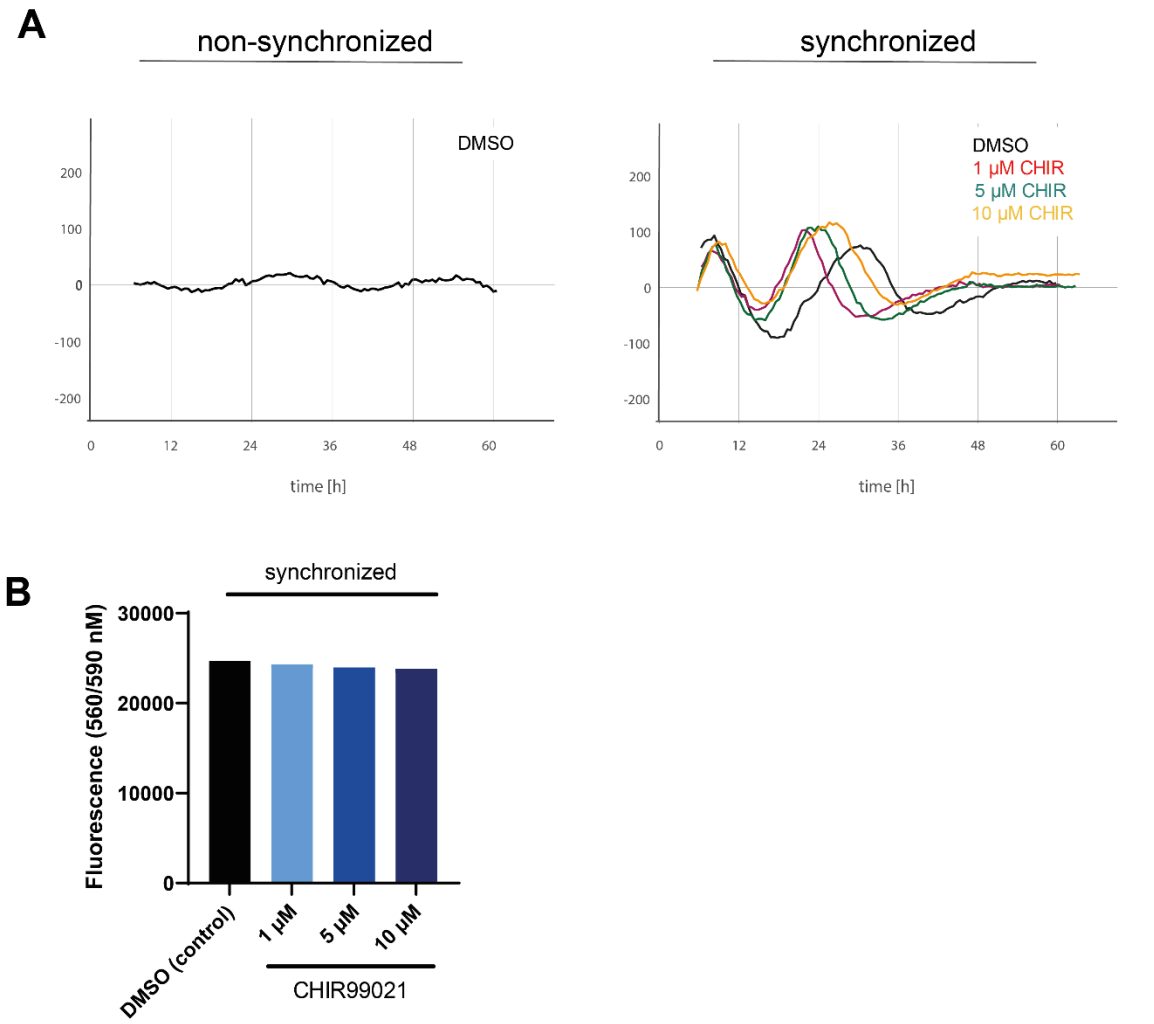

Figure 37: GSK3β inhibition by CHIR99021 disturbs the circadian synchrony in *PER2* luciferase reporter HME1 cells
A) Representative curves of fitted bioluminescence measurements of non-synchronized and synchronized *PER2* luciferase reporter HME1 (HME_PLB) cells treated with DMSO and the GSK3β inhibitor, CHIR99021 (1 µM, 5 µM, and 10 µM). For the synchronized condition, the cells were 100 % confluent and treated with 1 µM dexamethasone for 1 h to achieve synchronization. The cells were monitored for at least 72 h, and the bioluminescence was recorded every 30 min. GSK3β inhibition by CHIR99021 disturbed the circadian expression of the *PER2* gene, i.e. the circadian rhythmicity of the cells, by reducing the period of the oscillation in dependence on the CHIR99021 concentration (n=4). B) Representative cell viability assay of the HME1_PLB cells shown in A) by using CellTiter-Blue® and measuring the fluorescence at 560/ 590 nM wavelength. No cell death was observed, verifying the effect of CHIR99021 on the circadian synchrony. (n=2).

3.12.2 Disruption of the circadian *CYP1A1* induction by CHIR99021-mediated GSK3β inhibition

The effect of CHIR99021, i.e. the inactivation of GSK3β, on the circadian *CYP1A1* expression was analyzed by RT-qPCR to elucidate a possible role of GSK3β on the circadian *CYP1A1* induction. Therefore, HME1_PLB cells were either synchronized or not and treated with TCDD, with or without CHIR99021, for a period of 48 h. Cells were exposed to DMSO or CHIR99021, as control. Samples were collected every 12 h and the *CYP1A1* expression was analyzed by RT-qPCR. Figure 38A, B, and C shows the fold change of the *CYP1A1* expression of non-synchronized and synchronized HME1_PLB cells treated with DMSO plus CHIR99021, TCDD, and TCDD plus CHIR99021, respectively, calculated to the DMSO control cells. As expected, non-synchronized and synchronized cells showed no circadian induction of *CYP1A1* in the absence of TCDD and treatment with CHIR99021. However, a slight decrease in the fold change of the *CYP1A1* expression was observed after 36 h and 48 h of treatment in the synchronized cells compared to non-synchronized cells (Figure 38A). Accordingly, as shown previously, synchronized cells showed a circadian pattern in the TCDD-mediated *CYP1A1* induction, peaking at 24 h and 48 h, compared to the non-synchronized cells (Figure 38B). Interestingly, this circadian pattern was lost with CHIR99021 treatment, indicating circadian disruption by either complete extinction of circadian synchrony or a phase shift of the oscillation (Figure 38C). Additionally, Figure 38C shows that in synchronized cells treated with TCDD plus CHIR99021, the highest fold change of *CYP1A1* expression was determined after 24 h of synchronization (150-fold), which decreased with time and reached a 21-fold change at 48 h after synchronization. On the other hand, in non-synchronized cell, the *CYP1A1* induction increased with time and reached the highest fold change after 48 h (215-fold). Last, comparing non-synchronized cells of Figure 38A, B, and C showed that the mixture of TCDD and CHIR99021 treatment enhanced the *CYP1A1* induction overall compared to only treatment with TCDD or CHIR99021. This induction is even higher than the induction observed in synchronized cells only treated with TCDD or the mixture of TCDD and CHIR99021. All in all, after GSK3β inactivation by CHIR99021, the circadian TCDD-mediated *CYP1A1* induction in synchronized cells was disrupted as well as non-synchronized and synchronized cells with TCDD-activated AhR signaling exhibit a significant different pattern in *CYP1A1* induction. This proposes that GSK3β is involved in the circadian regulation of the AhR pathway and can disrupt the circadian expression of TCDD-mediated *CYP1A1* induction.

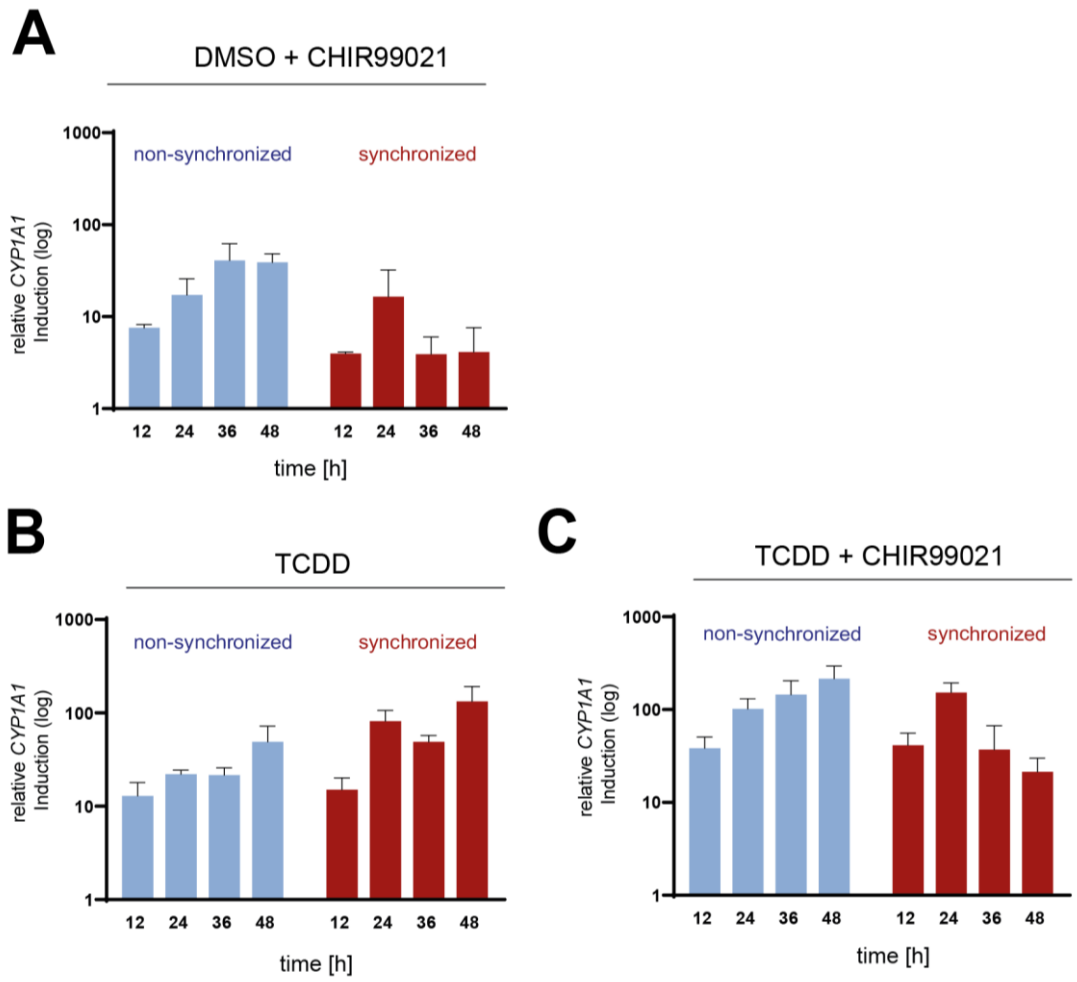

Figure 38: CHIR99021-mediated GSK3β inhibition disrupts the TCDD-mediated circadian *CYP1A1* expression
CYP1A1 fold induction at different timepoints in non-synchronized and synchronized cells upon A) DMSO plus CHIR, B) TCDD (0.5 nM), and C) DMSO plus CHIR99021 (5 µM) treatment. The cells were synchronized (or not) and treated for 12 h, 24 h, 36 h, and 48 h accordingly with DMSO (control), DMSO plus CHIR99021 (5 µM), TCDD (0.5 nM), and TCDD (0.5 nM) plus CHIR99021 (5 µM). CHIR99021 was used to inhibit GSK3β. The *CYP1A1* mRNA expression was analyzed by RT-qPCR and normalized to the endogenous control *B2M*. The fold change of *CYP1A1* expression upon TCDD or CHIR992021 treatment for each timepoint was calculated based to the control DMSO of the respective timepoint. The TCDD-mediated fold induction of *CYP1A1* shows a circadian pattern, with peaking at 24 h and 48 h, in synchronized cells, which is disrupted by inhibiting GSK3β with CHIR99021. (mean±SD, n=3).

Impairment of GSK3β changes the period of the circadian rhythm in HME1_PLB cells (Figure 37). This raised the question of whether the circadian *CYP1A1* induction is not disrupted per se, as indicated in Figure 38, but shifted similar as the circadian rhythm shown in Figure 37. To address this, different timepoints of synchronization were analyzed for *CYP1A1* expression. The period of the *PER2* circadian expression was decreased to 18 h upon CHIR99021 treatment (Figure 37) indicating a 6 h shift change to the control cells. Therefore, cells treated with TCDD or CHIR99021 were analyzed after 12 h, 18 h, 30 h, and

42 h of synchronization to identify a potential 6 h shifted circadian pattern in *CYP1A1* expression upon GSK3β inhibition. Figure 39 shows no 6 h-shifted circadian pattern in the fold change of *CYP1A1* expression after TCDD treatment and inhibition of GSK3β by CHIR99021. Instead, an increased fold change of 160-fold is observed at 30 h after synchronization and then a lower 50-fold change after 42 h of synchronization.

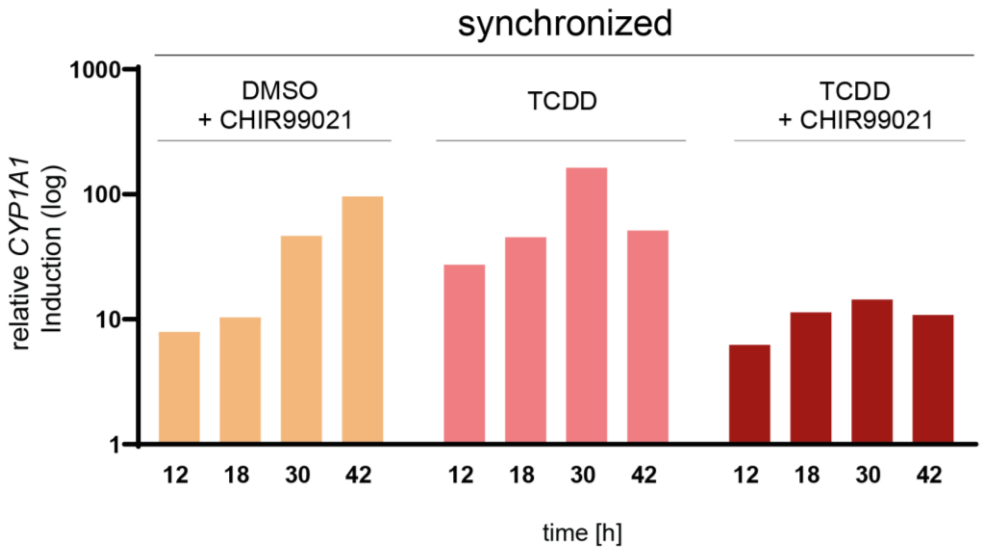

Figure 39: CHIR99021-mediated GSK3β inhibition causes no phase shift in the circadian TCDD-mediated *CYP1A1* expression
CYP1A1 induction at different timepoints in synchronized cells after TCDD (0.5 nM) and CHIR99021 treatment. The cells were synchronized for 12 h, 18 h, 30 h, and 42 h and treated accordingly with DMSO (control), and TCDD (0.5 nM). Also, GSK3β inhibition was achieved by using CHIR99021 (5 µM). The analysis of these timepoints was performed to identify whether there is a phase shift in the circadian TCDD-mediated *CYP1A1* induction, as observed in the circadian oscillation of the *PER2* gene, by visualizing the circadian synchrony via bioluminescence measurements. The *CYP1A1* mRNA expression was analyzed by RT-qPCR and normalized to the endogenous control *B2M*. The fold change of *CYP1A1* expression after TCDD, or CHIR99021 treatment for each timepoint was calculated based to the control DMSO of the respective timepoint. The TCDD-mediated fold induction of *CYP1A1* upon GSK3β inhibition showed no circadian pattern even with shortening the period by 6 h.

3.12.3 Analysis of GSK3β role on circadian rhythmicity and AhR-signaling by Western blot analysis

GSK3β has been described to phosphorylate AhR in a p23-manner. Thus, Western blot analysis of non-synchronized and synchronized HME1_PLB cells treated with TCDD and/or CHIR992021 was performed to identify whether an inhibition of GSK3β influences the p23 protein amount. Figure 40 shows the protein levels of p23 and GSK3β in non-synchronized and synchronized cells treated with DMSO, DMSO plus CHIR992021, TCDD, and TCDD plus CHIR992021. In both non-synchronized and synchronized cells, the GSK3β protein level is reduced after a 24 h exposure to CHIR992021 compared to the corresponding non-

exposed conditions. The GSK3β protein levels in the presence or absence of CHIR992021 are not affected after 12 h of treatment. These data suggest that CHIR992021 exposure successfully inhibits GSK3β after 24 h of exposure. However, GSK3β repression seems to have no influence on the protein levels of p23. The protein levels of both non-synchronized and synchronized cells remain the same despite the CHIR992021 exposure under DMSO or TCDD treatment.

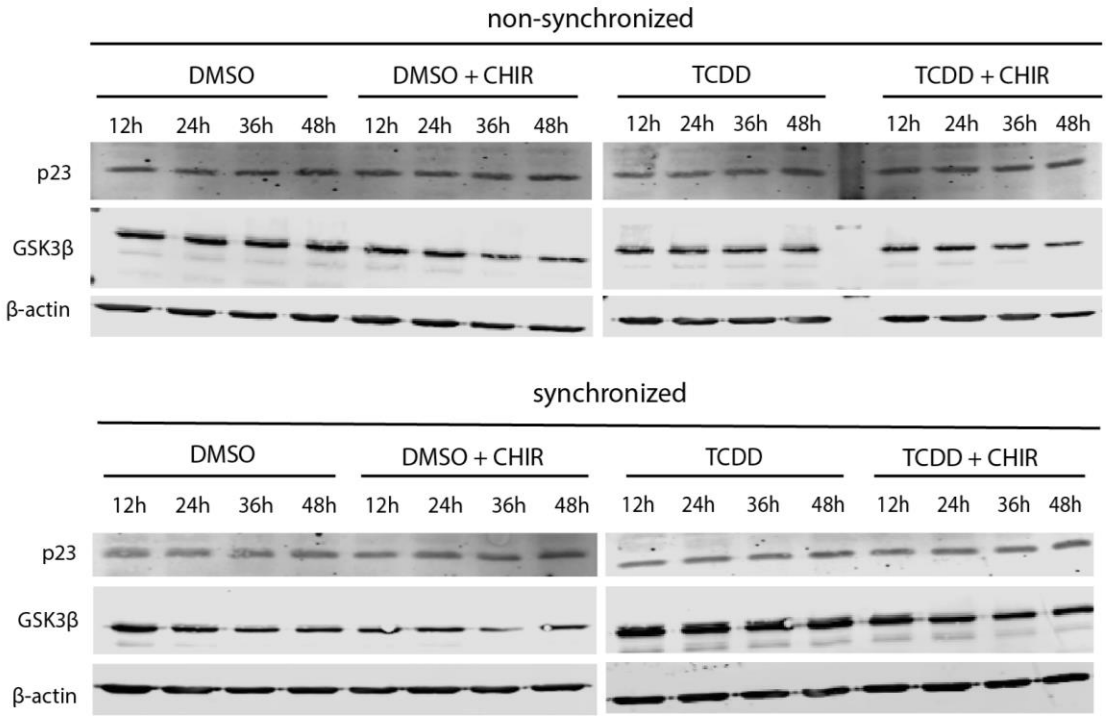

Figure 40: CHIR99021-mediated GSK3β inhibition has no effect on the p23 protein level
Representative Western blots of non-synchronized and synchronized cells treated with DMSO, DMSO plus CHIR992021 (5 µM), TCDD (0.5 µM), and TCDD (0.5 µM) plus CHIR992021 (5 µM) at different timepoints (12 h, 24 h, 36 h, and 48 h). The proteins were separated through SDS-PAGE. p23 (~25 kDa) and GSK3β (~25 kDa) protein levels were analyzed by Western blot. β-Actin was detected, at ~42 kDa, as loading control. No effect on p23 protein expression was identified by GSK3β inhibition with CHIR99021. Treatment of the cells with CHIR99021 shows GSK3β inhibition after 24 h of treatment. (n=2).

Next, BMAL1 protein levels after CHIR99021 exposure were analyzed by Western blot to address the regulation of GSK3β on BMAL1, which is also possible involved in the AhR signaling pathway, as shown in immunoprecipitation assays (3.11). In non-synchronized cells, no difference at the BMAL1 protein level was discovered between DMSO and CHIR99021 treated cells by direct comparison of the individual timepoints. Similarly, in non-synchronized cells, comparing the TCDD with the TCDD plus CHIR99021 exposure condition, exhibits the same BMAL1 protein level at any timepoint. Although in all four conditions, the BMAL1 protein level is lower at 12 h after treatment compared to 24 h, 36 h,

and 48 h. Further, in synchronized cells treated with DMSO, a circadian pattern in the protein level of BMAL1 was identified with the highest protein amount after 24 h and 48 h of synchronization. This circadian pattern was not observed in synchronized cells treated with DMSO plus CHIR9902. Instead, the BMAL1 protein expression was only decreased after 24 h of synchronization. However, the lowest protein amount was determined after 36 h of synchronization and treatment. Looking into each timepoint itself upon exposure to TCDD, CHIR99021 does not alter the BMAL1 protein level of the synchronized cells. On the other hand, the timeseries of the TCDD or TCDD plus CHIR99021 conditions revealed the highest BMAL1 protein level at 24 h and the lowest at 36 h and 48 h. Altogether, non-synchronized and synchronized HME1_PLB cells exhibit a different time-dependent pattern in BMAL1 protein level after inhibition of GSK3β with CHIR99021, which seems very similar to the *CYP1A1* induction shown in Figure 38.

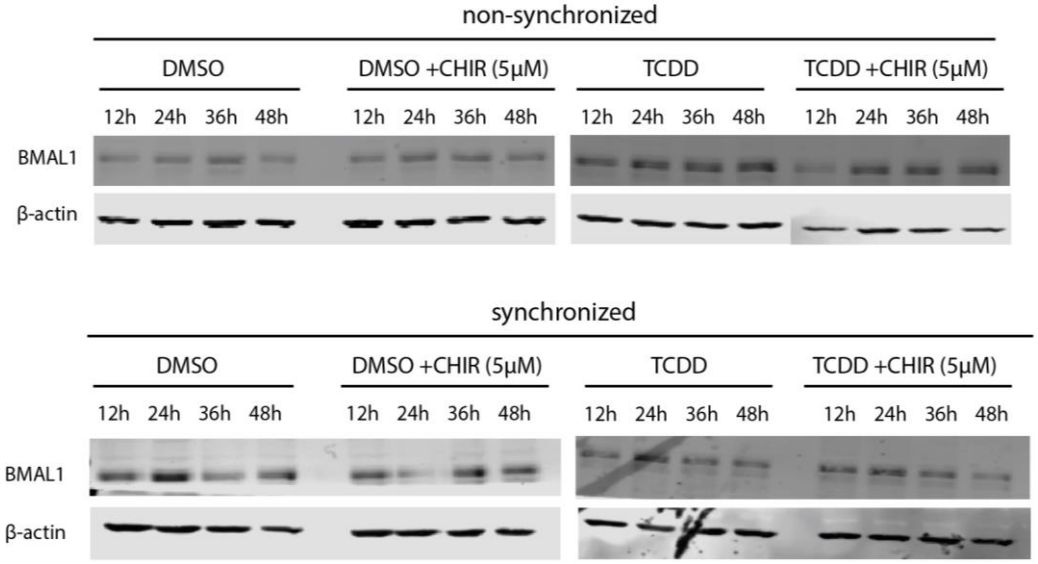

Figure 41: CHIR99021-mediated GSK3β inhibition alters BMAL1 protein levels upon synchronization and TCDD treatment
Representative Western blots of non-synchronized and synchronized cells treated with DMSO, DMSO plus CHIR992021(5 µM), TCDD (0.5 µM), and TCDD (0.5 µM) plus CHIR992021 (5 µM) for different timepoints (12 h, 24 h, 36 h, and 48 h). The proteins were separated through SDS-PAGE, and BMAL1 (~90 kDa) protein levels were analyzed by Western blot. β-Actin was detected, at ~ 42 kDa, as loading control. The BMAL1 protein levels were altered between non-synchronized and synchronized cells after GSK3β inhibition with CHIR99021 and TCDD treatment. (n=2).

4 Discussion

The importance of the AhR signaling pathway as well as the circadian rhythmicity in a plethora of processes has been highly addressed in the past years, as they play crucial roles in various biological processes and disease progression. However, their interplay has been poorly studied and not fully understood, yet. Moreover, even if the AhR pathway, as one of the most toxicological relevant pathways, is being used in the development of *in vitro* test systems for hazard identification, the circadian rhythm, which regulates equally important physiological processes, including xenobiotic metabolism, is often neglected. The common cell culture-based *in vitro* test systems, which disregard circadian synchrony, do not reflect the *in vivo* situation, and provide only limited information about the physiological cellular response to xenobiotics. In real life, humans and animals live in a circadian-dependent exposure regime and thus can respond differently to hazardous exposure at different times of the day. Test systems without circadian synchrony might underestimate potential higher health risks. For that reason, *in vitro* test methods need to be adapted and improved to mimic as closely as possible the *in vivo* situation found in animals and humans. As one possible strategy, the circadian rhythmicity could be included in these test systems. Moreover, understanding the regulatory framework, i.e. mechanism, behind the circadian regulation of toxicological relevant pathways, such as the AhR pathway, will help to generate more physiological relevant data.

Several studies have already shown that a restoration of the circadian synchrony in common *in vitro* systems, either by stimulation of the cells with dexamethasone or forskolin, or through serum shock, can improve their significance and sensitivity to obtain a biological relevant response [201, 230, 248]. Most of these studies focus on the AhR-CYP1A1 pathway and show the major relevance of the circadian rhythmicity to this pathway. However, none of them unravels the mechanism behind this regulation. In detail, Ndikung *et al*. showed that the expression of the AhR target genes, *CYP1A1* and *ALDH3A1*, is induced after exposure to various chemicals in synchronized human mammary epithelial cells, but the AhR expression itself remains the same between synchronized and non-synchronized cells [201]. Further, the TCDD-mediated target gene expression is time-dependent, showing a circadian pattern with a period of 24 h and peaking at 24 h and 48 h after synchronization. Based on these data, it was interesting to characterize the mechanism behind the circadian regulation of the AhR pathway and connect the circadian pathway with the xenobiotic metabolism to understand more about this interplay and its role in disease or adverse health effects. Indeed, several interesting insights of this regulation were identified in this thesis, which led to the proposal of a possible model of the mechanism mediating the circadian regulation of the AhR pathway.

4.1 Transcriptional circadian regulation of the AhR pathway

The activation of the AhR pathway with different ligands, e.g. TCDD, showed an increased and time-dependent induction of AhR target genes, such as *CYP1A1* and *ALDH3A1* upon synchronization of mammary epithelial cells (Figure 13). These data correlate with the findings from Ndikung *et al.* and Schmitt *et al.* suggesting a time-dependent sensitivity of the cells to AhR ligands, such as TCDD and BaP [201, 248]. Here, the AhR target gene, *AHRR*, which inhibits the binding of the AhR/ ARNT complex on the XRE promoter, was identified as an additional circadian regulated AhR target gene. Indeed, *AHRR* expression was induced in synchronized TCDD-treated cells compared to the non-synchronized ones (Figure 12), and its TCDD mediated induction was circadian regulated (Figure 14). This correlates with the TCDD-mediated *CYP1A1* and *ALDH3A1* induction upon synchronization, highly supporting the circadian regulation of the XRE promoter. In both non-synchronized and synchronized cells, the mRNA expression of AhR remains stable (Figure 15), supporting the findings of Ndikung *et al*. [201]. Additionally, the protein expression of AhR is unchanged over time but rather decreased upon TCDD exposure (Figure 16). Studies already showed that TCDD reduces the steady state of AhR, i.e. AhR protein level, by nuclear translocation and activating its degradation via ubiquitination [240, 249]. All this indicates a transcriptional circadian regulation of the AhR pathway that may be caused by a circadian regulation of the XRE promoter though enhanced binding and unbinding of the AhR/ARNT complex.

In M13SV1 cells, the promoter activity was enhanced upon synchronization, indicating a different regulation compared to non-synchronized cells. On contrary to the circadian induction of AhR target gene expression, no circadian pattern was identified in the *CYP1A1* promoter activity, but this increased with time (Figure 17). This data may not reflect the actual situation, as already mentioned before, the experiment setup was not ideal, and artificial promoter constructs do not always mimic the *in vivo* situation. The double transfection of the M13SV1 cells in combination with the cell density increasing with time could tamper with the amount of the transfected cells and subsequently, the luciferase measurements, i.e. promoter activity, over time. In the future, generating a stable M13SV1 cell line expressing these constructs could solve such issues. The Dual-Glo luciferase assay could not be performed in live cells and monitore them over a period of 48 h, which would enable live tracking of the promoter activity. A different approach to measure the promoter activity is to identify the *de novo* non-modified mRNA expression of the promoter target genes. Indeed, the expression of the *de novo CYP1A1* expression was circadian induced over time, with a peak at 24 h and 48 h, indicating a circadian regulation of the XRE promoter.

The transcriptional circadian regulation of the AhR pathway through the *XRE* promoter could be modulated by different events. One possible speculation is that the translocation of AhR from the cytoplasm to the nucleus occurs differently between the non-synchronized and synchronized cells. After ligand binding, the AhR is translocated rapidly in the nucleus, where it binds at the promoter, activates gene expression, and subsequently gets degraded. This process of either import or degradation could be circadian regulated, i.e. AhR amount could be transported into the nucleus or degraded at different rates depending on the circadian phase. However, preliminary data of cell fractionation and immunofluorescent staining analysis contradict this hypothesis. In both non-synchronized and synchronized cells, a TCDD-mediated translocation of AhR into the nucleus could be confirmed, as already described in the literature, but no difference in the amount of AhR translocating into the nucleus was identified between non-synchronized and synchronized conditions (Figure 27 and Figure 29). In the future, studies such as live cell imaging, could be performed to analyze more in detail the dynamic rate of the AhR and its cofactor nuclear export and import in dependence on circadian synchrony. However, our findings indicate that the circadian regulation of the AhR pathway is not happening at an import and export level. These rather suggest a direct interaction of AhR with circadian clock components or circadian regulated cofactors, which subsequently influences the formation of the AhR/ARNT/XRE interaction depending on the circadian phase.

4.2 p23 is a repressor of the circadian regulation of the AhR pathway

Analysis of the AhR signaling cofactors AIP, HSP90, p23, and ARNT at mRNA and protein level revealed no circadian expression after TCDD treatment and upon synchronization (Figure 19, Figure 20, and Figure 21). This suggests that none of these components are expressed in a circadian manner, which would explain the circadian regulation of the AhR pathway. Depletion of ARNT as well as AhR itself showed, as expected, a decrease in TCDD-mediated *CYP1A1* expression, correlating with studies showing that both AhR and ARNT are necessary for AhR target gene expression via the XRE promoter [138, 250]. In addition, downregulation of AIP results in a decrease of the *CYP1A1* expression upon TCDD, supporting the studies claiming that AIP is important for the AhR translocation to the nucleus [251]. Interestingly, p23 was identified as the only AhR signaling component that exclusively represses the TCDD-mediated *CYP1A1* induction in the synchronized cells. Vice versa, the ectopic overexpression of p23 decreased *CYP1A1* induction exclusively in circadian synchronized cells (Figure 23, Figure 24, and Figure 22). In addition, cell fractionation and immunofluorescent analysis showed that p23 is localized rather in the

cytoplasm than the nucleus upon synchronization (Figure 30). TCDD treatment reduces the translocation of p23 in the nucleus (Figure 28). All in all, this implies that p23 seems to be differently regulated or translocalized upon synchronization and appears to have a suppressive role in the circadian regulation of the *XRE* promoter activity and AhR target gene expression.

Looking into the literature, p23 is mainly described as a component of the HSP90-AIP-AhR complex that keeps AhR inactive in the absence of an AhR ligand [151], but it is also described to play a role in AhR stabilization [234, 252]. Pappas *et al.* showed that p23 directly interacts with AhR, correlating with the data shown in Figure 33, and suggested that in HeLa cells, p23 has an additional role beyond altering the AhR cytoplasmic complex dynamics, which is to protect AhR from ubiquitin meditated protein degradation despite the abundance of a ligand [234]. This contradicts our findings in mammary breast epithelial cells that p23 has a negative effect on the active AhR signaling pathway upon synchronization. Thus, p23 function on the AhR pathway probably varies depending not only on the organism but also on the cell type. Looking within a specific cell type, opens up the discussion of p23 possibly having a different role on the pathway upon exposure of an AhR ligand, depending on the circadian phase. Indeed, p23 could possibly stabilize AhR before reaching the maximum increase of *CYP1A1,* for example at 24 h, and then promotes its degradation or unbinding from the XRE promoter to undergo again the circadian cycle of *CYP1A1* expression, i.e. inhibits the AhR signaling pathway to not get overstimulated or overloaded. Summarizing, p23 is a negative regulator of the AhR pathway, possibly sensing when the promoter activation is overstimulated, enabling the maintenance of a proper steady state of the circadian expression of AhR target genes.

4.3 The role of GSK3β in the circadian regulation of the AhR pathway

Yang *et al.* showed that AhR is phosphorylated by GSK3β in a p23-dependent manner in HeLa cells for optimal ligand-dependent AhR target gene expression [253]. In addition, phosphorylation upon the absence of p23 leads rather to degradation via autophagy than ubiquitin-mediated lysosomal degradation modulated by GSK3β phosphorylation [253]. Besides that, GSK3β is involved in circadian rhythmicity by phosphorylating at least five clock control genes and maintaining their proper circadian oscillation in the SCN [254]. It also shows a diurnal variation in the phosphorylation state of the inactive GSK3β isoform. Our findings support the involvement of GSK3β in proper circadian oscillation of clock genes, specific *PER2* and *BMAL1*, as inhibition with CHIR99021 disturbs the

PER2:luciferase rhythmical activity by shortening the period (Figure 37) and also changing the BMAL1 protein expression pattern (Figure 41).

GSK3β inhibition with CHIR99021 interrupted the circadian TCDD-mediated *CYP1A1* expression upon synchronization (Figure 38). This could be explained either through the complete disruption of the circadian synchrony in the cells, or through GSK3β having a specific role in the circadian regulation of AhR target gene expression. Analyzing different timepoints of the *CYP1A1* induction could not exhibit a diurnal oscillation with a shortened period, indicating that possible GSK3β has a specific role in the AhR pathway and that the malfunction of the circadian *CYP1A1* induction is not due to the general impairment of the circadian synchrony (Figure 39). Moreover, upon GSK3β inhibition, the *CYP1A1* induction after 36 h is dramatically decreased in the synchronized cells compared to the non-synchronized cells, indicating that GSK3β may phosphorylates an important cofactor in the AhR pathway that influences either AhR stabilization, e.g. p23, or the interaction of AhR with other components, e.g. ARNT, leading to proper diurnal expression of AhR target genes (Figure 38). However, the protein levels of p23, AhR, and ARNT were not affected by GSK3β inhibition (Figure 40). Thus, no direct link between p23, AhR, and GSK3β phosphorylation could be identified. However, protein expression of BMAL1 after GSK3β inhibition and TCDD exposure showed a very similar pattern of *CYP1A1* induction under both synchronized and non-synchronized conditions, suggesting a crosslink of these components with the AhR pathway. Recent publications suggest that BMAL1 is inactivated and degraded through phosphorylation by GSK3β ensuring the maintenance of circadian rhythmicity. In addition, BMAL1 shares the same family as ARNT, i.e. they have a homology of 44,3%, supporting even more the crosslink between BMAL1, GSK3β phosphorylation and the AhR pathway [35, 157]. However, our findings contradict this, as no difference in BMAL1 protein expression after inhibition of GSK3β could be observed, neither in non-synchronized or synchronized mammary epithelial cells. Here, it is important to mention that, similar to p23, GSK3β could have different roles in regulation depending on the tissue.

4.4 Interaction of the AhR pathway with the clock machinery

The circadian clock is self-regulated through feedback loops of PER and CRY or BMAL1 and CLOCK interacting with each other, but it also senses and adapts to external environmental changes through the PAS domains of these proteins. Similar AhR and ARNT are composed of bHLH domains and PAS structural motifs that enable not only ligand binding but also heterodimerization with other proteins containing similar PAS sequences. This suggests that AhR can interact with several other proteins containing a PAS domain and possibly activate or regulate other signaling pathways. Here, an interaction between

AhR and BMAL1 was observed in breast epithelial cells (Figure 35). Already, studies have shown this interaction in ovarian and hepatic cells, supporting our data [129, 131].

The AhR immunoprecipitation assays also verified the interaction between AhR and ARNT after TCDD exposure, which seems to vary depending on the circadian phase (Figure 34). Accordingly, BMAL1 also shows some evidence that there is a possible circadian phase-dependent interaction with AhR, but more immunoprecipitation experiments must be conducted to provide a better overview (Figure 35). Perhaps these are the first evidence supporting that BMAL1 and ARNT might compete on AhR binding upon the abundance of AhR ligand driving the circadian expression of the target genes. We could speculate that under constant TCDD exposure for 48 h, BMAL1 is expressed in a circadian pattern with a 24 h period, as it is already shown that TCDD does not disrupt circadian synchrony, leading to different, time-dependent interactions with AhR and formation of the AhR:ARNT complex. This could also explain the mechanism behind the variation in cell response to AhR ligands depending on the circadian phase of the cells upon exposure. That means after exposure of the cells to an AhR ligand, AhR travels into the nucleus, and depending on the circadian phase of exposure, i.e. the abundance of the BMAL1 protein, it binds enhanced or reduced with ARNT on the *XRE* promoter, releasing a different cell response. More studies need to be conducted to have a more comprehensive idea about the exact interaction of BMAL1 and ARNT with AhR during different circadian phases. One proposal would be to change the expression of each of these genes and observe how the interaction with the other components behaves during different circadian phases. Summarizing these preliminary data, an interaction between BMAL1 and AhR could be verified for the first time in human breast epithelial cells, leading to speculation about a circadian-phase-dependent competing relationship between BMAL1 and ARNT on AhR binding.

4.5 Circadian expression of the AhR cofactor SP1

A promising cofactor of the AhR signaling pathway, possibly driving its circadian regulation, could be the transcription factor SP1. SP1 is a zinc finger transcription factor that binds to GC-rich sequences (5'-(G/T)GGGCGG(G/A)(G/A)(C/T)-3') of promoters (also called BTE (basic transcription element)) and belongs to the SP/KLF family [255]. In detail, it contains three zinc finger protein motifs at the C-terminus that can bind directly to DNA, allowing interaction with other transcriptional regulators, such as AhR. Indeed, DNA sequence analysis has shown that *XRE* and *BTE* elements are often found in promoters that are activated by polycyclic aromatic hydrocarbons, such as TCDD and benzo(a)pyrene [241]. Moreover, Fitzgerald *et al.* showed in mice that *AhR* basal expression is regulated by SP1-like factors [256], and Kobayashi *et al.* suggested, in HepG2 cells, that SP1 binds on the

BTE of the AhR target gene promoter and works cooperatively with the AhR/ARNT complex, which binds on the XRE, to induce *CYP1A1* expression [241]. The findings of Kobayashi *et al.* were also confirmed in MCF-7 and Hepa1c1c7 cells [257]. Interestingly, in pigs, AhR, although it plays an important role, is possibly not the main transcription factor of the basal *CYP1A1* expression but SP1 instead [258].

Analyzing the effect of SP1 on the AhR pathway in breast epithelial cells revealed that it plays an important role in TCDD-mediated *CYP1A1* expression upon synchronization. Specifically, SP1 downregulation altered the TCDD-mediated *CYP1A1* induction only in the synchronized cells but independently of the time of synchronization (Figure 25). Our findings suggest that SP1 plays an important role in modulating the AhR-driven *CYP1A1* induction exclusively in synchronized cells. Additionally, the TCDD dose curves depicted in Figure 26 revealed that suppression or ectopic overexpression of SP1 enhanced and reduced *CYP1A1* induction, respectively, in synchronized cells. Even if SP1 is not the main transcription factor of *CYP1A1* expression, it may be the key regulator mediating the circadian dependent expression of *CYP1A1* in the mammary epithelial cells. Supporting the theory, SP1 was identified as the only AhR signaling cofactor with a circadian expression at protein level (Figure 21). At this point, it can be hypothesized that AhR binds to the XRE element with ARNT and activates the AhR target gene expression, and subsequently SP1 is recruited to the BTE element, either initiating or maintaining circadian expression regulated by the competition between the AhR:BMAL1 and AhR:ARNT interactions on the XRE element. Moreover, we could show an interaction between AhR and SP1 independently of ligand exposure upon synchronization, which would enhance the theory that AhR and SP1 bind both on the promoter even for the basal expression of *CYP1A1* [245, 259]. In addition, the transcription factor SP1 is phosphorylated at several serine and threonine positions, and proteomic analysis suspects S728-p and S732-p sites as potential SP1 phosphorylation sites for GSK3β [260, 261]. A potential inhibition of GSK3β could lead to a deregulation of SP1 by alterations in its GSK3β-mediated phosphorylation, and this could possibly explain the circadian disruption in the TCDD-mediated *CYP1A1* induction after CHIR99021 exposure shown in Figure 38. In the future, it should be of highest interest to conduct more complicated and time-consuming experiments specific to the GSK3β-mediated phosphorylation of SP1 to understand whether there is a crosslink between these components and the circadian regulation of the AhR pathway.

4.6 Proposed model of the mechanism behind the circadian regulation of the AhR pathway

All the findings of this work can be summarized in a proposal for a mechanistic model, graphically depicted in Figure 42. Upon ligand exposure, e.g. TCDD, AhR translocates into the nucleus and binds with ARNT and the circadian rhythm regulator, BMAL1. Preliminary data indicate that these two components compete for AhR binding depending on the circadian phase regulating the circadian *XRE* promoter activity and the oscillation of AhR target gene expression upon ligand exposure. We could hypothesize that in a circadian phase with reduced BMAL1 expression, AhR would be more prone to bind with ARNT, and thus, the cellular response would be enhanced upon activation of AhR signaling by a ligand. Although, more experiments are required to confirm this theory. Additionally, we identified that SP1 plays an important role in the maintenance of this circadian regulation of AhR target gene expression, and p23 is a negative regulator of this promoter activation. Here, it could be again speculated that possibly p23 could help the mechanism not be overstimulated and sense its maximum capacity. Beside all this, GSK3β seems to have a specific role in the circadian regulation of the AhR pathway, which needs to be further elucidated. Possibly, GSK3β can modulate the circadian regulation of SP1 at protein level, as it is predicted that GSK3β phosphorylates SP1 at the following phosphorylation sites, S728-p and S732-p. Also, it could may be that GSK3β has a specific role in the BMAL1/ AhR interaction, as it is described to phosphorylate BMAL1. More experiments need to be performed to understand the exact effect of p23, SP1, and GSK3β on ARNT and BMAL1 binding to AhR and the circadian regulation of the AhR signaling pathway.

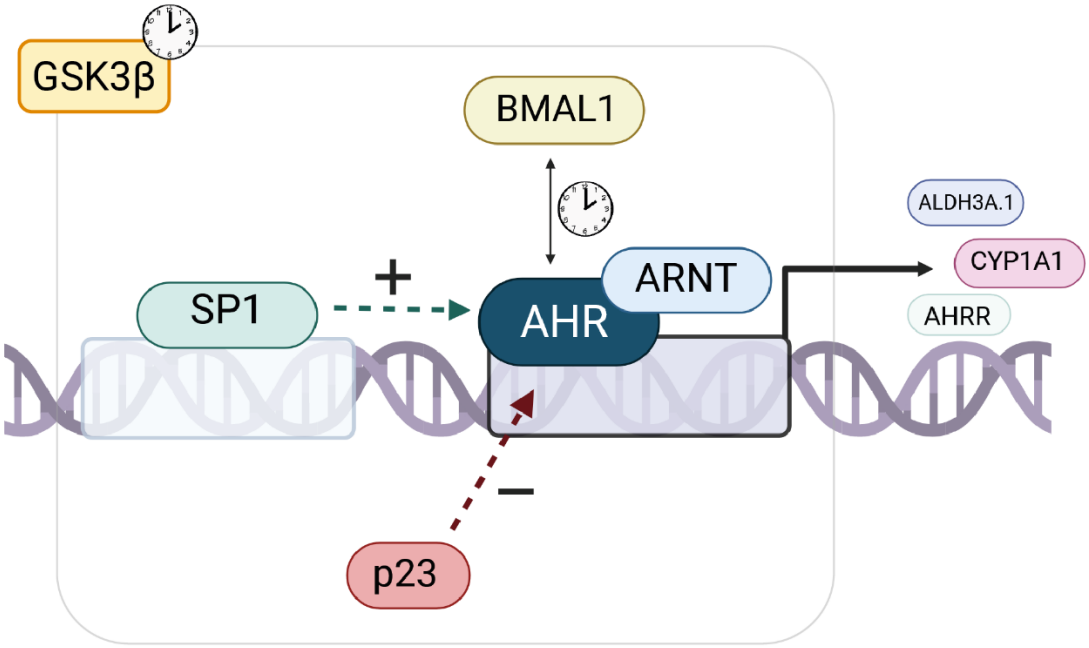

Figure 42: Proposed molecular mechanism of the circadian regulation of the AhR signaling AhR:ARNT heterodimer binds to the XRE sequence of the AhR target gene promoter, depending on the circadian phase. Also, BMAL1 binds with AhR and possibly competes with ARNT for AhR binding in a circadian manner. Thus, one theory could be that in the circadian phase, where BMAL1 is more expressed, exposure to an AhR ligand would probably lead to a reduced cellular response, as a decreased AHR/ ARNT complex would be formed and bind to the XRE promoter for target gene expression. Further, p23 negatively regulates promoter activation, and SP1 plays an important role in the maintenance of the circadian oscillation of the target gene transcription by binding to the BTE sequence of the promoter, probably in a circadian manner, as it shows a circadian pattern in protein level. GSK3β seems to have a specific role in the circadian regulation of the AhR pathway and could be proposed as a possible candidate modulating the SP1 circadian expression or BMAL1/ AhR interaction. (The illustration was created with BioRender.com).

4.7 The importance of understanding the regulatory framework of the circadian regulation of the AhR pathway

The development of *in vitro* systems mimicking as best as possible the situation in living organisms and simultaneously consider its complex regulatory network is of highest priority for biomedical and toxicological research. In the last years, reconstructing 3D tissue structures, i.e. developing *in vitro* 3D organoids, has been in the spotlight of biomedical and toxicological research. However, these quickly were identified as inappropriate for a large scale testing system, as several problems in handling and reproducibility appeared [262]. The next step was to develop organ-on-chip technologies that not only have the 3D structure of the tissues but also mimic the physiological constant flow of nutrients, metabolites, and signaling molecules, necessary in distinct compartments, facilitating functional interactions between different organs. This is an even more complex approach than the 3D cultures, with various standardization and transferability difficulties, making it

not easily applied by standard laboratories [263]. For years, both of these technologies neglected physiological and metabolic regulatory pathways such as the circadian rhythms, which is actually involved in almost every biological process (described in detail in chapter 1.3). Indeed, circadian rhythm playing a significant role in xenobiotic metabolism, for example in AhR signaling, which is one of the most toxicological relevant pathways, should be of particular interest in assay development, providing information about the response of exposure to industrial and environmental chemicals as well as drugs used for disease treatment. The ideal would be, at some point, to fuse circadian rhythms and 3D strategies (organoids or the organ on a chip), but until then, it could be easily incorporated in already existing 2D *in vitro* assays, enhancing the sensitivity of these test systems for the highest possible biological relevance. At this point, it is important to mention, that 3D systems fulfill all the requirements to incorporate circadian rhythmicity, but that would also mean adding another layer of complexity, and a lot of 2D systems are not suitable to transfer into 3D culture [109].

Although implementing circadian synchrony in 3D systems would mean adding another level of complexity, several already existing 2D *in vitro* systems could be easily leveled up by adding the simple step of circadian synchronization. The cultured cells could be stimulated with dexamethasone or forskolin for 0.5- 1 h to synchronize in the same circadian phase reflecting the *in vivo* situation, and available luciferase or other reporter gene cell lines that allow visualization of the circadian rhythmicity could be used to verify a successful synchronization [264]. The only disadvantage of this approach is that several 2D test systems employ cancer cells that are particularly hard or impossible to synchronize. But instead of using these cell lines for circadian regulation assays, they could be compared with synchronized non-cancerous cells to extract information about regulatory and cellular response differences between physiological and pathological conditions. Further, these elevated *in vitro* systems could be applied to study the effects and regulatory pathways of different *ze*itgebers, such as glucocorticoids and temperature [264, 265]. Interestingly, temperature has already been identified, as an *in vivo zeitgeber* and regulator of the expression of core clock genes in a posttranscriptional level by temperature-controlled alternative splicing processes [266]. Several studies have already shown that implementing circadian synchrony in *in vitro* systems significantly elevates the sensitivity of the cell response and leads to more accurate biological relevant data, such as the definition of the optimal treatment window to achieve the best biological relevant response [201, 230, 248]. This would allow us to screen substances and unravel molecular mechanisms that have a higher impact on human biological processes depending on the time of exposure or analysis. For example, in this thesis, the mechanism of the circadian regulation of the AhR

pathway was thoroughly analyzed to understand its exact function in xenobiotic metabolism or other biological processes by using the already established, elevated by synchronization 2D, *in vitro* system by Ndikung *et al.* [201]. Last, the results obtained from improved *in vitro* assays could improve physiologically based pharmacokinetic (PBPK) modelling, which is used to transfer in vitro obtained data for human application through in IVIVE (*in vitro* - *in vivo* extrapolation) techniques [267]. All in all, advanced *in vitro* systems provide more reliable biological relevant data by incorporating the regulatory framework of specific important processes for risk assessment and pharmaceutical drug development.

On the other hand, it is important not only to implement circadian rhythm in the *in vitro* systems for their improvement, but it is also of highest interest to understand itself and ensure human health. Specifically, studying the circadian regulation of the AhR pathway would not only give answers to how the circadian rhythm influences xenobiotic metabolism, specifically AhR signaling, but could also be used as an endpoint to understand the extent of the effect of circadian disruption on the AhR pathway and cell response. It is well described that circadian disruption due to modern lifestyle, i.e. light pollution, abnormal food consumption, and time or temperature changing environment, can lead to various diseases. However, to what extent this is affecting the xenobiotic metabolism and the risk probability for several hazards is not fully understood. Several studies have crosslinked chemicals with circadian disruption, but the exact influence of environmental and industrial chemicals on circadian rhythm and disease development remains unknown. Indeed, the circadian rhythm and xenobiotic metabolism seem to be tightly connected in common human diseases, such as cancer, cardiovascular, or metabolic diseases, but their mechanistic connection is often neglected in toxicological and biomedical research, and the outcome of this interplay is not fully discovered. Understanding the crosslink of circadian disruption and xenobiotic metabolism on disease development and progression should be of highest priority to become a novel toxicological endpoint in chemical and drug assessment. Moreover, unraveling toxicity pathways, such as the AhR signaling, could be used in developing guides, such as AOPs (adverse outcome pathways) and networks for efficient and human relevant testing assessment strategies [268, 269]. Although studies in non-human models have already shown that several metals, biocides, pesticides, polychlorinated biphenyls, hormones, and endocrine active substances are potential circadian disruptors, it is time to apply *in vitro* assays based on human cells or tissues to discover potential circadian disruptors more relevant to humans. Indeed, plenty of different circadian reporter systems in various tissues have already been established and could be employed in drug or chemical assessment.

Summarizing, implementing the circadian rhythm into *in vitro* test systems would lead to more biological relevant data to humans as well as unraveling its role in different toxicological pathways would lead to the development of more successful and innovative strategies in regulatory testing. Moreover, identifying circadian disruptors and their role in different pathways that lead to disease development and progression would improve the toxicological assessment of chemicals (environmental or industrial) and drugs (pharmaceutical). All this would hopefully enlighten us about the impact of the circadian regulation on human health and disease, which would lead to the development of novel health protective and therapeutic strategies. Here, specifically, unraveling the circadian regulation of the AhR pathway and subsequently broadening the knowledge of this very important toxicological pathway in correlation with the circadian rhythms will hopefully impact the development of more precise in vitro test systems for drug and chemical assessment to ensure human health.

4.8 Perspectives

Proposing a possible mechanism for the circadian regulation of the AhR signaling sets the foundation for future studies to fully understand this regulation and have an impact on improving *in vitro* test systems. In the near future, more experiments targeting the components p23 and SP1 should be performed to understand their exact role in this regulation by making stable knockdown or overexpression cell lines and studying the *CYP1A1* induction upon time. Also, studies targeting GSK3β, which could possibly mediate the circadian regulation of AhR signaling through p23 or SP1, should be performed to identify its exact role in this pathway. These could imply performing GSK3β mediated phosphorylation studies or further analysis of the predicted GSK3β phosphorylation sites of SP1. Last, more time-consuming, and complex AhR, BMAL1, and ARNT immunoprecipitation assays should be performed over time to verify the circadian competition of BMAL1 and ARNT on AhR binding. The immunoprecipitants could also be submitted for mass spectrometry and proteomic analysis to achieve a more precise quantification. Performing these further experiments would provide an even better understanding of the circadian regulation of the AhR pathway, and this mechanism could be used in developing new strategies in regulatory testing or drug development. All in all, fully characterizing the circadian regulation of an important toxicological pathway, such as the AhR, may directs the research towards unraveling even more mechanisms of pathways regulated by the circadian rhythms, and acknowledge the importance of the circadian clock in the field of toxicology.

5 References

1. Huang RC (2018) The discoveries of molecular mechanisms for the circadian rhythm: The 2017 Nobel Prize in Physiology or Medicine. Biomed J 41:5–8. https://doi.org/10.1016/j.bj.2018.02.003
2. Fuhr L, Abreu M, Pett P, Relogio A (2015) Circadian systems biology: When time matters. Comput Struct Biotechnol J 13:417–426. https://doi.org/10.1016/j.csbj.2015.07.001
3. de Mairan J (1729) Observation botanique. Hist. Acad. Roy. Sci. 35–36. In: Hist. Acad. Roy. pp 35–36
4. Kleitman N (1957) Sleep, wakefulness, and consciousness. Psychol. Bull. 54:354–359
5. Bünning E (1932) Die Erblichkeit der Tagesperiodizität bei Pflanzen. Naturwissenschaften 340–345
6. Takahashi JS, Zatz M (1982) Regulation of circadian rhythmicity. Science (80-) 217:1104–1111. https://doi.org/10.1126/science.6287576
7. Rosbash M (2017) A 50-year personal journey: Location, gene expression, and circadian rhythms. Cold Spring Harb Perspect Biol 9:. https://doi.org/10.1101/cshperspect.a032516
8. Dibner C, Schibler U (2015) Circadian timing of metabolism in animal models and humans. J Intern Med 277:513–527. https://doi.org/10.1111/joim.12347
9. Rosbash M, Hall JC (1989) The molecular biology of circadian rhythms. Neuron 3:387–398. https://doi.org/10.1016/0896-6273(89)90199-2
10. Bhadra U, Thakkar N, Das P, Pal Bhadra M (2017) Evolution of circadian rhythms: from bacteria to human. Sleep Med 35:49–61. https://doi.org/10.1016/j.sleep.2017.04.008
11. Bell-Pedersen D, Cassone VM, David J. Earnest, Susan S. Golden, Paul E. Hardin, Terry L. Thomas MJZ (2005) Circadian rhythms from multiple oscillators: Lessons from diverse organisms. Nat Rev Genet 6:544–556. https://doi.org/10.1161/CIRCULATIONAHA.110.956839
12. Aschoff J (1960) Exogenous and endogenous components in circadian rhythms. Cold Spring Harb Symp Quant Biol 25:11–28. https://doi.org/10.1101/sqb.1960.025.01.004
13. Vitaterna MH, Takahashi JS, Turek FW (2001) Overview of circadian rhythms. Alcohol Res Heal 25:85–93
14. Pittendrigh CS (1960) Circadian rhythms and the circadian organization of living systems. Cold Spring Harb Symp Quant Biol 25:159–184. https://doi.org/10.1101/sqb.1960.025.01.015
15. Berson DM, Dunn FA, Motoharu T (2002) Phototransduction by Retinal Ganglion Cells That Set the Circadian Clock. Science (80-) 295:1070–1073
16. Dibner C, Schibler U, Albrecht U (2009) The mammalian circadian timing system: Organization and coordination of central and peripheral clocks
17. Nicolas C, Paolo S-C (2000) Multilevel regulation of the ciracadian clock. Nat Rev Mol Cell Biol 1:59–67
18. Albrecht U (2012) Timing to Perfection: The Biology of Central and Peripheral Circadian Clocks. Neuron 74:246–260. https://doi.org/10.1016/j.neuron.2012.04.006
19. Mohawk JA, Green CB, Takahashi JS (2012) Central and Peripheral Circadian Clocks in Mammals. Annu Rev Neurosci 35:445–462. https://doi.org/10.1146/annurev-neuro-060909-153128
20. Vansteensel MJ, Michel S, Meijer JH (2008) Organization of cell and tissue circadian pacemakers: A comparison among species. Brain Res Rev 58:18–47. https://doi.org/10.1016/j.brainresrev.2007.10.009
21. Robinson I, Reddy AB (2014) Molecular mechanisms of the circadian clockwork in mammals. FEBS Lett 588:2477–2483. https://doi.org/10.1016/j.febslet.2014.06.005
22. Anafi RC, Francey LJ, Hogenesch JB, Kim J (2017) CYCLOPS reveals human transcriptional rhythms in health and disease. Proc Natl Acad Sci U S A 114:5312–5317. https://doi.org/10.1073/pnas.1619320114
23. Wittenbrink N, Ananthasubramaniam B, Munch M, et al (2018) High-accuracy determination of internal circadian time from a single blood sample. J Clin Invest 128:3826–3839. https://doi.org/10.1172/jci120874
24. Zhang R, Lahens NF, Ballance HI, et al (2014) A circadian gene expression atlas in mammals: implications for biology and medicine. Proc Natl Acad Sci U S A 111:16219–16224. https://doi.org/10.1073/pnas.1408886111

25. Yu W, Nomura M, Ikeda M (2002) Interactivating feedback loops within the mammalian clock: BMAL1 is negatively autoregulated and upregulated by CRY1, CRY2, and PER2. Biochem Biophys Res Commun 290:933–941. https://doi.org/10.1006/bbrc.2001.6300

26. Partch CL, Green CB, Takahashi JS (2014) Molecular Architecture of the Mammalian Circadian Clock. Trends Cell Biol 24:90–99. https://doi.org/10.1016/j.tcb.2013.07.002.Molecular

27. Ohsaki K, Oishi K, Kozono Y, et al (2008) The role of β-TrCP1 and β-TrCP2 in circadian rhythm generation by mediating degradation of clock protein PER2. J Biochem 144:609–618. https://doi.org/10.1093/jb/mvn112

28. Asher G, Gatfield D, Stratmann M, et al (2008) SIRT1 Regulates Circadian Clock Gene Expression through PER2 Deacetylation. Cell 134:317–328. https://doi.org/10.1016/j.cell.2008.06.050

29. Lee HM, Chen R, Kim H, et al (2011) The period of the circadian oscillator is primarily determined by the balance between casein kinase 1 and protein phosphatase 1. Proc Natl Acad Sci U S A 108:16451–16456. https://doi.org/10.1073/pnas.1107178108

30. Narasimamurthy R, Hunt SR, Lu Y, et al (2018) CK1δ/e protein kinase primes the PER2 circadian phosphoswitch. Proc Natl Acad Sci U S A 115:5986–5991. https://doi.org/10.1073/pnas.1721076115

31. Brown SA, Kowalska E, Dallmann R (2012) (Re)inventing the Circadian Feedback Loop. Dev Cell 22:477–487. https://doi.org/10.1016/j.devcel.2012.02.007

32. Lee J, Lee S, Chung S, et al (2016) Identification of a novel circadian clock modulator controlling BMAL1 expression through a ROR/REV-ERB-response element-dependent mechanism. Biochem Biophys Res Commun 469:580–586. https://doi.org/10.1016/j.bbrc.2015.12.030

33. Lee C, Etchegaray J-P, Cagampang FRA, et al (2001) Posttranslational Mechanisms Regulate the Mammalian Circadian Clock. Cell 107:855–867. https://doi.org/10.1136/bjo.2008.139840

34. Yoo S-H, Mohawk JA, Siepka SM, et al (2013) Competing E3 Ubiquitin Ligases Determine Circadian Period by Regulated Degradation of CRY in Nucleus and Cytoplasm. Cell 152:1091–1105. https://doi.org/10.1016/j.cell.2013.01.055.Competing

35. Sahar S, Zocchi L, Kinoshita C, et al (2010) Regulation of BMAL1 protein stability and circadian function by GSK3β-mediated phosphorylation. PLoS One 5:. https://doi.org/10.1371/journal.pone.0008561

36. Yin L, Wang J, Klein PS, Lazar1 MA (2006) Nuclear Receptor Rev-erba Is a Critical Lithium-Sensitive Component of the Circadian Clock. Science (80-) 311:1002–1006

37. Garg A, Orru R, Ye W, et al (2019) Structural and mechanistic insights into the interaction of the circadian transcription factor BMAL1 with the KIX domain of the CREB-binding protein. J Biol Chem 294:16604–16619. https://doi.org/10.1074/jbc.RA119.009845

38. Soni SK, Basu P, Singaravel M, et al (2021) Sirtuins and the circadian clock interplay in cardioprotection: focus on sirtuin 1. Cell Mol Life Sci 78:2503–2515. https://doi.org/10.1007/s00018-020-03713-6

39. Lee J, Lee Y, Lee MJ, et al (2008) Dual Modification of BMAL1 by SUMO2/3 and Ubiquitin Promotes Circadian Activation of the CLOCK/BMAL1 Complex. Mol Cell Biol 28:6056–6065. https://doi.org/10.1128/mcb.00583-08

40. Stojkovic K, Wing SS, Cermakian N (2014) A central role for ubiquitination within a circadian clock protein modification code. Front Mol Neurosci 7:1–7. https://doi.org/10.3389/fnmol.2014.00069

41. Chen LC, Hsieh YL, Tan GYT, et al (2021) Differential effects of SUMO1 and SUMO2 on circadian protein PER2 stability and function. Sci Rep 11:1–13. https://doi.org/10.1038/s41598-021-93933-y

42. Patke A, Young MW, Axelrod S (2020) Molecular mechanisms and physiological importance of circadian rhythms. Nat. Rev. Mol. Cell Biol. 21:67–84

43. Boivin DB, Boudreau P, Kosmadopoulos A (2022) Disturbance of the Circadian System in Shift Work and Its Health Impact. J. Biol. Rhythms 37:3–28

44. Xie Y, Tang Q, Chen G, et al (2019) New insights into the circadian rhythm and its related diseases. Front. Physiol. 10

45. Young ME, Laws FA, Goodwin GW, Taegtmeyer H (2001) Reactivation of Peroxisome Proliferator-activated Receptor α Is Associated with Contractile Dysfunction in Hypertrophied Rat Heart. J Biol Chem 276:44390–44395. https://doi.org/10.1074/jbc.M103826200

46. Thosar SS, Butler MP, Shea SA (2018) Role of the circadian system in cardiovascular disease. J. Clin. Invest. 128:2157–2167

47. Douma LG, Gumz ML (2018) Circadian clock-mediated regulation of blood pressure. Free Radic. Biol. Med. 119:108–114

48. Ruger M, Scheer FAJL (2009) Effects of circadian disruption on the cardiometabolic system. Rev. Endocr. Metab. Disord. 10:245–260

49. Gutenbrunner C (2000) Circadian variations of the serum creatine kinase level: A masking effect? Chronobiol Int 17:583–590. https://doi.org/10.1081/CBI-100101065

50. Curtis AM, Cheng Y, Kapoor S, et al (2007) Circadian variation of blood pressure and the vascular response to asynchronous stress. PNAS 104:3450–3455

51. Takeda N, Maemura K (2011) Circadian clock and cardiovascular disease. J. Cardiol. 57:249–256

52. Martino TA, Oudit GY, Herzenberg AM, et al (2008) Circadian rhythm disorganization produces profound cardiovascular and renal disease in hamsters. Am J Physiol Regul Integr Comp Physiol 294:1675–1683. https://doi.org/10.1152/ajpregu.00829.2007.-Sleep

53. Alibhai FJ, LaMarre J, Reitz CJ, et al (2017) Disrupting the key circadian regulator CLOCK leads to age-dependent cardiovascular disease. J Mol Cell Cardiol 105:24–37. https://doi.org/10.1016/j.yjmcc.2017.01.008

54. Vyas M V., Garg AX, Iansavichus A V., et al (2012) Shift work and vascular events: Systematic review and meta-analysis. BMJ 345:. https://doi.org/10.1136/bmj.e4800

55. Scheiermann C, Kunisaki Y, Frenette PS (2013) Circadian control of the immune system. Nat. Rev. Immunol. 13:190–198

56. Haus E, Smolensky MH (1999) Biologic rhythms in the immune system. Chronobiol Int 16:581–622. https://doi.org/10.3109/07420529908998730

57. Geiger SS, Fagundes CT, Siegel RM (2015) Chrono-immunology: Progress and challenges in understanding links between the circadian and immune systems. Immunology 146:349–358. https://doi.org/10.1111/imm.12525

58. Méndez-Ferrer S, Lucas D, Battista M, Frenette PS (2008) Haematopoietic stem cell release is regulated by circadian oscillations. Nature 452:442–447. https://doi.org/10.1038/nature06685

59. Mohren DCL, Jansen NWH, Kant I, et al (2002) Prevalence of Common Infections Among Employees in Different Work Schedules. JOEM1003 44:1003–1011. https://doi.org/10.1097/01.jom.0000034348.94005.74

60. Fatima Y, Bucks RS, Mamun AA, et al (2021) Shift work is associated with increased risk of COVID-19: Findings from the UK Biobank cohort. J Sleep Res 30:. https://doi.org/10.1111/jsr.13326

61. Jerigova V, Zeman M, Okuliarova M (2022) Circadian Disruption and Consequences on Innate Immunity and Inflammatory Response. Int. J. Mol. Sci. 23

62. Challet E (2019) The circadian regulation of food intake. Nat Rev Endocrinol 15:393–405. https://doi.org/10.1038/s41574-019-0210-x

63. Cornélissen G (2021) Circadian disruption and metabolic disease risk. Funct Foods Nutraceuticals Metab Non-communicable Dis 509–516. https://doi.org/10.1016/B978-0-12-819815-5.00004-5

64. Liu J, Zhou B, Yan M, et al (2016) Clock and BMAL1 regulate muscle insulin sensitivity via SIRT1 in male mice. Endocrinology 157:2259–2269. https://doi.org/10.1210/en.2015-2027

65. Turek FW, Joshu C, Kohsaka A, et al (2005) Obesity and metabolic syndrome in circadian Clock mutant nice. Science (80-) 308:1043–1045. https://doi.org/10.1126/science.1108750

66. Yang S, Liu A, Weidenhammer A, et al (2009) The role of mPer2 clock gene in glucocorticoid and feeding rhythms. Endocrinology 150:2153–2160. https://doi.org/10.1210/en.2008-0705

67. Lakatua DJ, Halberg F, Haus E, et al (1976) Timing of single daily meals serves to manipulate relations among human circadian plasma growth hormone, cortisol, insulin and cardiovascular rhythms. Endocrinology 98:456

68. Shi SQ, Ansari TS, McGuinness OP, et al (2013) Circadian disruption leads to insulin resistance and obesity. Curr Biol 23:372–381. https://doi.org/10.1016/j.cub.2013.01.048

69. Halberg F, Visscher MB (1952) Effect of light and of availability of food upon the 24-hour rhythm in number of circulating eosinophils in mice. Am J Physiol 171:732

70. La Fleur SE, Kalsbeek A, Wortel J, Buijs RM (1999) A suprachiasmatic nucleus generated rhythm in basal glucose concentrations. J Neuroendocrinol 11:643–652. https://doi.org/10.1046/j.1365-2826.1999.00373.x

71. Coomans C, Saaltink DJ, Deboer T, et al (2021) Doublecortin-like expressing astrocytes of the suprachiasmatic nucleus are implicated in the biosynthesis of vasopressin and influences circadian rhythms. Glia 69:2752–2766. https://doi.org/10.1002/glia.24069

72. Marcheva B, Ramsey KM, Peek CB, et al (2013) Circadian clocks and metabolism. Handb Exp Pharmacol 127–155. https://doi.org/10.1007/978-3-642-25950-0_6

73. Wondmkun YT (2020) Obesity, insulin resistance, and type 2 diabetes: Associations and therapeutic implications. Diabetes, Metab. Syndr. Obes. 13:3611–3616

74. Xiao W, Wang RS, Handy DE, Loscalzo J (2018) NAD(H) and NADP(H) Redox Couples and Cellular Energy Metabolism. Antioxidants Redox Signal. 28:251–272

75. Jordan SD, Lamia KA (2013) AMPK at the crossroads of circadian clocks and metabolism. Mol. Cell. Endocrinol. 366:163–169

76. Chang HC, Guarente L (2014) SIRT1 and other sirtuins in metabolism. Trends Endocrinol. Metab. 25:138–145

77. Reinke H, Asher G (2019) Crosstalk between metabolism and circadian clocks. Nat. Rev. Mol. Cell Biol. 20:227–241

78. Hardeland R, Coto-Montes A, Poeggeler B (2003) Circadian Rhythms, Oxidative Stress, and Antioxidative Defense Mechanisms. Chronobiol. Int. 20:921–962

79. Gamble KL, Berry R, Frank SJ, Young ME (2014) Circadian clock control of endocrine factors. Nat Rev Endocrinol 10:466–475. https://doi.org/10.1038/nrendo.2014.78

80. Bottalico LN, Weljie AM (2021) Cross-species physiological interactions of endocrine disrupting chemicals with the circadian clock. Gen. Comp. Endocrinol. 301

81. Neumann AM, Schmidt CX, Brockmann RM, Oster H (2019) Circadian regulation of endocrine systems. Aut Neurosci 216:1–8. https://doi.org/10.1016/j.autneu.2018.10.001

82. Brown GM (1994) Light, Melatonin and the Sleep-Wake Cycle. J ofPsychiatry Neurosci 19:

83. Delgado-Lara DL, González-Enríquez G V., Torres-Mendoza BM, et al (2020) Effect of melatonin administration on the PER1 and BMAL1 clock genes in patients with Parkinson's disease. Biomed Pharmacother 129:. https://doi.org/10.1016/j.biopha.2020.110485

84. Korf HW, von Gall C (2006) Mice, melatonin and the circadian system. Mol Cell Endocrinol 252:57–68. https://doi.org/10.1016/j.mce.2006.03.005

85. Lewy AJ, Ahmed S, Sack RL (1996) Phase shifting the human circadian clock using melatonin. Behav Brain Res 73:131–134

86. Sanchez REA, Kalume F, de la Iglesia HO (2022) Sleep timing and the circadian clock in mammals: Past, present and the road ahead. Semin. Cell Dev. Biol. 126:3–14

87. de Assis LVM, Oster H (2021) The circadian clock and metabolic homeostasis: entangled networks. Cell. Mol. Life Sci. 78:4563–4587

88. Koop S, Oster H (2022) Eat, sleep, repeat – endocrine regulation of behavioural circadian rhythms. FEBS J. 289:6543–6558

89. Oster H, Challet E, Ott V, et al (2017) The functional and clinical significance of the 24-hour rhythm of circulating glucocorticoids. Endocr. Rev. 38:3–45

90. Tsang AH, Astiz M, Friedrichs M, Oster H (2016) Endocrine regulation of circadian physiology. J. Endocrinol. 230:R1–R11

91. Gi HS, Chung S, Han KC, et al (2008) Adrenal peripheral clock controls the autonomous circadian rhythm of glucocorticoid by causing rhythmic steroid production. Proc Natl Acad Sci U S A 105:20970–20975. https://doi.org/10.1073/pnas.0806962106

92. Tsang AH, Barclay JL, Oster H (2013) Interactions between endocrine and circadian systems. J. Mol. Endocrinol. 52

93. Stiefel C, Stintzing F (2023) Endocrine-active and endocrine-disrupting compounds in food – occurrence, formation and relevance. NFS J 31:57–92. https://doi.org/10.1016/j.nfs.2023.03.004

94. Gamble KL, Berry R, Frank SJ, Young ME (2014) Circadian clock control of endocrine factors. Nat. Rev. Endocrinol. 10:466–475

95. Zhang Q, Jiang C, Li H, et al (2020) Effect of the Interaction Between Cadmium Exposure and CLOCK Gene Polymorphisms on Thyroid Cancer: a Case-Control Study in China. Biol Trace Elem Res 196:86–95. https://doi.org/10.1007/s12011-019-01904-2

96. Bahougne T, Angelopoulou E, Jeandidier N, Simonneaux V (2020) Individual evaluation of luteinizing hormone in aged C57BL/6 J female mice. GeroScience 42:323–331. https://doi.org/10.1007/s11357-019-00104-z

97. Zhao Y, Zhang K, Fent K (2018) Regulation of zebrafish (Danio rerio) locomotor behavior and circadian rhythm network by environmental steroid hormones. Environ Pollut 232:422–429. https://doi.org/10.1016/j.envpol.2017.09.057

98. Kabir ER, Rahman MS, Rahman I (2015) A review on endocrine disruptors and their possible impacts on human health. Environ. Toxicol. Pharmacol. 40:241–258

99. Zhang Y, Meng N, Bao H, et al (2019) Circadian gene PER1 senses progesterone signal during human endometrial decidualization. J Endocrinol. https://doi.org/10.1530/JOE-19-0284

100. Gery S, Virk RK, Chumakov K, et al (2007) The clock gene Per2 links the circadian system to the estrogen receptor. Oncogene 26:7916–7920. https://doi.org/10.1038/sj.onc.1210585

101. Francavilla A, Eagon PK, DiLeo A, et al (1986) Circadian rhythm of hepatic cytosolic and nuclear estrogen receptors. Gastroenterology 91:182–188. https://doi.org/10.3109/07420528609079538

102. Salamanca-Fernández E, Rodríguez-Barranco M, Guevara M, et al (2018) Night-shift work and breast and prostate cancer risk: Updating the evidence from epidemiological studies. An. Sist. Sanit. Navar. 41:211–226

103. Omiecinski CJ, Vanden Heuvel JP, Perdew GH, Peters JM (2011) Xenobiotic metabolism, disposition, and regulation by receptors: From biochemical phenomenon to predictors of major toxicities. Toxicol. Sci. 120

104. DeBruyne JP, Weaver DR, Dallmann R (2014) The hepatic circadian clock modulates xenobiotic metabolism in mice. J Biol Rhythms 29:277–287. https://doi.org/10.1177/0748730414544740

105. Dallmann R, Okyar A, Levi F (2016) Dosing-Time Makes the Poison: Circadian Regulation and Pharmacotherapy. Trends Mol Med 22:430–445. https://doi.org/10.1016/j.molmed.2016.03.004

106. Meléndez-Fernández OH, Liu JA, Nelson RJ (2023) Circadian Rhythms Disrupted by Light at Night and Mistimed Food Intake Alter Hormonal Rhythms and Metabolism. Int. J. Mol. Sci. 24

107. Bicker J, Alves G, Falcão A, Fortuna A (2020) Timing in drug absorption and disposition: The past, present, and future of chronopharmacokinetics. Br. J. Pharmacol. 177:2215–2239

108. Dobrek L (2021) Chronopharmacology in therapeutic drug monitoring—dependencies between the rhythmics of pharmacokinetic processes and drug concentration in blood. Pharmaceutics 13

109. Mihelakis M, Ndikung J, Oelgeschläger M, Ertych N (2022) The 4th dimension of in vitro systems – Time to level up. Environ Int 164:. https://doi.org/10.1016/j.envint.2022.107256

110. Claudel T, Cretenet G, Saumet A, Gachon F (2007) Crosstalk between xenobiotics metabolism and circadian clock. FEBS Lett. 581:3626–3633

111. Tani N, Ikeda T, Ishikawa T (2023) Relationship between clock gene expression and CYP2C19 and CYP3A4 with benzodiazepines. Hum Exp Toxicol 42:1–9. https://doi.org/10.1177/09603271231171643

112. Sundekilde UK, Kristensen CM, Olsen MA, et al (2022) Time-dependent regulation of hepatic cytochrome P450 mRNA in male liver-specific PGC-1α knockout mice. Toxicology 469:. https://doi.org/10.1016/j.tox.2022.153121

113. Li H, Wang Y-G, Ma Z-C, et al (2021) A high-throughput cell-based gaussia luciferase reporter assay for measurement of CYP1A1, CYP2B6, and CYP3A4 induction. Xenobiotica 51:752–763. https://doi.org/10.1080/00498254.2021.1918800

114. Zhang T, Guo L, Yu F, et al (2019) The nuclear receptor Rev-erbα participates in circadian regulation of Ugt2b enzymes in mice. Biochem Pharmacol 161:89–97. https://doi.org/https://doi.org/10.1016/j.bcp.2019.01.010

115. Guo L, Yu F, Zhang T, Wu B (2018) The clock protein BMAL1 regulates circadian expression and activity of sulfotransferase 1A1 in mice. Drug Metab Dispos 46:1403–1410. https://doi.org/10.1124/dmd.118.082503

116. Xu YQ, Zhang D, Jin T, et al (2012) Diurnal Variation of Hepatic Antioxidant Gene Expression in Mice. PLoS One 7:3–10. https://doi.org/10.1371/journal.pone.0044237

117. Filipski E, Berland E, Ozturk N, et al (2014) Optimization of irinotecan chronotherapy with P-glycoprotein inhibition. Toxicol Appl Pharmacol 274:471–479. https://doi.org/10.1016/j.taap.2013.12.018

118. Zhou C, Yu F, Zeng P, et al (2019) Circadian sensitivity to the cardiac glycoside oleandrin is associated with diurnal intestinal P-glycoprotein expression. Biochem Pharmacol 169:113622. https://doi.org/https://doi.org/10.1016/j.bcp.2019.08.024

119. Sanchez RI, Kauffman FC (210AD) Regulation of Xenobiotic Metabolism in the Liver. Compr Toxicol 9:109–128

120. Xu C, Yong-Tao Li C, Tony Kong A-N (2005) Induction of Phase I, II and III Drug Metabolism/Transport by Xenobiotics

121. Claudel T, Cretenet G, Saumet A, Gachon F (2007) Crosstalk between xenobiotics metabolism and circadian clock. FEBS Lett 581:3626–3633. https://doi.org/10.1016/j.febslet.2007.04.009

122. Ferrell JM, Chiang JYL (2015) Circadian rhythms in liver metabolism and disease. Acta Pharm. Sin. B 5:113–122

123. Gachon F (2007) Physiological function of PARbZip circadian clock-controlled transcription factors. Ann. Med. 39:562–571

124. Mackowiak B, Wang H (2016) Mechanisms of xenobiotic receptor activation: Direct vs. indirect. Biochim Biophys Acta - Gene Regul Mech 1859:1130–1140. https://doi.org/10.1016/j.bbagrm.2016.02.006

125. Yang X (2010) A wheel of time: The circadian clock, nuclear receptors, and physiology. Genes Dev. 24:741–747

126. Gachon F, Olela FF, Schaad O, et al (2006) The circadian PAR-domain basic leucine zipper transcription factors DBP, TEF, and HLF modulate basal and inducible xenobiotic detoxification. Cell Metab 4:25–36. https://doi.org/10.1016/j.cmet.2006.04.015

127. Panda S, Antoch MP, Miller BH, et al (2002) Coordinated Transcription of Key Pathways in the Mouse by the Circadian Clock dian oscillator directs transcription of the photosyn-thetic machinery to the daylight hours, thereby ensuring efficient assimilation of light energy. In mammals, circa-dian consolidation of locomotor activity to time of food availability and predator avoidance functions to improve

128. Gachon F, Fonjallaz P, Damiola F, et al (2004) The loss of circadian PAR bZip transcription factors results in epilepsy. Genes Dev 18:1397–1412. https://doi.org/10.1101/gad.301404

129. Jaeger C, Tischkau SA (2016) Role of Aryl Hydrocarbon Receptor in Circadian Clock Disruption and Metabolic Dysfunction. Environ. Health Insights 10

130. Tischkau SA (2011) AHR and the Circadian Clock. In: The AH Receptor in Biology and Toxicology. John Wiley and Sons, pp 511–522

131. Tischkau SA (2020) Mechanisms of circadian clock interactions with aryl hydrocarbon receptor signalling. Eur J Neurosci 51:379–395. https://doi.org/10.1111/ejn.14361

132. Tanimura N, Kusunose N, Matsunaga N, et al (2011) Aryl hydrocarbon receptor-mediated Cyp1a1 expression is modulated in a CLOCK-dependent circadian manner. Toxicology 290:203–207. https://doi.org/10.1016/j.tox.2011.09.007

133. Kou Z, Dai W (2021) Aryl hydrocarbon receptor: Its roles in physiology. Biochem. Pharmacol. 185

134. Barouki R, Coumoul X, Fernandez-Salguero PM (2007) The aryl hydrocarbon receptor, more than a xenobiotic-interacting protein. FEBS Lett. 581:3608–3615

135. Lin L, Dai Y, Xia Y (2022) An overview of aryl hydrocarbon receptor ligands in the Last two decades (2002–2022): A medicinal chemistry perspective. Eur. J. Med. Chem. 244

136. Nebert DW (2017) Aryl hydrocarbon receptor (AHR): "pioneer member" of the basic-helix/loop/helix per-Arnt-sim (bHLH/PAS) family of "sensors" of foreign and endogenous signals. Prog. Lipid Res. 67:38–57

137. Larigot L, Juricek L, Dairou J, Coumoul X (2018) AhR signaling pathways and regulatory functions. Biochim. Open 7:1–9

138. Haidar R, Henkler F, Kugler J, et al (2021) The role of DNA-binding and ARNT dimerization on the nucleo-cytoplasmic translocation of the aryl hydrocarbon receptor. Sci Rep 11:. https://doi.org/10.1038/s41598-021-97507-w

139. Wu D, Potluri N, Kim Y, Rastinejad F (2013) Structure and Dimerization Properties of the Aryl Hydrocarbon Receptor PAS-A Domain. Mol Cell Biol 33:4346–4356. https://doi.org/10.1128/mcb.00698-13

140. Schulte KW, Green E, Wilz A, et al (2017) Structural Basis for Aryl Hydrocarbon Receptor-Mediated Gene Activation. Structure 25:1025-1033.e3. https://doi.org/10.1016/j.str.2017.05.008

141. Labrecque M, Prefontaine G, Beischlag T (2013) The Aryl Hydrocarbon Receptor Nuclear Translocator (ARNT) Family of Proteins: Transcriptional Modifiers with Multi-Functional Protein Interfaces. Curr Mol Med 13:. https://doi.org/10.2174/15665240113139990042

142. Kahalehili HM, Newman NK, Pennington JM, et al (2021) Dietary Indole-3-Carbinol Activates AhR in the Gut, Alters Th17-Microbe Interactions, and Exacerbates Insulitis in NOD Mice. Front Immunol 11:.

https://doi.org/10.3389/fimmu.2020.606441

143. Larigot L, Benoit L, Koual M, et al (2022) Annual Review of Pharmacology and Toxicology Aryl Hydrocarbon Receptor and Its Diverse Ligands and Functions: An Exposome Receptor INTRODUCTION: THE DISCOVERY OF THE AhR SIGNALING PATHWAY AND DETOXICATION FUNCTIONS. Annu Rev Pharmacol Toxicol 62:383–404. https://doi.org/10.1146/annurev-pharmtox-052220

144. Bjeldanes LF, Kim J-Y, Grose KR, et al (1991) Aromatic hydrocarbon responsiveness-receptor agonists generated from indole-3-carbinol in vitro and in vivo: Comparisons with 2,3,7,8-tetrachlorodibenzo-p-dioxin (anticarcinogen/Brassica oleracea/indolo[3,2-b4carbazole)

145. Denison MS, Pandini A, Nagy SR, et al (2002) Ligand binding and activation of the Ah receptor. Chem Biol Interact 141:3–24. https://doi.org/10.1016/S0009-2797(02)00063-7

146. Heath-Pagliuso S, Rogers WJ, Tullis K, et al (1998) Activation of the Ah receptor by tryptophan and tryptophan metabolites. Biochemistry 37:11508–11515. https://doi.org/10.1021/bi980087p

147. Chevrier J, Warner M, Gunier RB, et al (2014) Serum Dioxin concentrations and thyroid hormone levels in the seveso women's health study. Am J Epidemiol 180:490–498. https://doi.org/10.1093/aje/kwu160

148. Furue M, Tsuji G (2019) Chloracne and hyperpigmentation caused by exposure to hazardous aryl hydrocarbon receptor ligands. Int. J. Environ. Res. Public Health 16

149. World Health Organization, International Agency for Research on Cancer (1997) Polychlorinated Dibenzo- para -Dioxins and Polychlorinated Dibenzofurans - Summary of Data Reported and Evaluation. IARC Monogr Eval Carcinog Risks to Humans Vol 69:

150. Barouki R, Aggerbeck M, Aggerbeck L, Coumoul X (2012) The aryl hydrocarbon receptor system. Drug Metabol. Drug Interact. 27

151. Cox MB, Miller III CA (2004) Cooperation of heat shock protein 90 and p23 in aryl hydrocarbon receptor signaling. Cell Stress Society International

152. Xie J, Huang X, Park MS, et al (2014) Differential suppression of the aryl hydrocarbon receptor nuclear translocator-dependent function by an aryl hydrocarbon receptor PAS-A-derived inhibitory molecule. Biochem Pharmacol 88:253–265. https://doi.org/10.1016/j.bcp.2014.01.021

153. Davarinos NA, Pollenz RS (1999) Aryl Hydrocarbon Receptor Imported into the Nucleus following Ligand Binding Is Rapidly Degraded via the Cytosplasmic Proteasome following Nuclear Export*. J Biol Chem 270:28708–28715

154. Pongratz I, Mason$ GGF, Poellingerf L (1992) Dual Roles of the 90-kDa Heat Shock Protein hsp90 in Modulating Functional Activities of the Dioxin Receptor. J Biol Chem 267:13728–13734

155. Kazlauskas A, Sundström S, Poellinger L, Pongratz I (2001) The hsp90 Chaperone Complex Regulates Intracellular Localization of the Dioxin Receptor. Mol Cell Biol 21:2594–2607. https://doi.org/10.1128/mcb.21.7.2594-2607.2001

156. Nguyen PM, Wang D, Wang Y, et al (2012) P23 co-chaperone protects the aryl hydrocarbon receptor from degradation in mouse and human cell lines. Biochem Pharmacol 84:838–850. https://doi.org/10.1016/j.bcp.2012.06.018

157. Yang Y, Chan WK (2021) Glycogen synthase kinase 3 beta regulates the human aryl hydrocarbon receptor cellular content and activity. Int J Mol Sci 22:. https://doi.org/10.3390/ijms22116097

158. Mimura J, Ema M, Sogawa K, Fujii-Kuriyama Y (1999) Identification of a novel mechanism of regulation of Ah (dioxin) receptor function. Genes (Basel) 13:20–25

159. Tsuji N, Fukuda K, Nagata Y, et al (2014) The activation mechanism of the aryl hydrocarbon receptor (AhR) by molecular chaperone HSP90. FEBS Open Bio 4:796–803. https://doi.org/10.1016/j.fob.2014.09.003

160. Zhu K, Meng Q, Zhang Z, et al (2019) Aryl hydrocarbon receptor pathway: Role, regulation and intervention in atherosclerosis therapy (Review). Mol Med Rep 20:4763–4773. https://doi.org/10.3892/mmr.2019.10748

161. Haarmann-Stemmann T, Abel J (2006) The arylhydrocarbon receptor repressor (AhRR): Structure, expression, and function. Biol. Chem. 387:1195–1199

162. Hu J, Ding Y, Liu W, Liu S (2023) When AHR signaling pathways meet viral infections. Cell Commun. Signal. 21

163. Long WP, Pray-Grant M, Tsai JC, Perdew GH (1998) Protein kinase C activity is required for aryl hydrocarbon receptor pathway-mediated signal transduction. Mol Pharmacol 53:. https://doi.org/10.1124/mol.53.4.691

164. Wright EJ, Pereira De Castro K, Joshi AD, Elferink CJ (2017) Canonical and non-canonical aryl hydrocarbon receptor signaling pathways. Curr. Opin. Toxicol. 2:87–92

165. Degner SC, Papoutsis AJ, Selmin O, Romagnolo DF (2009) Targeting of aryl hydrocarbon receptor-mediated activation of cyclooxygenase-2 expression by the indole-3-carbinol metabolite 3,3 -diindolylmethane in breast cancer cells 1,2. J Nutr 139:26–32. https://doi.org/10.3945/jn.108.099259

166. Sondermann NC, Faßbender S, Hartung F, et al (2023) Functions of the aryl hydrocarbon receptor (AHR) beyond the canonical AHR/ARNT signaling pathway. Biochem. Pharmacol. 208

167. Grishanova AY, Klyushova LS, Perepechaeva ML (2023) AhR and Wnt/β-Catenin Signaling Pathways and Their Interplay. Curr. Issues Mol. Biol. 45:3848–3876

168. Wilson SR, Joshi AD, Elferink CJ (2013) The tumor suppressor kruppel-like factor 6 is a novel aryl hydrocarbon receptor DNA binding partner. J Pharmacol Exp Ther 345:419–429. https://doi.org/10.1124/jpet.113.203786

169. Matsumura F, Vogel CFA (2006) Evidence supporting the hypothesis that one of the main functions of the aryl hydrocarbon receptor is mediation of cell stress responses. Biol. Chem. 387:1189–1194

170. Procházková J, Kabátková M, Bryja V, et al (2011) The interplay of the aryl hydrocarbon receptor and β-catenin alters both AhR-dependent transcription and wnt/β-catenin signaling in liver progenitors. Toxicol Sci 122:349–360. https://doi.org/10.1093/toxsci/kfr129

171. Braeuning A, Köhle C, Buchmann A, Schwarz M (2011) Coordinate regulation of cytochrome P450 1a1 expression in mouse liver by the aryl hydrocarbon receptor and the β-catenin pathway. Toxicol Sci 122:16–25. https://doi.org/10.1093/toxsci/kfr080

172. Luecke-Johansson S, Gralla M, Rundqvist H, et al (2017) A Molecular Mechanism To Switch the Aryl Hydrocarbon Receptor from a Transcription Factor to an E3 Ubiquitin Ligase Molecular and Cellular Biology. Mol Cell Biol 37:630–646

173. Barouti N, Mainetti C, Fontao L, Sorg O (2015) L-tryptophan as a novel potential pharmacological treatment for wound healing via aryl hydrocarbon receptor activation. Dermatology 230:332–339. https://doi.org/10.1159/000371876

174. Kober C, Roewe J, Schmees N, et al (2023) Targeting the aryl hydrocarbon receptor (AhR) with BAY 2416964: a selective small molecule inhibitor for cancer immunotherapy. J Immunother Cancer 11:e007495. https://doi.org/10.1136/jitc-2023-007495

175. Sayed TS, Maayah ZH, Zeidan HA, et al (2022) Insight into the physiological and pathological roles of the aryl hydrocarbon receptor pathway in glucose homeostasis, insulin resistance, and diabetes development. Cell. Mol. Biol. Lett. 27

176. Zhang N (2011) The role of endogenous aryl hydrocarbon receptor signaling in cardiovascular physiology. J. Cardiovasc. Dis. Res. 2:91–95

177. Perdew GH, Esser C, Snyder M, et al (2023) The Ah Receptor from Toxicity to Therapeutics: Report from the 5th AHR Meeting at Penn State University, USA, June 2022. Int J Mol Sci 24:. https://doi.org/10.3390/ijms24065550

178. Guerra-Ojeda S, Suarez A, Valls A, et al (2023) The Role of Aryl Hydrocarbon Receptor in the Endothelium: A Systematic Review. Int. J. Mol. Sci. 24

179. Tanos R, Patel RD, Murray IA, et al (2012) Aryl hydrocarbon receptor regulates the cholesterol biosynthetic pathway in a dioxin response element-independent manner. Hepatology 55:1994–2004. https://doi.org/10.1002/hep.25571

180. Wang J, Lu P, Xie W (2022) Atypical functions of xenobiotic receptors in lipid and glucose metabolism. Med. Rev. 2:611–624

181. da Silva JF, Bolsoni JA, da Costa RM, et al (2022) Aryl hydrocarbon receptor (AhR) activation contributes to high-fat diet-induced vascular dysfunction. Br J Pharmacol 179:2938–2952. https://doi.org/10.1111/bph.15789

182. Girer NG, Tomlinson CR, Elferink CJ (2021) The Aryl Hydrocarbon Receptor in Energy Balance: The Road from Dioxin-Induced Wasting Syndrome to Combating Obesity with Ahr Ligands. Int J Mol Sci 22:. https://doi.org/10.3390/ijms2201

183. Xu CX, Wang C, Zhang ZM, et al (2015) Aryl hydrocarbon receptor deficiency protects mice from diet-induced adiposity and metabolic disorders through increased energy expenditure. Int J Obes 39:1300–1309. https://doi.org/10.1038/ijo.2015.63

184. Dong F, Perdew GH (2020) The aryl hydrocarbon receptor as a mediator of host-microbiota interplay. Gut Microbes 12

185. Vasquez A, Atallah-Yunes N, Smith FC, et al (2003) Cardiac Abnormalities in AhRKO Mice A Role for the Aryl Hydrocarbon Receptor in Cardiac Physiology and Function as Demonstrated by AhR Knockout Mice

186. Mulero-Navarro S, Fernandez-Salguero PM (2016) New trends in Aryl hydrocarbon receptor biology. Front. Cell Dev. Biol. 4

187. Gutiérrez-Vázquez C, Quintana FJ (2018) Regulation of the Immune Response by the Aryl Hydrocarbon Receptor. Immunity 48:19–33

188. Nguyen NT, Kimura A, Nakahama T, et al (2010) Aryl hydrocarbon receptor negatively regulates dendritic cell immunogenicity via a kynurenine-dependent mechanism. Proc Natl Acad Sci U S A 107:19961–19966. https://doi.org/10.1073/pnas.1014465107

189. Litzenburger UM, Opitz CA, Sahm F, et al (2014) Constitutive IDO expression in human cancer is sustained by an autocrine signaling loop involving IL-6, STAT3 and the AHR. Oncotarget 5:1038–1051. https://doi.org/10.18632/oncotarget.1637

190. Quintana FJ, Sherr DH (2013) Aryl hydrocarbon receptor control of adaptive immunity. Pharmacol. Rev. 65:1148–1161

191. Shimba S, Watabe Y (2009) Crosstalk between the AHR signaling pathway and circadian rhythm. Biochem. Pharmacol. 77:560–565

192. Wang C, Zhang ZM, Xu CX, Tischkau SA (2014) Interplay between dioxin-mediated signaling and circadian clock: A possible determinant in metabolic homeostasis. Int. J. Mol. Sci. 15:11700–11712

193. Xu CX, Krager SL, Liao DF, Tischkau SA (2010) Disruption of CLOCK-BMAL1 transcriptional activity is responsible for aryl hydrocarbon receptor-mediated regulation of period1 gene. Toxicol Sci 115:98–108. https://doi.org/10.1093/toxsci/kfq022

194. Gu Y-Z, Hogenesch JB, Bradfield CA (2000) THE PAS SUPERFAMILY: Sensors of Environmental and Developmental Signals

195. Takahata S, Sogawa K, Kobayashi A, et al (1998) Transcriptionally Active Heterodimer Formation of an Arnt-like PAS Protein, Arnt3, with HIF-1a, HLF, and Clock

196. Hogenesch JB, Chan WK, Jackiw VH, et al (1997) Characterization of a Subset of the Basic-Helix-Loop-Helix-PAS Superfamily That Interacts with Components of the Dioxin Signaling Pathway*. J Biol Chem 272:8581–8593

197. Jaeger C, Khazaal AQ, Xu C, et al (2017) Aryl Hydrocarbon Receptor Deficiency Alters Circadian and Metabolic Rhythmicity. J Biol Rhythms 32:109–120. https://doi.org/10.1177/0748730417696786

198. Mukai M, Tischkau SA (2007) Effects of tryptophan photoproducts in the circadian timing system: Searching for a physiological role for aryl hydrocarbon receptor. Toxicol Sci 95:172–181. https://doi.org/10.1093/toxsci/kfl126

199. Fader KA, Nault R, Doskey CM, et al (2019) 2,3,7,8-Tetrachlorodibenzo-p-dioxin abolishes circadian regulation of hepatic metabolic activity in mice. Sci Rep 9:. https://doi.org/10.1038/s41598-019-42760-3

200. Garrett RW, Gasiewicz TA (2006) The aryl hydrocarbon receptor agonist 2,3,7,8-tetrachlorodibenzo-p-dioxin alters the circadian rhythms, quiescence, and expression of clock genes in murine hematopoietic stem and progenitor cells. Mol Pharmacol 69:. https://doi.org/10.1124/mol.105.021006

201. Ndikung J, Storm D, Violet N, et al (2020) Restoring circadian synchrony in vitro facilitates physiological responses to environmental chemicals. Environ Int 134:. https://doi.org/10.1016/j.envint.2019.105265

202. Qu X, Metz RP, Porter WW, et al (2010) The clock genes period 1 and period 2 mediate diurnal rhythms in dioxin-induced Cyp1A1 expression in the mouse mammary gland and liver. Toxicol Lett 196:28–32. https://doi.org/10.1016/j.toxlet.2010.03.020

203. Pendergast JS, Yamazaki S (2012) The mammalian circadian system is resistant to dioxin. J Biol Rhythms 27:156–163. https://doi.org/10.1177/0748730411434405

204. Huang P, Ceccatelli S, Rannug A (2002) A study on diurnal mRNA expression of CYP1A1, AHR, ARNT, and PER2 in rat pituitary and liver

205. Richardson VM, Santostefano MJ, Birnbaum LS (1998) Daily Cycle of bHLH-PAS Proteins, Ah Receptor and Arnt, in Multiple Tissues of Female Sprague-Dawley Rats 1. Biochem Biophys Res Commun 252:225–231

206. Qu X, Metz RP, Porter WW, et al (2007) Disruption of clock gene expression alters responses of the aryl hydrocarbon receptor signaling pathway in the mouse mammary gland. Mol Pharmacol 72:. https://doi.org/10.1124/mol.107.039305

207. Takiguchi T, Tomita M, Matsunaga N, et al (2007) Molecular basis for rhythmic expression of CYP3A4 in serum-shocked HepG2 cells. Wolters Kluwer Health | Lippincott Williams & Wilkins

208. Dallmann R, Brown SA, Gachon F (2014) Chronopharmacology: New insights and therapeutic implications. Annu. Rev. Pharmacol. Toxicol. 54:339–361

209. Tian J, Feng Y, Fu H, et al (2015) The Aryl Hydrocarbon Receptor: A Key Bridging Molecule of External and Internal Chemical Signals. Environ Sci Technol 49:9518–9531. https://doi.org/10.1021/acs.est.5b00385

210. Andreeva-Gateva P, Bakalov D, Sabit Z, Tafradjiiska-Hadjiolova R (2020) Aryl hydrocarbon receptors as potential therapeutic targets. Pharmacia 67:311–315. https://doi.org/10.3897/pharmacia.67.e47298

211. Levi F, Okyar A, Dulong S, et al (2010) Circadian timing in cancer treatments. Annu. Rev. Pharmacol. Toxicol. 50:377–421

212. Ozturk N, Ozturk D, Kavakli IH, Okyar A (2017) Molecular aspects of circadian pharmacology and relevance for cancer chronotherapy. Int. J. Mol. Sci. 18

213. Okazaki F, Matsunaga N, Hamamura K, et al (2017) Administering xCT Inhibitors Based on Circadian Clock Improves Antitumor Effects. Cancer Res 77:6603–6613. https://doi.org/10.1158/0008-5472.can-17-0720

214. Sulli G, Lam MTY, Panda S (2019) Interplay between Circadian Clock and Cancer: New Frontiers for Cancer Treatment. Trends in Cancer 5:475–494

215. Sancar A, Van Gelder RN (2021) Clocks, cancer, and chronochemotherapy. Science (80-.). 371

216. Ramos A, Sadeghi S, Tabatabaeian H (2021) Battling chemoresistance in cancer: Root causes and strategies to uproot them. Int. J. Mol. Sci. 22

217. Savvidis C, Koutsilieris M (2012) Circadian rhythm disruption in cancer biology. Mol Med 18:1249–1260. https://doi.org/10.2119/molmed.2012.00077

218. Huang C, Zhang C, Cao Y, et al (2023) Major roles of the circadian clock in cancer. Cancer Biol. Med. 20:1–24

219. Zhou L, Zhang Z, Nice E, et al (2022) Circadian rhythms and cancers: the intrinsic links and therapeutic potentials. J. Hematol. Oncol. 15

220. Paris A, Tardif N, Galibert MD, Corre S (2021) AhR and cancer: From gene profiling to targeted therapy. Int. J. Mol. Sci. 22:1–22

221. Wittenbrink N, Ananthasubramaniam B, Münch M, et al (2018) High-accuracy determination of internal circadian time from a single blood sample. J Clin Invest 128:3826–3839. https://doi.org/10.1172/JCI120874

222. Kessler K, Hornemann S, Rudovich N, et al (2020) Saliva Samples as A Tool to Study the Effect of Meal Timing on Metabolic And Inflammatory Biomarkers. Nutrients 12:. https://doi.org/10.3390/nu12020340

223. Takuma M, Ushijima K, Kumazaki M, et al (2015) Influence of dioxin on the daily variation of insulin sensitivity in mice. Env Toxicol Pharmacol 40:349–351. https://doi.org/10.1016/j.etap.2015.07.008

224. Miura N, Yoshioka H, Ashimori A, et al (2017) Multidirectional analyses of hepatic chronotoxicity induced by cadmium in mice. J Toxicol Sci 42:597–604

225. Levi F, Blazsek I, Ferle-Vidovic A (1988) Circadian and seasonal rhythms in murine bone marrow colony-forming cells affect tolerance for the anticancer agent 4'-O-tetrahydropyranyladriamycin (THP). Exp Hematol 16:696–701

226. Froy O (2009) Cytochrome P450 and the Biological Clock in Mammals. Curr Drug Metab 10:. https://doi.org/10.2174/138920009787522179

227. Gängler S, Charisiadis P, Seth R, et al (2018) Time of the day dictates the variability of biomarkers of exposure to disinfection byproducts. Environ Int 112:33–40. https://doi.org/10.1016/j.envint.2017.12.013

228. Miura N, Yoshioka H, Ashimori A, et al (2017) Multidirectional analyses of hepatic chronotoxicity induced by cadmium in mice. J Toxicol Sci 42:597–604. https://doi.org/10.2131/jts.42.597

229. Schmitt EE, Barhoumi R, Metz RP, Porter WW (2017) Circadian regulation of benzo[a]pyrene metabolism and DNA adduct formation in breast cells and the mouse mammary gland. Mol Pharmacol 91:178–188. https://doi.org/10.1124/mol.116.106740

230. Ávila-Rosales OS, Díaz-Muñoz M, Camacho-Carranza R, et al (2021) Daytime restricted feeding modifies the temporal expression of CYP1A1 and attenuated damage induced by benzo[a]pyrene in rat liver when administered before CYP1A1 acrophase. Toxics 9:. https://doi.org/10.3390/toxics9060130

231. Burgdorf T, Piersma AH, Landsiedel R, et al (2019) Workshop on the validation and regulatory acceptance of innovative 3R approaches in regulatory toxicology – Evolution versus revolution. Toxicol. Vitr. 59:1–11

232. Relógio A, Thomas P, Medina-Pérez P, et al (2014) Ras-Mediated Deregulation of the Circadian Clock in Cancer. PLoS Genet 10:. https://doi.org/10.1371/journal.pgen.1004338

233. Kao CY, Nomata K, Oakley CS, et al (1995) Two types of normal human breast epithelial cells derived from reduction mammoplasty: Phenotypic characterization and response to SV40 transfection. Carcinogenesis 16:531–538. https://doi.org/10.1093/carcin/16.3.531

234. Pappas B, Yang Y, Wang Y, et al (2018) p23 protects the human aryl hydrocarbon receptor from degradation via a heat shock protein 90-independent mechanism. Biochem Pharmacol 152:34–44. https://doi.org/10.1016/j.bcp.2018.03.015

235. Yoo SH, Yamazaki S, Lowrey PL, et al (2004) PERIOD2::LUCIFERASE real-time reporting of circadian dynamics reveals persistent circadian oscillations in mouse peripheral tissues. Proc Natl Acad Sci U S A 101:5339–5346. https://doi.org/10.1073/pnas.0308709101

236. Brown SA, Fleury-Olela F, Nagoshi E, et al (2005) The period length of fibroblast circadian gene expression varies widely among human individuals. PLoS Biol 3:. https://doi.org/10.1371/journal.pbio.0030338

237. Schulthess P, Löffler A, Vetter S, et al (2015) Signal integration by the CYP1A1 promoter - A quantitative study. Nucleic Acids Res 43:5318–5330. https://doi.org/10.1093/nar/gkv423

238. Schindelin J, Arganda-Carrera I, Frise E, et al (2009) Fiji - an Open platform for biological image analysis. Nat Methods 9:. https://doi.org/10.1038/nmeth.2019.Fiji

239. Goni R, García P, Foissac S (2009) The qPCR data statistical analysis. Control 1:1–9

240. Ma Q, Baldwin KT (2000) 2,3,7,8-tetrachlorodibenzo-p-dioxin-induced degradation of aryl hydrocarbon receptor (AhR) by the ubiquitin-proteasome pathway. Role of the transcription activaton and DNA binding of AhR. J Biol Chem 275:8432–8438. https://doi.org/10.1074/jbc.275.12.8432

241. Kobayashi A, Sogawa K, Fujii-Kuriyama Y (1996) Cooperative interaction between AhR·Arnt and Sp1 for the drug-inducible expression of CYP1A1 gene. J Biol Chem 271:12310–12316. https://doi.org/10.1074/jbc.271.21.12310

242. Tomita S, Sinal CJ, Yim SH, Gonzalez FJ (2000) Conditional disruption of the aryl hydrocarbon receptor nuclear translocator (Arnt) gene leads to loss of target gene induction by the aryl hydrocarbon receptor and hypoxia-inducible factor 1alpha. Mol Endocrinol 14:1674–1681. https://doi.org/10.1210/mend.14.10.0533

243. Hollingshead BD, Petrulis JR, Perdew GH (2004) The aryl hydrocarbon (Ah) receptor transcriptional regulator hepatitis B virus X-associated protein 2 antagonizes p23 binding to Ah receptor-Hsp90 complexes and is dispensable for receptor function. J Biol Chem 279:45652–45661. https://doi.org/10.1074/jbc.M407840200

244. Kuwahara J, Azumano M, Takeda T (1999) Nuclear localization of transcription factor Sp1. Nucleic Acids Symp Ser 293–294. https://doi.org/10.1093/nass/42.1.293

245. Ye W, Chen R, Chen X, et al (2019) AhR regulates the expression of human cytochrome P450 1A1 (CYP1A1) by recruiting Sp1. FEBS J 286:4215–4231. https://doi.org/10.1111/febs.14956

246. Zelin E, Zhang Y, Toogun OA, et al (2012) The p23 Molecular Chaperone and GCN5 Acetylase Jointly Modulate Protein-DNA Dynamics and Open Chromatin Status. Mol Cell 48:459–470. https://doi.org/10.1016/j.molcel.2012.08.026

247. Iitaka C, Miyazaki K, Akaike T, Ishida N (2005) A role for glycogen synthase kinase-3β in the mammalian circadian clock. J Biol Chem 280:29397–29402. https://doi.org/10.1074/jbc.M503526200

248. Schmitt EE, Barhoumi R, Metz RP, Porter WW (2017) Circadian Regulation of Benzo[a]Pyrene Metabolism and DNA Adduct Formation in Breast Cells and the Mouse Mammary Gland. Mol Pharmacol 91:178–188. https://doi.org/10.1124/mol.116.106740

249. Davarinos NA, Pollenz RS (1999) Aryl Hydrocarbon Receptor Imported into the Nucleus following Ligand Binding Is Rapidly Degraded via the Cytosplasmic Proteasome following Nuclear Export*. J Biol Chem 274:28708–28715

250. Luecke-Johansson S, Gralla M, Rundqvist H, et al (2017) A Molecular Mechanism To Switch the Aryl Hydrocarbon Receptor from a Transcription Factor to an E3 Ubiquitin Ligase. Mol Cell Biol 37:. https://doi.org/10.1128/mcb.00630-16

251. Petrulis JR, Hord NG, Perdew GH (2000) Subcellular localization of the aryl hydrocarbon receptor is modulated by the immunophilin homolog hepatitis B virus X-associated protein 2. J Biol Chem

275:37448–37453. https://doi.org/10.1074/jbc.M006873200

252. Kazlauskas A, Poellinger L, Pongratz I (1999) Evidence that the co-chaperone p23 regulates ligand responsiveness of the dioxin (aryl hydrocarbon) receptor. J Biol Chem 274:13519–13524. https://doi.org/10.1074/jbc.274.19.13519

253. Yang Y, Chan WK (2020) Selective autophagy maintains the aryl hydrocarbon receptor levels in HeLa cells: A mechanism that is dependent on the p23 co-chaperone. Int J Mol Sci 21:14–16. https://doi.org/10.3390/ijms21103449

254. Lingala SM, Ghany MGMMhs (2015) Circadian Rhythmicity of Active Gsk3 Isoforms Modulates Molecular Clock Gene Rhythms in the Scn. 25:289–313. https://doi.org/10.1177/0748730415573167.Circadian

255. O'Connor L, Gilmour J, Bonifer C (2016) The role of the ubiquitously expressed transcription factor Sp1 in tissue-specific transcriptional regulation and in disease. Yale J Biol Med 89:513–525

256. Fitzgerald CT, Nebert DW, Puga A (1998) Regulation of mouse Ah receptor (Ahr) gene basal expression by members of the Sp family of transcription factors. DNA Cell Biol 17:811–822. https://doi.org/10.1089/dna.1998.17.811

257. Wang F, Wang W, Safe S (1999) Regulation of constitutive gene expression through interactions of Sp1 protein with the nuclear aryl hydrocarbon receptor complex. Biochemistry 38:11490–11500. https://doi.org/10.1021/bi982578f

258. Xie X, Jiang J, Ye W, et al (2018) Sp1, instead of AhR, regulates the basal transcription of porcine CYP1A1 at the proximal promoter. Front Pharmacol 9:1–10. https://doi.org/10.3389/fphar.2018.00927

259. Garrison PM, Denison MS (2000) Analysis of the murine AhR gene promoter. J Biochem Mol Toxicol 14:1–10. https://doi.org/10.1002/(SICI)1099-0461(2000)14:1<1::AID-JBT1>3.0.CO;2-4

260. Spengler ML, Guo LW, Brattain MG (2008) Phosphorylation mediates Sp1 coupled activities of proteolytic processing, desumoylation and degradation. Cell Cycle 7:623–630. https://doi.org/10.4161/cc.7.5.5402

261. Mir R, Sharma A, Pradhan SJ, Galande S (2018) Regulation of Transcription Factor SP1 by the β -Catenin Destruction Complex Modulates Wnt Response . Mol Cell Biol 38:1–22. https://doi.org/10.1128/mcb.00188-18

262. Antoni D, Burckel H, Josset E, Noel G (2015) Three-dimensional cell culture: A breakthrough in vivo. Int J Mol Sci 16:5517–5527. https://doi.org/10.3390/ijms16035517

263. Schneider MR, Oelgeschlaeger M, Burgdorf T, et al (2021) Applicability of organ-on-chip systems in toxicology and pharmacology. Crit Rev Toxicol 51:540–554. https://doi.org/10.1080/10408444.2021.1953439

264. Balsalobre A, Brown SA, Marcacci L, et al (2000) Resetting of circadian time in peripheral tissues by glucocorticoid signaling. Science (80-) 289:2344–2347

265. Brown SA, Zumbrunn G, Fleury-Olela F, et al (2002) Rhythms of mammalian body temperature can sustain peripheral circadian clocks. Curr Biol 12:1574–1583. https://doi.org/10.1016/S0960-9822(02)01145-4

266. Preußner M, Heyd F (2018) Temperature-controlled Rhythmic Gene Expression in Endothermic Mammals: All Diurnal Rhythms are Equal, but Some are Circadian. BioEssays 40:1–10. https://doi.org/10.1002/bies.201700216

267. Wambaugh JF, Hughes MF, Ring CL, et al (2018) Evaluating in vitro-in vivo extrapolation of toxicokinetics. Toxicol Sci 163:152–169. https://doi.org/10.1093/toxsci/kfy020

268. Ankley GT, Bennett RS, Erickson RJ, et al (2010) Adverse outcome pathways: a conceptual framework to support ecotoxicology research and risk assessment. Env Toxicol Chem 29:730–741. https://doi.org/10.1002/etc.34

269. Burden N, Sewell F, Andersen ME, et al (2015) Adverse Outcome Pathways can drive non-animal approaches for safety assessment. J Appl Toxicol 35:971–975. https://doi.org/10.1002/jat.3165

Publications

Journal Publications

M. Mihelakis, J. Ndikung, M. Oelgeschläger, and N. Ertych, "**The 4th dimension of *in vitro* systems – Time to level up**" *Environ. Int.*, vol. 164, Jun. 2022, doi: 10.1016/j.envint.2022.107256

M. Mihelakis, T. Flore, G. Schönfelder, M. Oelgeschläger and N. Ertych "**SP1 and p23 orchestrate circadian target gene induction of activated aryl hydrocarbon receptor in human breast cells**" (in preparation)

Poster Presentations

The mechanism of the circadian regulated AhR-signaling pathway

Melina Mihelakis, Norman Ertych, and Michael Oelgeschlaeger

AhR symposium, 19th- 23rd July, 2022, Pennsylvania State University, US